Award Number: W81XWH-10-1-0823

TITLE: Determine the Role of Canonical Wnt Signaling in Ovarian Tumorigenesis

PRINCIPAL INVESTIGATOR: Rugang Zhang, Ph.D.

CONTRACTING ORGANIZATION: The Wistar Institute, Philadelphia, PA 19104

REPORT DATE: October 2012

TYPE OF REPORT: Annual

PREPARED FOR: U.S. Army Medical Research and Materiel Command
Fort Detrick, Maryland 21702-5012

REPORT DOCUMENTATION PAGE

Form Approved
OMB No. 0704-0188

1. REPORT DATE	2. REPORT TYPE	3. DATES COVERED
1 October 2012	Annual	15 September 2011 - 14 September 2012

4. TITLE AND SUBTITLE

Determine the Role of Canonical Wnt Signaling in Ovarian Tumorigenesis

5a. CONTRACT NUMBER

5b. GRANT NUMBER
W81XWH-10-1-0823

5c. PROGRAM ELEMENT NUMBER

6. AUTHOR(S)

Rugang Zhang, Ph.D.

E-Mail: rzhang@wistar.org

5d. PROJECT NUMBER

5e. TASK NUMBER

5f. WORK UNIT NUMBER

7. PERFORMING ORGANIZATION NAME(S) AND ADDRESS(ES)

The Wistar Institue
Philadelphia, PA 19104

8. PERFORMING ORGANIZATION REPORT NUMBER

9. SPONSORING / MONITORING AGENCY NAME(S) AND ADDRESS(ES)
U.S. Army Medical Research and Materiel Command
Fort Detrick, Maryland 21702-5012

10. SPONSOR/MONITOR'S ACRONYM(S)

11. SPONSOR/MONITOR'S REPORT NUMBER(S)

12. DISTRIBUTION / AVAILABILITY STATEMENT
Approved for Public Release; Distribution Unlimited

13. SUPPLEMENTARY NOTES

14. ABSTRACT

Ovarian cancer ranks first as the cause of death for gynecological cancers. Obviously, there is an urgent need to develop novel treatment methods for ovarian cancer. To do this, we must better understand key events associated with ovarian cancer development. In order to combat cancer, a normal cell's typical response to a tumor-promoting genetic alteration is irreversible growth arrest, consequently preventing the normal human cell from progressing towards becoming a cancer cell. This process is termed senescence. When this process fails, those cells containing tumor-promoting genetic alterations can grow without control and become a tumor. The potential use of cellular senescence for cancer therapy would rely on reactivation of this process in cancer cells. We have previously discovered a pathway that opposes the beneficial process of senescence. This pathway is referred to as the canonical Wnt signaling pathway. Therefore, we hypothesize that canonical Wnt signaling pathway contributes to the development of ovarian cancer through bypassing senescence. The proposed studies may lead to development of strategies for ovarian cancer treatment using reactivation of cellular senescence as a novel mechanism by targeting ovarian cancer promoting canonical Wnt signaling.

15. SUBJECT TERMS
Ovarian Cancer, Cellular Senescence, Wnt signaling

16. SECURITY CLASSIFICATION OF:			17. LIMITATION OF ABSTRACT	18. NUMBER OF PAGES	19a. NAME OF RESPONSIBLE PERSON
a. REPORT	b. ABSTRACT	c. THIS PAGE			USAMRMC
U	U	U	UU	67	19b. TELEPHONE NUMBER *(include area code)*

Table of Contents

Introduction:

The role of Wnt signaling in epithelial ovarian cancer (EOC) development remains largely elusive. We have evidence to suggest that canonical Wnt signaling is activated through downregulation of Wnt5a in EOC. Wnt5a is a non-canonical Wntligand that acts as an antagonist of canonical Wnt signaling. Furthermore, inhibition of canonical Wnt signaling or restoration of Wnt5a expression inhibits the growth of EOC cells. The overall hypothesis of this proposal is that canonical Wnt signaling activated by loss of Wnt5a contributes to EOC development by abrogation of OIS. The objectives of the proposed studies are to determine the role of canonical Wnt signaling in regulating OIS of ovarian epithelial cells during progression of benign ovarian tumors into invasive EOCs, and to investigate the effects of inhibition of the canonical Wnt signaling on malignant behavior of EOC cells. The specific aims are: 1): Elucidate the mechanisms by which inhibition of canonical Wnt signaling inhibits the growth of EOC cells; 2): Determine whether loss of Wnt5a contributes to EOC development by abrogation of OIS; 3): Investigate the effects of inhibition of canonical Wnt signaling on malignant behavior of EOC cells in immunodeficient mice.

Body:

1. Research accomplishments associated with each task outlined in the approved Statement of Work.

Task 1. Determine whether inhibition of canonical Wnt signaling inhibits the growth of EOC cells through inducing cell senescence. (Months 1-12)

Specifically, we will determine whether inhibition of canonical Wnt signaling induces the expression of markers of senescence in human EOC cells.

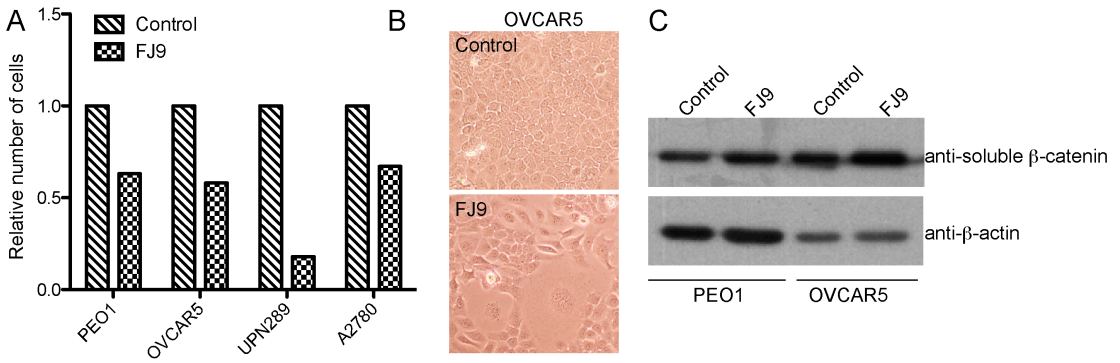

Figure 1. FJ9 suppresses the growth of human EOC cells via Wnt/β-catenin independent mechanisms. (A) Equal number of indicated EOC cell lines were treated with 100uM FJ9 or vehicle control (dissolved in 0.01% DMSO). After 72 hours of treatment, the number of cells were counted and calculated as relative number of cells. (B) same as (A) but examined for cell morphology changes using phase contrast microscopy. (C) Same as (A) but examined for expression of soluble b-catenin and b-actin in indicated human EOC cell lines treated with FJ9 or vehicle control by immunoblotting using indicated antibodies.

Progress report: FJ9 has previously been demonstrated as an inhibitor of canonical Wnt signaling [1]. We showed that FJ9 inhibits the growth of human EOC cells in a panel of human EOC cell lines (Figure 1A). Consistent with the idea that this is due to senescence induction, cells treated with FJ9 demonstrated features of senescence such as a large flat cell morphology (Figure 1B). However, examination of markers of canonical Wnt signaling in FJ9 treated or control cells showed that there is no evidence to suggest the observed effects are due to inhibition of canonical Wnt/β-catenin pathway. For example, the levels of soluble β-catenin, a marker of active canonical Wnt/β-catenin pathway were not decreased by FJ9 treatment (Figure 1C). This result suggests that FJ9 inhibits the growth of human EOC cells via canonical Wnt signaling independent mechanisms.

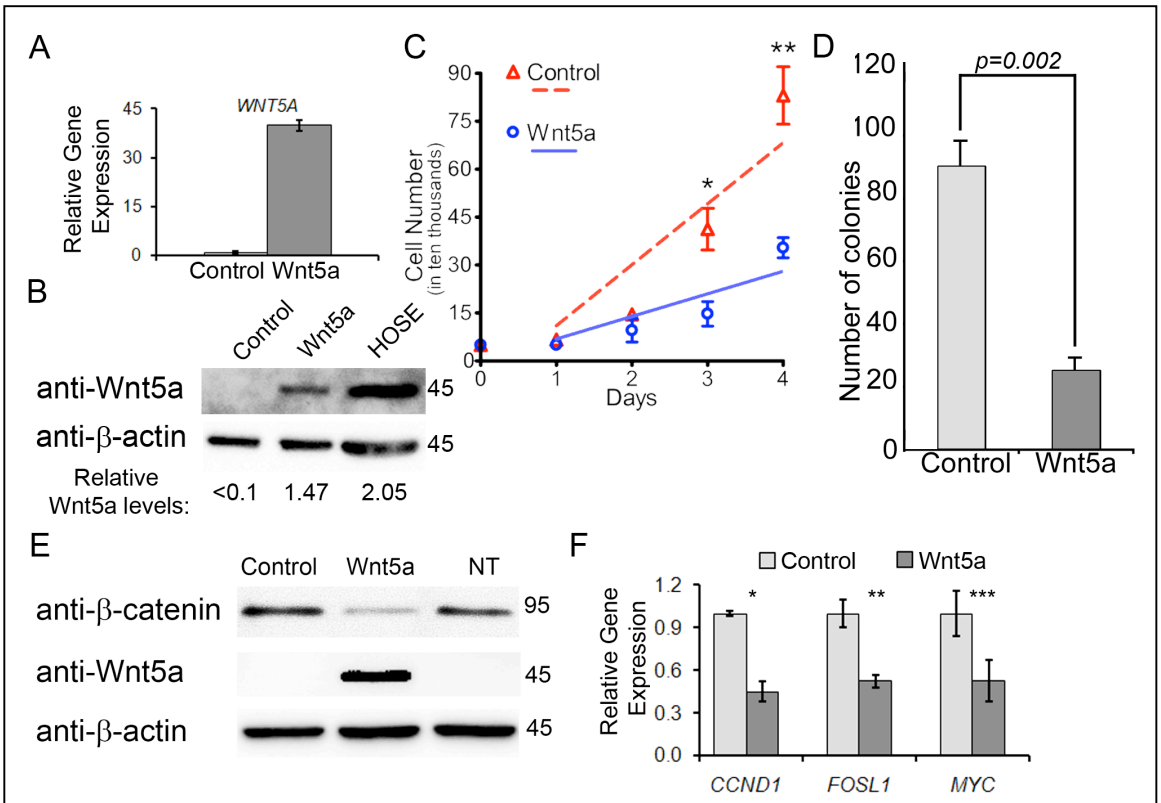

Figure 2. Wnt5a restoration inhibits the growth of human EOC cells by antagonizing canonical Wnt/β-catenin signaling. (A) OVCAR5 cells were transduced with a control or Wnt5a encoding puromycin resistant retrovirus. The infected cells were drug-selected with 3 μg/ml puromycin. Expression of Wnt5a mRNA in drug-selected cells was determined by qRT-PCR. **(B)** Same as (A), but examined for expression of Wnt5a and β-actin in control or Wnt5a-infected OVCAR5 and primary HOSE cells by immunoblotting. Relative levels of Wnt5a expression was indicated based on densitometric analysis using NIH Image J software. **(C)** Same as (A), but equal number (5000) of drug-selected control (open triangles and dotted line) or Wnt5a-infected cells (open circles and solide line) were cultured on plastic plates for 4 days, and the number of cells was counted (Control ± SD or Wnt5a ± SD (n=3); student *t-test* was used for calculating p value) *p = 0.0038 and **p = 0.001. Mean of three independent experiments with SD and linear regression. **(D)** Same as (C), but grown under anchorage-independent condition in soft-agar. The number of colonies was counted 2 weeks after initial inoculation. Mean of three independent experiments with SD. **(E)** Same as (A), but examined for the levels of soluble β-catenin and β-actin expression by immunoblotting (NT = non-treated). **(F)** Same as (A), but examined for expression of indicated β–catenin target genes by qRT-PCR. Expression of *β*-2-microglobulin was used to normalize the expression of indicated genes. * p = 0.0095, ** p = 0.0012 and *** p = 0.0286 compared with controls.

We sought to determine the effects of Wnt5a reconstitution in human EOC cells. Wnt5a expression was reconstituted in the OVCAR5 EOC cell line via retroviral transduction. Ectopically expressed Wnt5a was confirmed by both qRT-PCR and immunoblotting in

OVCAR5 cells stably expressing Wnt5a or a vector control (Figure 2A-B). Of note, the levels of ectopically expressed Wnt5a in OVCAR5 cells are comparable to the levels observed in primary HOSE cells (Figure 2B). Interestingly, Wnt5a reconstitution in OVCAR5 human EOC cells significantly inhibited both anchorage-dependent and anchorage-independent growth in soft-agar compared with vector controls (Figure 2C-D). In addition, similar growth inhibition by Wnt5a reconstitution was also observed in the PEO1 human EOC cell line (Figure 3A-C), suggesting that this effect is not cell line specific. Based on these results, we conclude that Wnt5a reconstitution inhibits the growth of human EOC cells in vitro.

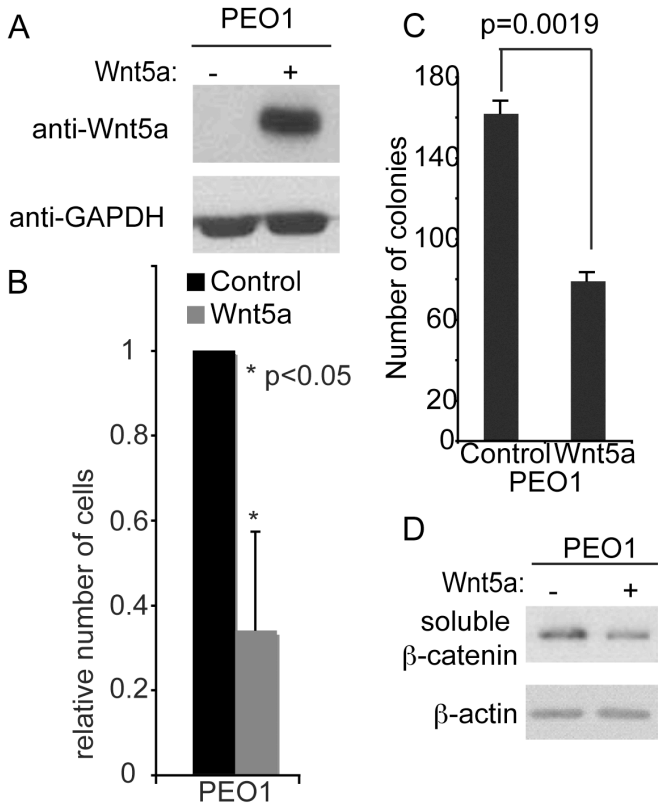

Figure 3. Wnt5a restoration inhibits the growth of PEO1 EOC cells by antagonizing canonical Wnt signaling. **(A)** PEO1 cells were transduced with a control- or Wnt5a-encoding puromycin resistant retrovirus. The infected cells were drug-selected with 1 μg/ml puromycin for 3 days. Expression of Wnt5a and GAPDH in drug-selected cells was determined by immunoblotting. **(B)** Same as (A) but an equal number of drug-selected control and Wnt5a infected PEO1 cells were cultured on plastic plate for 5 days and the number of cells were counted using trypan blue exclusion assay. Mean of three independent experiments with SD. **(C)** Same as (B) but grown under anchorage-independent conditions in soft-agar. The number of colonies were counted 2 weeks after initial inoculation. Mean of 3 independent experiments with SD. **(D)** Same as (A), but examined for soluble β-catenin expression by immunoblotting.

Canonical Wnt signaling promotes cell proliferation and Wnt5a has been demonstrated to antagonize the canonical Wnt/ β-catenin signaling in certain cell contexts [2-5]. We hypothesized that Wnt5a would suppress the growth of human EOC cells by antagonizing canonical Wnt/β-catenin signaling. To test our hypothesis, we examined the effect of Wnt5a reconstitution on expression of markers of active Wnt/β-catenin signaling in human EOC cells, namely the levels of "active" soluble β-catenin[6-8] and expression of β-catenin target genes such as CCND1, c-MYC and FOSL1 [9, 10]. Indeed, we observed a decrease in soluble β-catenin in Wnt5a reconstituted OVCAR5 cells compared with vector controls (Figure 2E). Consistently, we also observed a

significant decrease in the levels of β-catenin target genes in these cells, namely CCND1 (p = 0.0095), FOSL1 (p = 0.0012) and c-MYC (p = 0.0286) (Figure 2F). Similar effects of Wnt5a reconstitution on expression of markers of active Wnt/β-catenin signaling (such as decreased levels of soluble β-catenin) were also observed in PEO1 human EOC cells (Figure 3D), suggesting that this is not cell line specific. Based on these results, we conclude that Wnt5a suppresses the growth of human EOC cells by antagonizing canonical Wnt/β-catenin signaling in human EOC cells.

Next, we sought to determine the cellular mechanism whereby Wnt5a inhibits the growth of human EOC cells. We sought to determine whether Wnt5a restoration might induce senescence in human EOC cells. To do so, we determined whether Wnt5a restoration induces SA-β-gal activity, a universal marker of cellular senescence [11]. Indeed, SA-β-gal activity was notably induced by Wnt5a reconstitution in both OVCAR5 and PEO1 human EOC cells compared with controls (Figure 4).

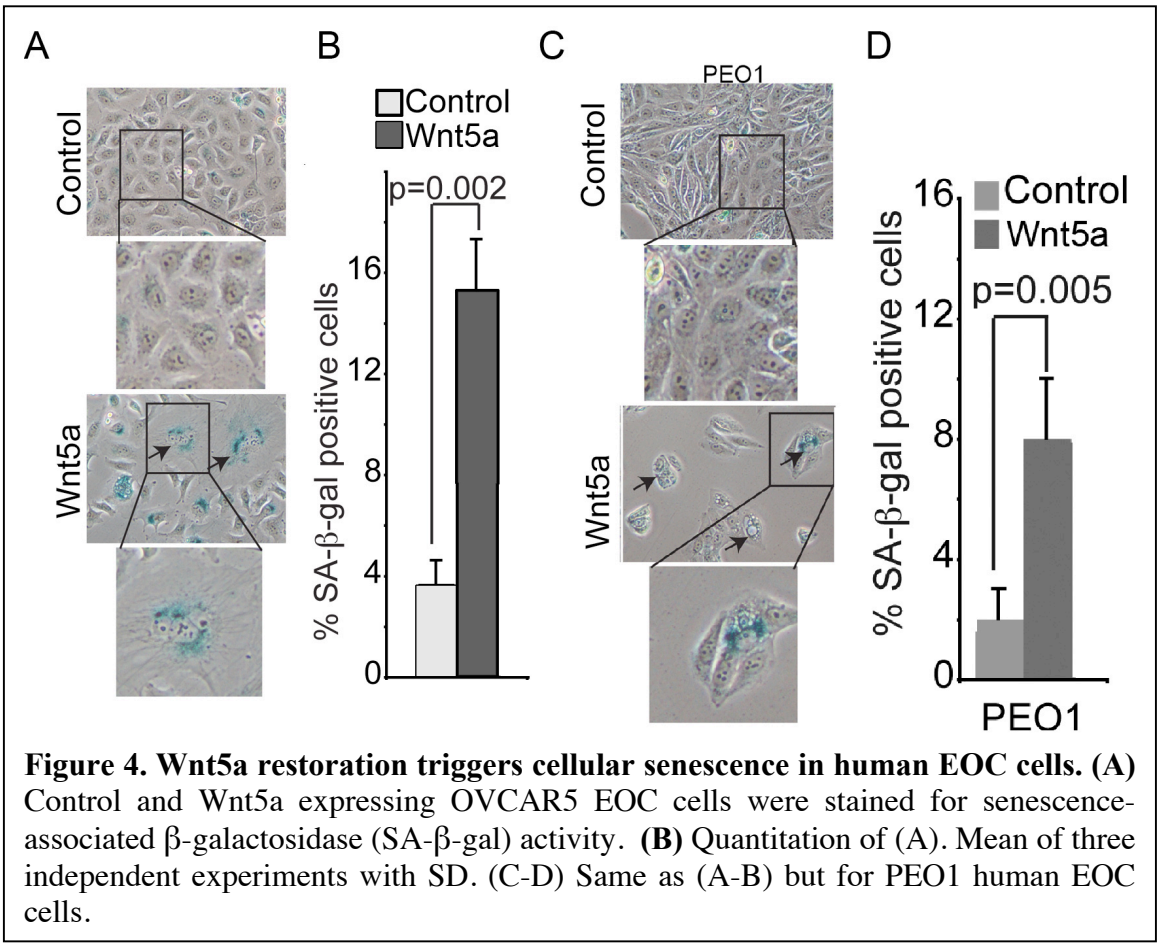

Figure 4. Wnt5a restoration triggers cellular senescence in human EOC cells. (A) Control and Wnt5a expressing OVCAR5 EOC cells were stained for senescence-associated β-galactosidase (SA-β-gal) activity. **(B)** Quantitation of (A). Mean of three independent experiments with SD. (C-D) Same as (A-B) but for PEO1 human EOC cells.

Task 2. Determine the effects of inhibition of Wnt/β-catenin signaling on key senescence-regulating pathways in human EOC cells. (Month 13-24)

Specifically, we will determine the effects of inhibition of Wnt/β-catenin signaling by FJ9 treatment or enforced Wnt5a expression on status of p53, pRB and HIRA/PML pathways.

Progress report: Since FJ9 failed to inhibit canonical Wnt signaling (Figure 1C), we focused on our study on using Wnt5a restoration as a way to inhibit canonical Wnt signaling (Figure 2 and 3). We have previously shown that suppression of canonical Wnt signaling promotes cellular senescence in primary human fibroblasts by activating the senescence-promoting histone repressor A (HIRA)/ promyelocyticleukemia (PML) pathway [8]. PML bodies are 20-30 dot-like structures in the nucleus of virtually all human cells. PML bodies are sites of poorly defined tumor suppressor activity, and are disrupted in acute promyelocytic leukemia [12]. PML has been implicated in regulating cellular senescence. For example, the foci number and size of PML bodies increase during senescence [12, 13] and inactivation of PML suppresses senescence [14]. Activation of the HIRA/PML pathway is reflected by the recruitment of HIRA into PML bodies [15].

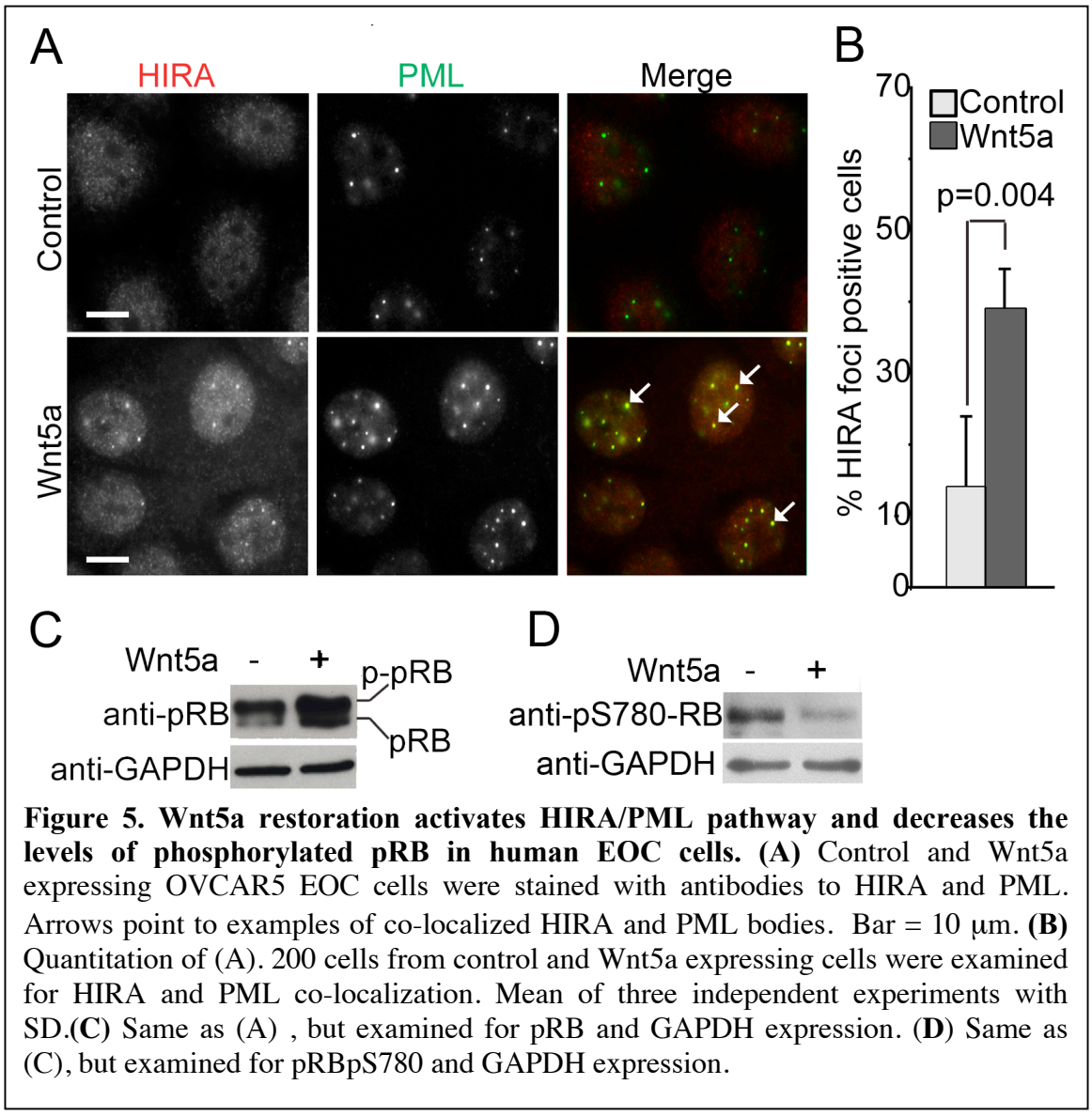

Figure 5. Wnt5a restoration activates HIRA/PML pathway and decreases the levels of phosphorylated pRB in human EOC cells. (A) Control and Wnt5a expressing OVCAR5 EOC cells were stained with antibodies to HIRA and PML. Arrows point to examples of co-localized HIRA and PML bodies. Bar = 10 μm. **(B)** Quantitation of (A). 200 cells from control and Wnt5a expressing cells were examined for HIRA and PML co-localization. Mean of three independent experiments with SD.**(C)** Same as (A) , but examined for pRB and GAPDH expression. (**D**) Same as (C), but examined for pRBpS780 and GAPDH expression.

As Wnt5a antagonizes canonical Wnt signaling in human EOC cells (Figure 2E-F), we sought to determine whether Wnt5a restoration might activate the senescence-promoting HIRA/PML pathway in human EOC cells. Towards this goal, we examined the localization of HIRA in OVCAR5 EOC cells reconstituted with Wnt5a or vector

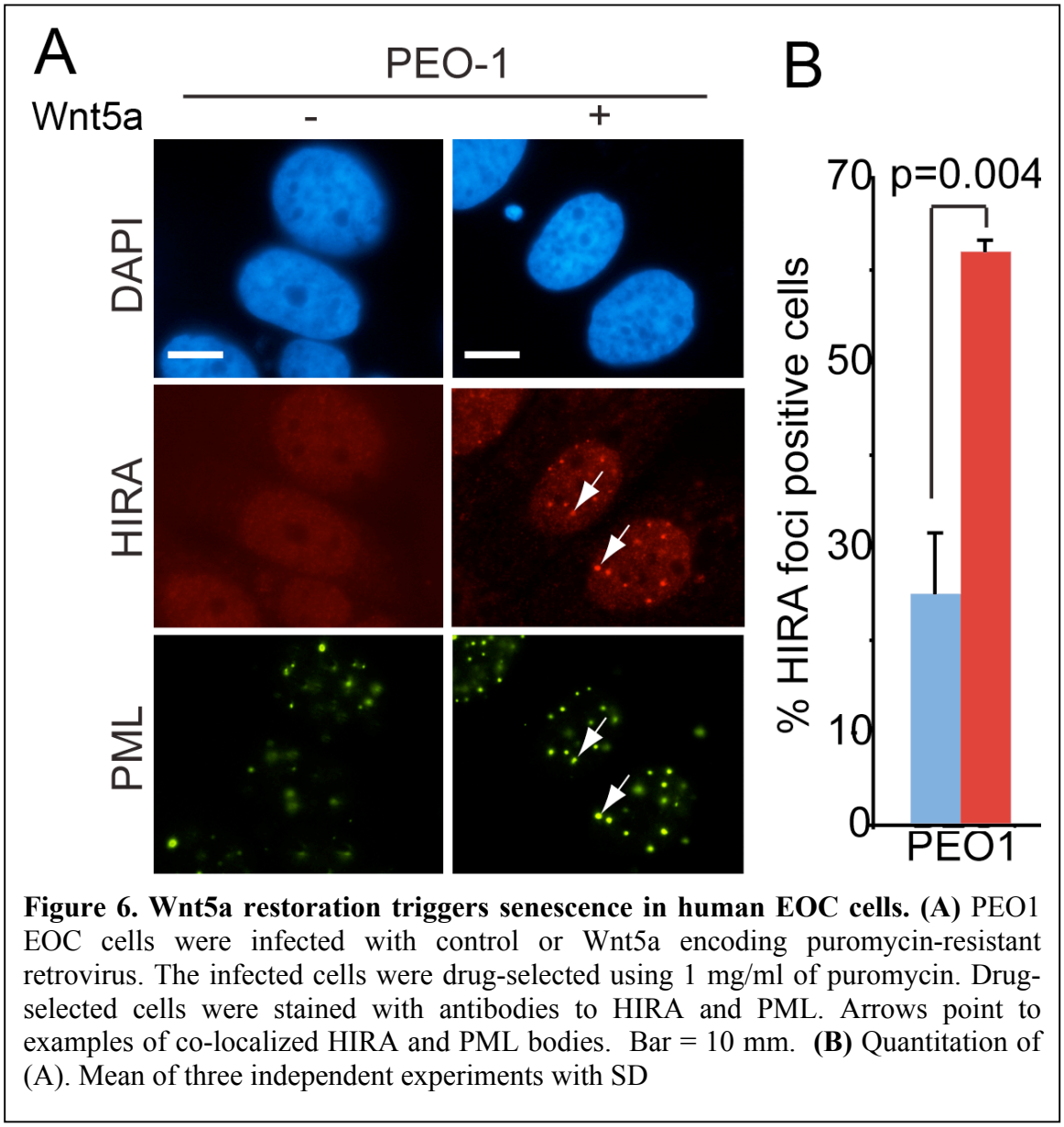

Figure 6. Wnt5a restoration triggers senescence in human EOC cells. (A) PEO1 EOC cells were infected with control or Wnt5a encoding puromycin-resistant retrovirus. The infected cells were drug-selected using 1 mg/ml of puromycin. Drug-selected cells were stained with antibodies to HIRA and PML. Arrows point to examples of co-localized HIRA and PML bodies. Bar = 10 mm. **(B)** Quantitation of (A). Mean of three independent experiments with SD

control. Notably, there was a significant increase in the percentage of cells with HIRA localized to PML bodies in Wnt5a restored human EOC cells compared with controls (Figure 5A-B, $p = 0.004$). In addition, we also observed an increase in the number and size of PML bodies in the Wnt5a restored OVCAR5 EOC cells (Figure 5A), which are also established markers of cellular senescence [14, 16].

The p53 and pRB tumor suppressor pathways play a key role in regulating senescence [11]. Thus, we sought to determine the effects of Wnt5a on the p53 and pRB

pathways. Interestingly, $p16^{INK4a}$, the upstream repressor of pRB, is deleted in OVCAR5 human EOC cell line [17]. In addition, the levels of total phosphorylated pRB were not decreased by Wnt5a, while the levels of cyclin D1/CKD4-mediated Serine 780 phosphorylation on pRB (pRBpS780) were decreased by Wnt5a [18] (Figure 4C-D). Further, p53 is null in OVCAR5 cells [19]. We conclude that cellular senescence induced by Wnt5a restoration is independent of both p53 and $p16^{INK4a}$.

Similarly, we observed activation of the HIRA/PML pathway by Wnt5a restoration in PEO1 human EOC cells (Figure 6A-B), suggesting that the observed effects are not cell line specific. Together, we conclude that Wnt5a reconstitution activates the HIRA/PML senescence pathway.

Based on these results, we concluded that Wnt5a restoration induced senescence of human EOC cells by activating the HIRA/PML senescence pathway.

Key Research Accomplishments:

- FJ9 suppresses the growth of human EOC cells but likely through canonical Wntsignaling independent mechanisms.
- Wnt5a suppresses the growth of human EOC cells.
- Wnt5a inhibits canonical Wnt signaling.
- Wnt5a induces cellular senescence.
- Cellular senescence induced by Wnt5a restoration is independent of both p53 and p16.
- Cellular senescence induced by Wnt5a restoration correlates with activation of the HIRA/PML senescence-promoting pathway.
- Cellular senescence induced by Wnt5a restoration correlates with a decreased level of serine 780 phosphorylated pRB.

Reportable Outcomes:

Manuscripts:

1. Aird K.M., **Zhang R.*** Detection of senescence-associated heterochromatin foci. ***Methods Mol. Biol***. *in press.*
2. Li H., Cai Q., Wu H., Vathipadiekal V., Dobbin Z.C., Li T., Hua X., Landen C.N., Birrer M. J., Sanchez-Beato M., **Zhang R.*** SUZ12 promotes human epithelial ovarian cancer by suppressing apoptosis via silencing HRK. ***Mol Cancer Res.*** *In press*.

3. Tu Z., Aird K.M. and **Zhang R.*** RAS, cellular senescence and transformation: the BRCA1 DNA repair pathway at the crossroads. ***Small GTPases*** 3: 162-167, **2012**.

4. Li H., Bitler B.G., Maradeo M.E., Slifker M., Vathipadiekal V., Careasy C., Tummino P., Cairns P., Birrer M.J., **Zhang R.*** ALDH1A1 is a novel EZH2 target gene in epithelial ovarian cancer identified by genome-wide approaches. ***Cancer Prev Res.*** 5: 484-91, **2012**.

5. Tu Z., Nicodemus J., Beehary N., Xia B., Yen T. and **Zhang R.*** Oncogenic Ras regulates BRIP1 expression to induce dissociation of BRCA1 from chromatin, inhibit DNA repair, and promote senescence. ***Dev. Cell*** 21: 1077-91, **2011**.

6. Bitler B.G., Nicodemus J.P., Li H., Cai Q., Wu H., Hua X., Li T., Birrer M.J., Godwin A.K., Cairns P., **Zhang R.*** Wnt5a suppresses epithelial ovarian cancer by promoting cellular senescence. ***Cancer Res.*** 71:6184-94, **2011**.

7. Li H., Cai Q., Godwin A.K. and **Zhang R***. Enhancer of zeste homology 2 promotes the proliferation and invasion of human epithelial cells. ***Mol. Cancer Res.*** 8: 1610-1618, **2010**.

Abstracts:
An abstract based on this study has been published by American Association of Cancer Research.

An abstract based on this study has been published by the 3rd International Symposium on Ovarian Cancer

Presentations:
A poster has been presented at 2011 AACR annual meeting.

A talk has been presented at the 3rd International Symposium on Ovarian Cancer

Patents:
A patent has been filed based on the funded studies.
U.S. Patent Application Serial Number: 61/445, 145.

Conclusions:

Wnt5a promotes senescence of human EOC cells by suppressing the proliferation promoting canonical Wnt/β-catenin pathway. We suggest that strategies to drive senescence in EOC cells by reconstituting Wnt5a signaling may offer an effective new strategy for EOC therapy

References:

1. Fujii, N., et al., *An antagonist of dishevelled protein-protein interaction suppresses beta-catenin-dependent tumor cell growth*. Cancer Res, 2007. **67**(2): p. 573-9.
2. Liang, H., et al., *Wnt5a inhibits B cell proliferation and functions as a tumor suppressor in hematopoietic tissue*. Cancer Cell, 2003. **4**(5): p. 349-60.
3. Mikels, A.J. and R. Nusse, *Purified Wnt5a protein activates or inhibits beta-catenin-TCF signaling depending on receptor context*. PLoS Biol, 2006. **4**(4): p. e115.
4. Topol, L., et al., *Wnt-5a inhibits the canonical Wnt pathway by promoting GSK-3-independent beta-catenin degradation*. J Cell Biol, 2003. **162**(5): p. 899-908.
5. McDonald, S.L. and A. Silver, *The opposing roles of Wnt-5a in cancer*. Br J Cancer, 2009. **101**(2): p. 209-14.
6. Cheyette, B.N., et al., *Dapper, a Dishevelled-associated antagonist of beta-catenin and JNK signaling, is required for notochord formation*. Dev Cell, 2002. **2**(4): p. 449-61.
7. Reya, T. and H. Clevers, *Wnt signalling in stem cells and cancer*. Nature, 2005. **434**(7035): p. 843-50.
8. Ye, X., et al., *Downregulation of Wnt signaling is a trigger for formation of facultative heterochromatin and onset of cell senescence in primary human cells*. Mol Cell, 2007. **27**(2): p. 183-96.
9. Katoh, M., *WNT signaling pathway and stem cell signaling network*. Clin Cancer Res, 2007. **13**(14): p. 4042-5.
10. Mann, B., et al., *Target genes of beta-catenin-T cell-factor/lymphoid-enhancer-factor signaling in human colorectal carcinomas*. Proc Natl Acad Sci U S A, 1999. **96**(4): p. 1603-8.
11. Kuilman, T., et al., *The essence of senescence*. Genes Dev, 2010. **24**(22): p. 2463-79.
12. Bernardi, R. and P.P. Pandolfi, *Structure, dynamics and functions of promyelocytic leukaemia nuclear bodies*. Nat Rev Mol Cell Biol, 2007. **8**(12): p. 1006-16.
13. Mallette, F.A., et al., *Human fibroblasts require the Rb family of tumor suppressors, but not p53, for PML-induced senescence*. Oncogene, 2004. **23**(1): p. 91-9.
14. Ferbeyre, G., et al., *PML is induced by oncogenic ras and promotes premature senescence*. Genes Dev, 2000. **14**(16): p. 2015-27.
15. Salomoni, P. and P.P. Pandolfi, *The role of PML in tumor suppression*. Cell, 2002. **108**(2): p. 165-70.
16. Pearson, M., et al., *PML regulates p53 acetylation and premature senescence induced by oncogenic Ras*. Nature, 2000. **406**(6792): p. 207-10.
17. Watson, J.E., et al., *Identification and characterization of a homozygous deletion found in ovarian ascites by representational difference analysis*. Genome Res, 1999. **9**(3): p. 226-33.
18. Lundberg, A.S. and R.A. Weinberg, *Functional inactivation of the retinoblastoma protein requires sequential modification by at least two distinct cyclin-cdk complexes*. Mol Cell Biol, 1998. **18**(2): p. 753-61.

19. Yaginuma, Y. and H. Westphal, *Abnormal structure and expression of the p53 gene in human ovarian carcinoma cell lines*. Cancer Res, 1992. **52**(15): p. 4196-9.

Appendices:

Manuscripts:

1. Tu Z., Aird K.M. and **Zhang R.*** RAS, cellular senescence and transformation: the BRCA1 DNA repair pathway at the crossroads. ***Small GTPases*** 3: 162-167, **2012**.

2. Li H., Bitler B.G., Maradeo M.E., Slifker M., Vathipadiekal V., Careasy C., Tummino P., Cairns P., Birrer M.J., **Zhang R.*** ALDH1A1 is a novel EZH2 target gene in epithelial ovarian cancer identified by genome-wide approaches. ***Cancer Prev Res.*** 5: 484-91, **2012**.

3. Tu Z., Nicodemus J., Beehary N., Xia B., Yen T. and **Zhang R.*** Oncogenic Ras regulates BRIP1 expression to induce dissociation of BRCA1 from chromatin, inhibit DNA repair, and promote senescence. ***Dev. Cell*** 21: 1077-91, **2011**.

4. Bitler B.G., Nicodemus J.P., Li H., Cai Q., Wu H., Hua X., Li T., Birrer M.J., Godwin A.K., Cairns P., **Zhang R.*** Wnt5a suppresses epithelial ovarian cancer by promoting cellular senescence. ***Cancer Res.*** 71:6184-94, **2011**.

5. Li H., Cai Q., Godwin A.K. and **Zhang R***. Enhancer of zeste homology 2 promotes the proliferation and invasion of human epithelial cells. ***Mol. Cancer Res.*** 8: 1610-1618, **2010**.

Abstracts:

An abstract based on this study has been published by American Association of Cancer Research.

An abstract based on this study has been published by the 3rd International Symposium on Ovarian Cancer

Small GTPases 3:3, 163-167; July/August/September 2012; © 2012 Landes Bioscience

RAS, cellular senescence and transformation

The BRCA1 DNA repair pathway at the crossroads

Zhigang Tu, Katherine M. Aird and Rugang Zhang[†,*]

Women's Cancer Program and Epigenetics and Progenitor Cell Keystone Program; Fox Chase Cancer Center; Philadelphia, PA USA

[†]Current affiliation: Gene Expression and Regulation Program; The Wistar Institute; Philadelphia, PA USA

The definition of an oncogene is a gene that actively promotes tumorigenesis. For example, activation of RAS oncogene promotes cell transformation and cancer. Paradoxically, in primary mammalian cells, oncogenic RAS typically triggers cellular senescence, a state of irreversible cell growth arrest. Oncogene-induced senescence is an important tumor suppression mechanism in vivo. Here, we discuss our recent evidence that RAS-induced suppression of DNA repair response via dissociation of BRCA1 from chromatin promotes senescence while predisposing cells to senescence bypass and transformation by allowing for secondary hits. The molecular mechanism we uncovered helps reconcile the tumor-promoting nature of oncogenic RAS with the tumor-suppressing role of oncogene-induced senescence.

Keywords: oncogene, RAS, cellular senescence, cell transformation, DNA damage, BRCA1, BRIP1, B-Myb

Abbreviations: PI3K, phosphatidylinositol-3-kinase; shB-Myb, short hairpins RNA to the human B-Myb gene; SA-β-gal, senescence-associated beta-galactosidase activity

Submitted: 02/08/12

Accepted: 03/02/12

http://dx.doi.org/10.4161/sgtp.19884

*Correspondence to: Rugang Zhang; Email: rzhang@wistar.org

Commentary to: Tu Z, Aird KM, Bitler BG, Nicodemus JP, Beeharry N, Xia B, et al. Oncogenic RAS regulates BRIP1 expression to induce dissociation of BRCA1 from chromatin, inhibit DNA repair, and promote senescence. Dev Cell 2011; 21:1077–91; PMID: 22137763.

Oncogenic mutations in the RAS gene are present in ~30% of human cancers.[1] Oncogenic RAS proteins promote cell transformation through the engagement of downstream pathways such as phosphatidylinositol-3-kinase (PI3K)/AKT and the RAF family of serine/threonine kinases such as BRAF.[2-4] Paradoxically, activation of the RAS oncogene in primary mammalian cells typically induces a status of irreversible cell growth arrest, known as cellular senescence.[5] By driving irreversible growth arrest of cancer progenitor cells harboring the initial oncogenic hit, oncogene-induced senescence is an important tumor suppression mechanism in vivo.[5] Further underscoring the importance of senescence in tumor suppression, reactivation of tumor suppressors such as p53 triggers cellular senescence and associated tumor regression due to activation of the innate immune response in mouse models.[6] Recently, the senescence-associated secretory phenotype has been proposed to be a cell non-autonomous mechanism by which senescent cells promote transformation of neighboring premalignant cells.[5,7] Here, we discuss our recent discovery of a novel cell-intrinsic mechanism by which oncogenic RAS drives cellular senescence while predisposing cells to secondary hits, which ultimately promotes senescence bypass in RAS-expressing primary human cells.[8]

Downstream effectors of RAS such as BRAF and AKT all possess the ability to induce senescence on their own in primary mammalian cells.[9,10] Likewise, inactivation of PTEN, a negative regulator of AKT, also triggers senescence in primary mammalian cells.[11] Notably, there are differences in the senescence induced by different oncogenes. For example, it has been demonstrated that the senescence induced by RAS or BRAF is associated with activation of the DNA damage response.[12] However, senescence induced by AKT or loss of PTEN is independent of the DNA damage response.[13,14] Accordingly, it has been proposed that DNA damage-independent senescence could be utilized as a novel mechanism for developing cancer therapeutics.[13,15] Aberrant DNA replication is thought to be the trigger of the DNA damage response during senescence induced by oncogenic RAS mutants.[12] Consistently, RAS-induced senescence is

dependent upon S phase progression, and inhibition of S phase progression by treating cells with Aphidicolin or contact inhibition blocks RAS-induced senescence.[13] In contrast, senescence induced by loss of PTEN is independent of S phase progression and can occur in quiescent cells.[13] Thus, the difference in DNA damage response observed in senescence induced by different oncogenes is likely due to their ability to trigger aberrant DNA replication.

Aberrant DNA replication induced by oncogenic RAS is transient and occurs only at the very early stages of senescence.[12] However, DNA damage accumulates in fully senescent cells days after aberrant DNA replication in primary human cells, which supposedly have intact DNA repair machinery.[12,14] This evidence suggests that the impairment of DNA repair might contribute to the accumulation of DNA damage during RAS-induced senescence. In support of this idea, we discovered that BRCA1 becomes dissociated from chromatin in RAS-infected primary human cells, and BRCA1-mediated DNA repair response is impaired in these cells.[8] This observation is unique in that other markers of DNA damage that have been reported in the literature, such as ATM, ATR, Chk1, Chk2, γH2A and 53BP1, are all activated during senescence induced by oncogenic RAS.[12,16] Importantly, BRCA1 chromatin dissociation occurs well before the RAS-induced cell cycle exit,[8] suggesting that this is not a consequence of the senescence-associated cell cycle exit. Moreover, senescence induced by AKT or loss of PTEN is not associated with BRCA1 chromatin dissociation, correlating with a lack in DNA damage response in these cells.[8] This observation further supports the hypothesis that BRCA1 chromatin dissociation is not merely a consequence of senescence. Additionally, BRCA1 chromatin dissociation displays the same kinetics as DNA damage accumulation, and suppression of BRCA1 chromatin dissociation is sufficient to inhibit DNA damage accumulation.[8] Further, BRCA1 knockdown triggers DNA damage and senescence in primary human cells.[8] Together, these findings further support the premise that BRCA1 chromatin dissociation contributes to the accumulation of DNA damage during RAS-induced senescence.

It is important to note that the levels of activated RAS oncogene determine the outcome of RAS expression. For example, in an inducible H-RAS^{G12V} transgenic mouse model, low levels of oncogenic RAS promote cell proliferation, while high levels of oncogenic RAS drive cell senescence.[17] Interestingly, tumorigenesis is associated with enrichment of high RAS induction, senescence and senescence bypass.[17] Notably, the levels of oncogenic H-RAS^{G12V} observed in T24, a human bladder cancer cell line, is sufficient to trigger BRCA1 chromatin dissociation in primary human cells.[8] This suggests that physiological level of RAS observed in human cancer cells is sufficient to trigger BRCA1 chromatin dissociation.

As stated previously, oncogene-induced BRCA1 chromatin dissociation well precedes the cell cycle exit during senescence. In addition, oncogenic RAS impairs BRCA1-mediated DNA repair response in cycling RAS-infected cells at a very early stage of senescence.[8] Together, a large time window is created for cells to accumulate secondary oncogenic hits prior to the senescence-associated cell cycle exit, which ultimately leads to senescence bypass in a minority of cells while the vast majority of cells eventually exit from the cell cycle and become senescent. Consistent with this model, RAS-expressing cells accumulate significantly greater DNA damage after IR treatment, and IR treatment promotes senescence bypass in RAS-infected cells.[8] In mouse models, activated oncogenes (such as RAS or BRAF) have been shown to initially induce senescence and formation of benign lesions. However, these lesions ultimately lead to the development of invasive cancer.[17-19] This is consistent with our model whereby oncogenic RAS induces senescence in the vast majority of cells while promoting senescence bypass in a minority of cells, which ultimately outgrow the majority of senescent cells and become transformed.

Interestingly, cells from BRCA1 exon 11 knockout mice display signs of cellular senescence.[20] Exon 11 of the mouse BRCA1 gene encodes for the two BRCT repeats of the BRCA1 protein. Recently, it has been demonstrated that BRCT repeats are essential for the tumor suppressive function of BRCA1.[21] Notably, we discovered that the C-terminus of BRCA1, which contains two BRCT repeats, is sufficient to be dissociated from chromatin in response to oncogenic RAS.[8] BRCT repeats of BRCA1 bind to phosphorylated partners such as BRIP1, Abbarax/RAP80 and CtIP to form three distinct complexes in a mutually exclusive manner.[22] These distinct complexes regulate activation of checkpoints in response to DNA damage.[22] We found that BRIP1, but not RAP80 or CtIP, is downregulated prior to BRCA1 chromatin dissociation. In addition, BRIP1 knockdown dissociates BRCA1 from chromatin, induces the DNA damage response and triggers cellular senescence. Conversely, ectopic BRIP1 suppresses BRCA1 chromatin dissociation, the DNA damage response and cellular senescence induced by oncogenic RAS.[8] Together, these findings suggest a key role of BRIP1 in regulating RAS-induced senescence.

BRIP1 was first described as a member of the DEAH helicase family that binds to the BRCT repeats of BRCA1.[23] The interaction between BRIP1 and BRCA1 depends upon the phosphorylation of BRIP1 at residue serine 990, which is regulated in a cell cycle-dependent manner.[24] The BRIP1-containing BRCA1 complex is implicated in regulating activation of S phase checkpoint.[25] For example, it has been demonstrated that BRIP1 is required for timely S phase progression.[25] In addition, BRIP1 and BRCA1 facilitate DNA replication during the S phase of the cell cycle by mediating the loading of CDC45L, the replication-licensing factor.[26] Thus, RAS-induced suppression of BRIP1 may promote senescence by driving aberrant DNA replication and activating S phase checkpoints during RAS-induced senescence.

The interaction between BRIP1 and BRCA1 suggests that BRIP1 might be linked to increased cancer risk. Indeed, it has been shown that germline mutations that alter its helicase function or disrupt its interaction with BRCA1 are associated with early-onset breast cancer.[27,28] Counter intuitively, the levels of BRIP1 are elevated in breast carcinoma, and higher levels of BRIP1 are associated with higher tumor

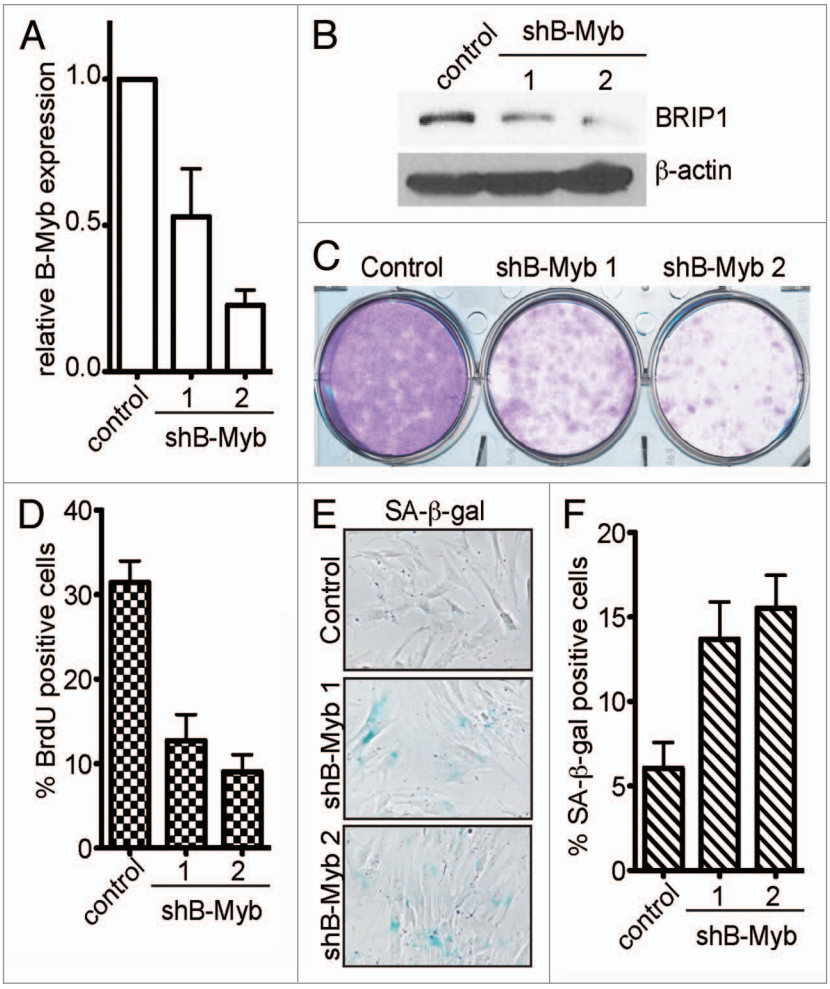

Figure 1. B-Myb knockdown suppresses the expression of BRIP1 and induces senescence. (A) IMR90 primary human fibroblasts were infected with lentivirus encoding two individual short hairpin RNAs to the human *B-Myb* gene (shB-Myb) or a control. The sense sequences for the shB-Myb are: 5'-GCT AAC AAC AAA GTT CCA CTT-3' and 5'-CCC AGA TCA GAA GTA CTC CAT-3'. Expression of B-Myb mRNA in the drug-selected cells was determined by qRT-PCR. (B) Same as (A), but examined for BRIP1 and β-actin expression by immunoblot. (C) Same as (A), but equal number of cells (1 x 10^4) were loaded in 6-well plates for 12 d and stained with 0.05% crystal violet for colony formation. (D) Same as (A), but labeled for 1 h with 10 μM BrdU, and the percentage of the BrdU positive cells was quantified by immunofluorescence staining. (E) Same as (A), but stained for SA-β-gal activity, a marker of cellular senescence. (F) Quantitation of (D). 100 cells from each of the indicated groups were examined for SA-β-gal activity. Mean of three independent experiments with SD.

grade.[29] In addition, high levels of BRIP1 positively correlate with HER2 status and expression of Ki67, a marker of cell proliferation.[29] It has been demonstrated that HER2 overexpression drives senescence in primary human mammary epithelial cells.[30] Thus, overexpression of BRIP1 may contribute to breast cancer by promoting proliferation of mammary epithelial cells through suppressing senescence induced by HER2 overexpression.

As discussed above, IR-treatment in RAS-infected cells promotes senescence bypass.[8] In IR-treatment-induced senescence bypassed cells, we show that BRIP1 remains downregulated and BRCA1 remains dissociated from chromatin.[8] This is likely due to selection pressure imposed by exogenous DNA damage treatment. In addition, we observed the accumulation of DNA damage in these senescence-bypassed cells compared with controls.[8] This suggests that DNA repair remains impaired in these RAS-expressing senescence-bypassed cells induced by IR-treatment. Consistently, it has previously been demonstrated that the DNA damage response is attenuated in RAS-expressing transformed cells.[31]

Interestingly, we observed rare colonies that bypassed RAS-induced senescence after extended culture without exogenous DNA damage treatment.[8] The formation of these colonies may reflect the rare senescence-bypassed cells that are associated with endogenous DNA damage triggered by oncogenic RAS. Thus, it will be interesting to examine the levels of BRIP1 expression and chromatin-associated BRCA1 levels in these cells. Because restoration of BRIP1 expression and suppression of BRCA1 chromatin dissociation inhibits RAS-induced senescence,[8] it is plausible that the senescence bypass observed in these rare colonies is due to restoration of BRIP1 expression and, consequently, rescuing BRCA1 chromatin dissociation. Our model would predict

that these senescence-bypassed cells with restored BRIP1 expression and chromatin-associated BRCA1 levels would be independent of the DNA damage response. Likewise, it will be interesting to determine the levels of DNA damage in HER2 positive breast carcinoma specimens with elevated levels of BRIP1.[29]

RAS-induced BRIP1 downregulation that triggers BRCA1 chromatin dissociation was due to suppression of B-Myb expression,[8] a known regulator of RAS-induced senescence. For example, ectopic B-Myb suppresses senescence of primary mouse embryonic fibroblasts induced by oncogenic RAS.[32] Similar to BRIP1, B-Myb expression is required for S phase entry and acts as a crucial factor for DNA replication during S phase.[33] Depletion of B-Myb triggers aberrant DNA replication and the DNA damage response.[33] Given its role in S phase entry and progression, it is not surprising that gene amplification or overexpression of B-Myb occurs in several types of cancer.[34,35]

B-Myb directly regulates BRIP1 by binding to the proximal promoter region of the human BRIP1 gene.[8] However, it remains to be determined whether B-Myb downregualtion is sufficient to induce BRCA1 downregulation and senescence. To address this question, we developed two individual short hairpins RNA to the human *B-Myb* gene (shB-Myb). The efficacy of B-Myb knockdown by the shB-Mybs was confirmed by qRT-PCR (**Fig. 1A**). Indeed, BRIP1 expression was downregulated in B-Myb knockdown cells (**Fig. 1B**). Further, B-Myb knockdown suppressed the proliferation of primary human fibroblasts as determined by decreased colony formation and BrdU incorporation (**Fig. 1C and D**). Consistent with the idea that growth inhibition induced by B-Myb knockdown is due to senescence, expression of SA-β-gal, a marker of cellular senescence,[36] was induced in B-Myb knockdown cells (**Fig. 1E and F**). Together, these data further support that premise that B-Myb is a key regulator of BRIP1 during senescence.

In summary, a very early stage of RAS-induced cellular senescence involves suppression of BRIP1 expression to dissociate BRCA1 from chromatin and thereby impair the BRCA1-mediated DNA repair. This promotes cellular senescence and senescence-associated accumulation of DNA damage while also allowing for subsequent secondary hits that may predispose rare clones of cells to escape senescence and ultimately contribute to cell transformation. Therefore, this newly discovered cell-intrinsic pathway reconciles the tumor-promoting nature of oncogenic RAS with the tumor-suppressing role of RAS-induced senescence.

Acknowledgments

R.Z. is an Ovarian Cancer Research Fund (OCRF) Liz Tilberis Scholar. This work was supported in part by an NCI FCCC-UPenn ovarian cancer SPORE (P50 CA083638) pilot project and SPORE career development award (to R.Z.), a DOD ovarian cancer academy award (OC093420 to R.Z.), a NIH/NCI grant (R01CA160331 to R.Z.), and an OCRF program project (to R.Z.).

References

1. Bos JL. ras oncogenes in human cancer: a review. Cancer Res 1989; 49:4682-9; PMID:2547513.
2. Rodriguez-Viciana P, Warne PH, Dhand R, Vanhaesebroeck B, Gout I, Fry MJ, et al. Phosphatidylinositol-3-OH kinase as a direct target of Ras. Nature 1994; 370:527-32; PMID:8052307; http://dx.doi.org/10.1038/370527a0.
3. Warne PH, Viciana PR, Downward J. Direct interaction of Ras and the amino-terminal region of Raf-1 in vitro. Nature 1993; 364:352-5; PMID:8332195; http://dx.doi.org/10.1038/364352a0.
4. Han M, Golden A, Han Y, Sternberg PW. *C. elegans* lin-45 raf gene participates in let-60 ras-stimulated vulval differentiation. Nature 1993; 363:133-40; PMID:8483497; http://dx.doi.org/10.1038/363133a0.
5. Campisi J. Senescent cells, tumor suppression and organismal aging: good citizens, bad neighbors. Cell 2005; 120:513-22; PMID:15734683; http://dx.doi.org/10.1016/j.cell.2005.02.003.
6. Xue W, Zender L, Miething C, Dickins RA, Hernando E, Krizhanovsky V, et al. Senescence and tumour clearance is triggered by p53 restoration in murine liver carcinomas. Nature 2007; 445:656-60; PMID:17251933; http://dx.doi.org/10.1038/nature05529.
7. Campisi J, d'Adda di Fagagna F. Cellular senescence: when bad things happen to good cells. Nat Rev Mol Cell Biol 2007; 8:729-40; PMID:17667954; http://dx.doi.org/10.1038/nrm2233.
8. Tu Z, Aird KM, Bitler BG, Nicodemus JP, Beeharry N, Xia B, et al. Oncogenic RAS regulates BRIP1 expression to induce dissociation of BRCA1 from chromatin, inhibit DNA repair and promote senescence. Dev Cell 2011; 21:1077-91; PMID:22137763; http://dx.doi.org/10.1016/j.devcel.2011.10.010.
9. Michaloglou C, Vredeveld LC, Soengas MS, Denoyelle C, Kuilman T, van der Horst CM, et al. BRAFE600-associated senescence-like cell cycle arrest of human naevi. Nature 2005; 436:720-4; PMID:16079850; http://dx.doi.org/10.1038/nature03890.
10. Krizhanovsky V, Xue W, Zender L, Yon M, Hernando E, Lowe SW. Implications of cellular senescence in tissue damage response, tumor suppression and stem cell biology. Cold Spring Harb Symp Quant Biol 2008; 73:513-22; PMID:19150958; http://dx.doi.org/10.1101/sqb.2008.73.048.
11. Chen Z, Trotman LC, Shaffer D, Lin HK, Dotan ZA, Niki M, et al. Crucial role of p53-dependent cellular senescence in suppression of Pten-deficient tumorigenesis. Nature 2005; 436:725-30; PMID:16079851; http://dx.doi.org/10.1038/nature03918.
12. Di Micco R, Fumagalli M, Cicalese A, Piccinin S, Gasparini P, Luise C, et al. Oncogene-induced senescence is a DNA damage response triggered by DNA hyper-replication. Nature 2006; 444:638-42; PMID:17136094; http://dx.doi.org/10.1038/nature05327.
13. Alimonti A, Nardella C, Chen Z, Clohessy JG, Carracedo A, Trotman LC, et al. A novel type of cellular senescence that can be enhanced in mouse models and human tumor xenografts to suppress prostate tumorigenesis. J Clin Invest 2010; 120:681-93; PMID:20197621; http://dx.doi.org/10.1172/JCI40535.
14. Kennedy AL, Morton JP, Manoharan I, Nelson DM, Jamieson NB, Pawlikowski JS, et al. Activation of the PIK3CA/AKT pathway suppresses senescence induced by an activated RAS oncogene to promote tumorigenesis. Mol Cell 2011; 42:36-49; PMID:21474066; http://dx.doi.org/10.1016/j.molcel.2011.02.020.
15. Nardella C, Clohessy JG, Alimonti A, Pandolfi PP. Pro-senescence therapy for cancer treatment. Nat Rev Cancer 2011; 11:503-11; PMID:21701512; http://dx.doi.org/10.1038/nrc3057.
16. Di Micco R, Sulli G, Dobreva M, Liontos M, Botrugno OA, Gargiulo G, et al. Interplay between oncogene-induced DNA damage response and heterochromatin in senescence and cancer. Nat Cell Biol 2011; 13:292-302; PMID:21336312; http://dx.doi.org/10.1038/ncb2170.
17. Sarkisian CJ, Keister BA, Stairs DB, Boxer RB, Moody SE, Chodosh LA. Dose-dependent oncogene-induced senescence in vivo and its evasion during mammary tumorigenesis. Nat Cell Biol 2007; 9:493-505; PMID:17450133; http://dx.doi.org/10.1038/ncb1567.
18. Dankort D, Filenova E, Collado M, Serrano M, Jones K, McMahon M. A new mouse model to explore the initiation, progression and therapy of $BRAF_{V600E}$-induced lung tumors. Genes Dev 2007; 21:379-84; PMID:17299132; http://dx.doi.org/10.1101/gad.1516407.
19. Dhomen N, Reis-Filho JS, da Rocha Dias S, Hayward R, Savage K, Delmas V, et al. Oncogenic Braf induces melanocyte senescence and melanoma in mice. Cancer Cell 2009; 15:294-303; PMID:19345328; http://dx.doi.org/10.1016/j.ccr.2009.02.022.
20. Cao L, Li W, Kim S, Brodie SG, Deng CX. Senescence, aging and malignant transformation mediated by p53 in mice lacking the Brca1 full-length isoform. Genes Dev 2003; 17:201-13; PMID:12533509; http://dx.doi.org/10.1101/gad.1050003.
21. Shakya R, Reid LJ, Reczek CR, Cole F, Egli D, Lin CS, et al. BRCA1 tumor suppression depends on BRCT phosphoprotein binding, but not its E3 ligase activity. Science 2011; 334:525-8; PMID:22034435; http://dx.doi.org/10.1126/science.1209909.
22. Huen MS, Sy SM, Chen J. BRCA1 and its toolbox for the maintenance of genome integrity. Nat Rev Mol Cell Biol 2010; 11:138-48; PMID:20029420; http://dx.doi.org/10.1038/nrm2831.
23. Cantor SB, Bell DW, Ganesan S, Kass EM, Drapkin R, Grossman S, et al. BACH1, a novel helicase-like protein, interacts directly with BRCA1 and contributes to its DNA repair function. Cell 2001; 105:149-60; PMID:11301010; http://dx.doi.org/10.1016/S0092-8674(01)00304-X.

24. Yu X, Chini CC, He M, Mer G, Chen J. The BRCT domain is a phospho-protein binding domain. Science 2003; 302:639-42; PMID:14576433; http://dx.doi.org/10.1126/science.1088753.
25. Kumaraswamy E, Shiekhattar R. Activation of BRCA1/BRCA2-associated helicase BACH1 is required for timely progression through S phase. Mol Cell Biol 2007; 27:6733-41; PMID:17664283; http://dx.doi.org/10.1128/MCB.00961-07.
26. Greenberg RA, Sobhian B, Pathania S, Cantor SB, Nakatani Y, Livingston DM. Multifactorial contributions to an acute DNA damage response by BRCA1/BARD1-containing complexes. Genes Dev 2006; 20:34-46; PMID:16391231; http://dx.doi.org/10.1101/gad.1381306.
27. Cantor S, Drapkin R, Zhang F, Lin Y, Han J, Pamidi S, et al. The BRCA1-associated protein BACH1 is a DNA helicase targeted by clinically relevant inactivating mutations. Proc Natl Acad Sci USA 2004; 101:2357-62; PMID:14983014; http://dx.doi.org/10.1073/pnas.0308717101.
28. De Nicolo A, Tancredi M, Lombardi G, Flemma CC, Barbuti S, Di Cristofano C, et al. A novel breast cancer-associated BRIP1 (FANCJ/BACH1) germ-line mutation impairs protein stability and function. Clin Cancer Res 2008; 14:4672-80; PMID:18628483; http://dx.doi.org/10.1158/1078-0432.CCR-08-0087.
29. Eelen G, Vanden Bempt I, Verlinden L, Drijkoningen M, Smeets A, Neven P, et al. Expression of the BRCA1-interacting protein Brip1/BACH1/FANCJ is driven by E2F and correlates with human breast cancer malignancy. Oncogene 2008; 27:4233-41; PMID:18345034; http://dx.doi.org/10.1038/onc.2008.51.
30. Ansieau S, Bastid J, Doreau A, Morel AP, Bouchet BP, Thomas C, et al. Induction of EMT by twist proteins as a collateral effect of tumor-promoting inactivation of premature senescence. Cancer Cell 2008; 14:79-89; PMID:18598946; http://dx.doi.org/10.1016/j.ccr.2008.06.005.
31. Abulaiti A, Fikaris AJ, Tsygankova OM, Meinkoth JL. Ras induces chromosome instability and abrogation of the DNA damage response. Cancer Res 2006; 66:10505-12; PMID:17079472; http://dx.doi.org/10.1158/0008-5472.CAN-06-2351.
32. Masselink H, Vastenhouw N, Bernards R. B-myb rescues ras-induced premature senescence, which requires its transactivation domain. Cancer Lett 2001; 171:87-101; PMID:11485831; http://dx.doi.org/10.1016/S0304-3835(01)00631-0.
33. Lorvellec M, Dumon S, Maya-Mendoza A, Jackson D, Frampton J, García P. B-Myb is critical for proper DNA duplication during an unperturbed S phase in mouse embryonic stem cells. Stem Cells 2010; 28:1751-9; PMID:20715180; http://dx.doi.org/10.1002/stem.496.
34. Bar-Shira A, Pinthus JH, Rozovsky U, Goldstein M, Sellers WR, Yaron Y, et al. Multiple genes in human 20q13 chromosomal region are involved in an advanced prostate cancer xenograft. Cancer Res 2002; 62:6803-7; PMID:12460888.
35. Thorner AR, Hoadley KA, Parker JS, Winkel S, Millikan RC, Perou CM. In vitro and in vivo analysis of B-Myb in basal-like breast cancer. Oncogene 2009; 28:742-51; PMID:19043454; http://dx.doi.org/10.1038/onc.2008.430.
36. Dimri GP, Lee X, Basile G, Acosta M, Scott G, Roskelley C, et al. A biomarker that identifies senescent human cells in culture and in aging skin in vivo. Proc Natl Acad Sci USA 1995; 92:9363-7; PMID:7568133; http://dx.doi.org/10.1073/pnas.92.20.9363.

Developmental Cell
Article

Oncogenic Ras Regulates BRIP1 Expression to Induce Dissociation of BRCA1 from Chromatin, Inhibit DNA Repair, and Promote Senescence

Zhigang Tu,[1] Katherine M. Aird,[1] Benjamin G. Bitler,[1] Jasmine P. Nicodemus,[1] Neil Beeharry,[2] Bing Xia,[3] Tim J. Yen,[2] and Rugang Zhang[1,2,*]
[1]Women's Cancer Program
[2]Epigenetics and Progenitor Cells Keystone Program
Fox Chase Cancer Center, 333 Cottman Avenue, Philadelphia, PA 19111, USA
[3]The Cancer Institute of New Jersey, University of Medicine & Dentistry of New Jersey, Robert Wood Johnson Medical School, New Brunswick, NJ 08901, USA
*Correspondence: rugang.zhang@fccc.edu
DOI 10.1016/j.devcel.2011.10.010

SUMMARY

Here, we report a cell-intrinsic mechanism by which oncogenic RAS promotes senescence while predisposing cells to senescence bypass by allowing for secondary hits. We show that oncogenic RAS inactivates the BRCA1 DNA repair complex by dissociating BRCA1 from chromatin. This event precedes senescence-associated cell cycle exit and coincides with the accumulation of DNA damage. Downregulation of BRIP1, a physiological partner of BRCA1 in the DNA repair pathway, triggers BRCA1 chromatin dissociation. Conversely, ectopic BRIP1 rescues BRCA1 chromatin dissociation and suppresses RAS-induced senescence and the DNA damage response. Significantly, cells undergoing senescence do not exhibit a BRCA1-dependent DNA repair response when exposed to DNA damage. Overall, our study provides a molecular basis by which oncogenic RAS promotes senescence. Because DNA damage has the potential to produce additional "hits" that promote senescence bypass, our findings may also suggest one way a small minority of cells might bypass senescence and contribute to cancer development.

INTRODUCTION

Activation of oncogenes (such as RAS) in primary mammalian cells typically triggers a cascade of molecular and cellular events, which ultimately culminates in a state of irreversible cell growth arrest (Campisi, 2005). This process is termed oncogene-induced senescence and is an important tumor suppression mechanism in vivo (Campisi, 2005). Paradoxically, the definition of an oncogene is a gene that actively promotes tumorigenesis. The mechanism underlying this paradox remains poorly understood.

Senescent cells display several hallmark morphological and molecular characteristics. These cells are positive for senescence-associated β-galactosidase (SA-β-gal) activity (Dimri et al., 1995). In addition, chromatin in the nuclei of senescent human cells often reorganizes to form specialized domains of facultative heterochromatin called senescence-associated heterochromatin foci (SAHF) (Braig et al., 2005; Narita et al., 2003, 2006; Zhang et al., 2005, 2007a). SAHF contain markers of heterochromatin, including di- and tri-methylated lysine 9 histone H3 (H3K9Me2/H3K9Me3), histone H2A variant mH2A, and HMGA (Narita et al., 2003, 2006; Zhang et al., 2005). SAHF formation contributes to senescence-induced cell cycle exit by directly sequestering and silencing proliferation-promoting genes (Narita et al., 2003; Zhang et al., 2007a).

Oncogene-induced senescence is often characterized by the accumulation of DNA damage; in particular, DNA double-strand breaks (DSBs) (Bartkova et al., 2006; Di Micco et al., 2006). For example, oncogenic RAS mutants induce DNA damage by triggering aberrant DNA replication (Di Micco et al., 2006). However, it remains to be determined whether impaired DNA repair contributes to the accumulation of DNA damage observed during oncogene-induced senescence.

BRCA1 plays an important role in DNA DSB repair (Scully and Livingston, 2000). Germline mutations in the *BRCA1* gene predispose women to breast and ovarian cancer (Scully and Livingston, 2000), and inactivation of BRCA1 contributes to cancer development by causing genomic instability (Turner et al., 2004). BRCA1 interacts with various DNA damage repair proteins through its two C terminus BRCA1 C-terminal (BRCT) repeats. The BRCT repeats of BRCA1 recognize cognate partners by binding to their phosphoserine residues (Manke et al., 2003; Yu et al., 2003), and their binding partners include BRCA1-interacting protein 1 (BRIP1), CtIP, and RAP80/Abraxas (Wang et al., 2007; Yu et al., 1998, 2003). In addition, BRCA1 interacts with partner and localizer of BRCA2 (PALB2), which is necessary for localization of BRCA2 to DNA DSBs (Xia et al., 2006). Functional BRCA1 is required for localizing/sustaining PALB2 at sites of DNA DSBs and error-free homologous recombination repair (Livingston, 2009; Sy et al., 2009; Zhang et al., 2009). A role for BRCA1 in senescence is implied by findings from the *BRCA1* exon 11 knockout mouse whose cells exhibit

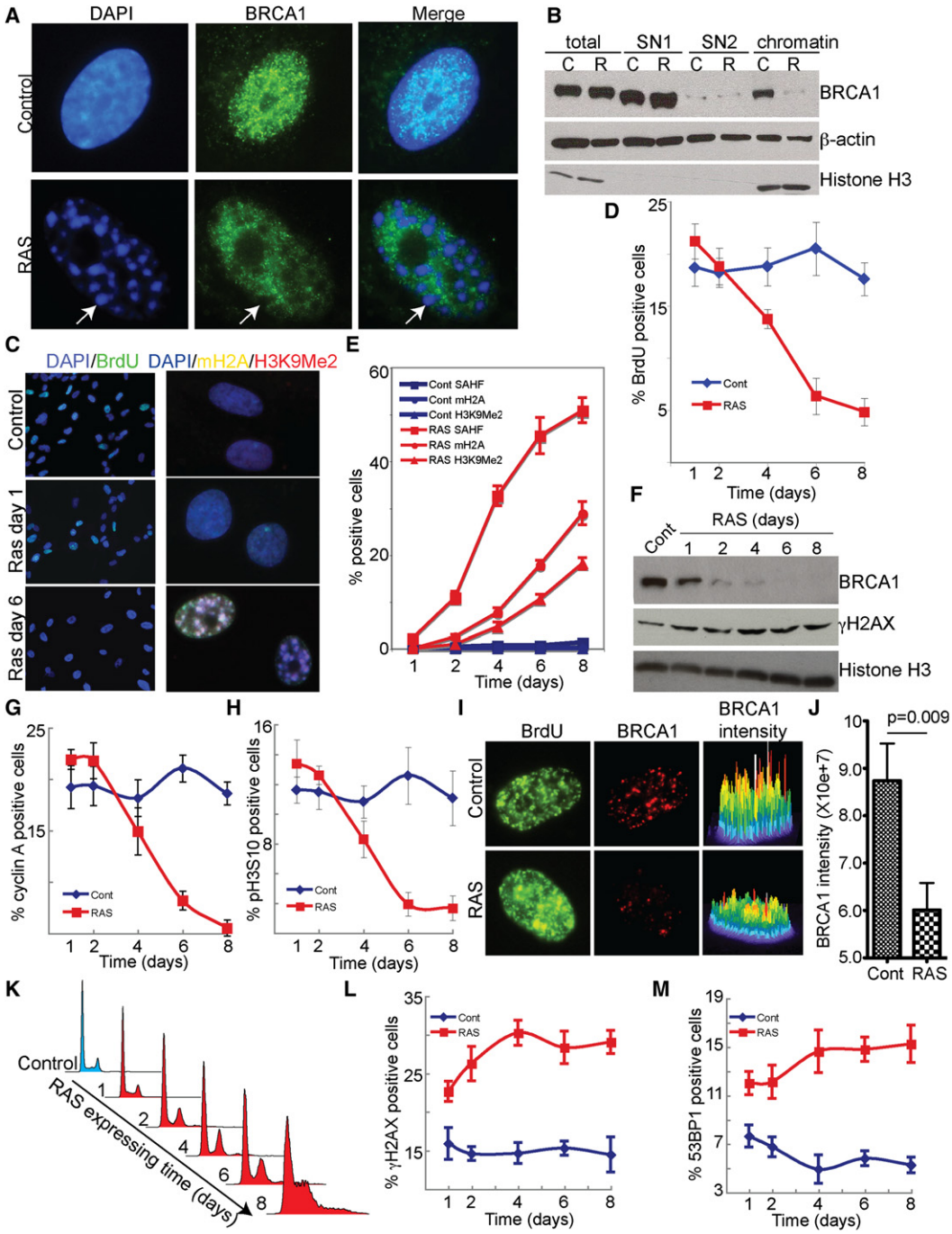

Figure 1. Oncogene-Induced Dissociation of BRCA1 from Chromatin Occurs prior to the Oncogene-Induced Cell Cycle Exit and Coincides with the Accumulation of DNA Damage during Senescence

(A) IMR90 cells were infected with retrovirus-encoding control or oncogenic RAS to induce senescence. Drug-selected cells were stained with DAPI to visualize SAHF and an anti-BRCA1 antibody at day 5. Arrows point to an example of BRCA1-excluded SAHF in senescent IMR90 cells.

(B) Same as (A) but examined for expression of BRCA1, β-actin, and histone H3 in soluble (cytoplasmic soluble fraction SN1 and nuclear soluble fraction SN2) and chromatin fractions of control (C) or RAS (R)-infected IMR90 cells by western blot. Note that equal amounts of total proteins were loaded for total cell lysates, SN1, SN2, and chromatin fractions.

(C) Same as (A). At days 1 and 6, control and RAS-infected cells were labeled with BrdU for 1 hr (left) or stained with DAPI to visualize SAHF and antibodies against mH2A and H3K9Me2 that form foci that colocalize with SAHF in senescent human cells (right).

(D and E) Time course of BrdU labeling (D) and formation of SAHF, mH2A, and H3K9Me2 foci (E) in control and RAS-infected IMR90 cells. Mean of three independent experiments with SD.

(F) Same as (D) but examined for expression of BRCA1, γH2AX, and histone H3 in the chromatin fractions of control and RAS-infected cells at the indicated time points by western blot.

signs of senescence (Cao et al., 2003). These observations suggest that senescence and tumorigenesis pathways may converge on BRCA1-associated DNA damage responses.

Here, we report a cell-intrinsic mechanism by which oncogenic RAS promotes senescence but at the same time predisposes cells to secondary hits, which ultimately leads to senescence bypass.

RESULTS

BRCA1 Becomes Dissociated from Chromatin during Oncogenic RAS-Induced Senescence

Senescent cells are characterized by the accumulation of DNA DSBs (Bartkova et al., 2006; Di Micco et al., 2006; Halazonetis et al., 2008), and one of the critical players in DSB repair is BRCA1 (Scully and Livingston, 2000). To test the hypothesis that changes in BRCA1 function occur during oncogene-induced senescence, we first examined changes in the subcellular distribution of BRCA1 during RAS-induced senescence of IMR90 primary human fibroblasts (see Figure S1A available online). BRCA1 immunofluorescence (IF) staining was performed in proliferating (control) and senescent IMR90 primary human fibroblasts induced by RAS. Notably, BRCA1 was excluded from SAHF in senescent cells (Figure 1A). In addition, similar results were obtained using multiple anti-BRCA1 antibodies (one rabbit polyclonal and two individual mouse monoclonal antibodies) (data not shown). We next fractionated protein from proliferating (control) and senescent IMR90 cells into soluble and chromatin fractions (Méndez and Stillman, 2000; Narita et al., 2006) and tested each for the presence of BRCA1. Compared with control cells, BRCA1 levels were dramatically decreased in the chromatin fractions of senescent IMR90 cells (Figure 1B; Figure S1B).

We next sought to exclude the possibility that BRCA1 chromatin dissociation was caused by supra-physiological levels of RAS. To do so, we titrated RAS expression in IMR90 cells to levels lower than those in the classic bladder cancer cell line T24 that harbors an oncogenic RAS mutation (H-RAS^{G12V}, the same RAS mutant used in the current study) (Hurlin et al., 1989) (Figure S1C). Importantly, we observed a decrease in BRCA1 levels in the chromatin fractions of RAS-infected IMR90 cells with lower RAS expression than the T24 cells (Figure S1C). Interestingly, BRCA1 levels in the chromatin fractions of T24 cells were also notably lower when compared to IMR90 cells, albeit similar levels of total BRCA1 levels were observed (Figure S1C). Together, our data show that the physiological levels of oncogenic RAS observed in cancerous cells are sufficient to dissociate BRCA1 from chromatin in primary cells.

Next, we asked whether BRCA1 chromatin dissociation is unique to IMR90 cells induced to senesce by RAS. To answer this question, primary WI38 and BJ human fibroblasts, which both senesce after oncogenic RAS is expressed (Ye et al., 2007; Zhang et al., 2005) (data not shown), were infected with control or RAS-encoding retrovirus. Compared with controls, BRCA1 levels were dramatically decreased in the chromatin fractions of RAS-infected WI38 and BJ cells (Figure S1D). Taken together, these data demonstrate that BRCA1 becomes dissociated from chromatin during RAS-induced senescence.

BRCA1 Chromatin Dissociation Precedes the Cell Cycle Exit during RAS-Induced Senescence

We next sought to determine whether BRCA1 chromatin dissociation occurs early or late during RAS-induced senescence. Toward this goal, we conducted a detailed time course analysis of chromatin-associated BRCA1, senescence-associated cell cycle exit (determined by BrdU incorporation or expression of cyclin A or serine 10 phosphorylated histone H3 [pH3S10]), and other markers of senescence (such as formation of SAHF, mH2A foci, and H3K9Me2 foci) in control and RAS-infected IMR90 cells (Figures 1C–1H). Strikingly, as early as day 1 (Figure S1A), BRCA1 was largely dissociated from chromatin (Figure 1F; Figure S1K), which is well before the senescence-associated cell cycle exit and accumulation of markers of senescence (Figures 1C–1H).

BRCA1 forms discrete nuclear foci during the S/G2 phases of the cell cycle in normal cycling cells (Durant and Nickoloff, 2005; Scully et al., 1997a; Xu et al., 2001). Therefore, we sought to determine whether RAS expression impairs BRCA1 foci formation in cycling cells. Toward this goal, at day 2, control and RAS-infected IMR90 cells were labeled with BrdU to identify S phase cells. We next pre-extracted soluble proteins from control and RAS-infected cells and stained these cells with antibodies against BRCA1 and BrdU. Indeed, the intensity of BRCA1 foci in BrdU-positive cells was significantly weaker in RAS-infected IMR90 cells compared with controls ($p = 0.009$) (Figures 1I and 1J). This is not simply a consequence of DNA damage because this did not occur in ionizing radiation (IR)-treated cells (Figures S1E and S1F). Furthermore, control and RAS-infected IMR90 cells were stained with antibodies against BRCA1 and cyclin A, a marker of the S/G2 phases of the cell cycle (Erlandsson et al., 2000; Sartori et al., 2007). Consistently, BRCA1 foci were either negative or notably weaker in cyclin A-positive RAS-infected cells compared with controls (Figures S1G and S1H). Finally, FACS analysis revealed that RAS-infected cells accumulated at the S and G2/M phases of the cell cycle compared with controls at this stage (day 2) (Figure 1K; Figures S1I and S1J). From these results, we conclude that oncogene-induced dissociation of BRCA1 from chromatin precedes the oncogene-induced cell cycle exit during senescence.

(G and H) Same as (D) but stained for cyclin A expression (using a mouse anti-cyclin A antibody) (G) or pH3S10 (H) by IF at the indicated time points.
(I and J) At day 2, control and RAS-infected cells were labeled with BrdU for 1 hr, and soluble proteins were pre-extracted (see Experimental Procedures for details). Pre-extracted cells were stained with antibodies against BRCA1 and BrdU. The intensity of BRCA1 staining in BrdU-positive control and RAS-infected cells was quantified using MetaMorph software (J) (n = 30).
(K) Same as (D) but examined for cell cycle distribution by flow cytometry.
(L and M) Same as (D) but examined for expression of γH2AX (L) or 53BP1 (M) expression by IF staining. A total of 200 cells from each of the indicated groups were examined for formation of γH2AX or 53BP1 foci. Mean of three independent experiments with SD.
See also Figure S1.

BRCA1 Chromatin Dissociation Coincides with the Accumulation of DNA Damage

We next asked whether BRCA1 chromatin dissociation plays a role in the DNA damage accumulation observed during RAS-induced senescence. Strikingly, accumulation of markers of DNA damage, including formation of γH2AX and 53BP1 foci, accumulation of γH2AX in chromatin fractions, and upregulation of p53 displayed the identical kinetics as dissociation of BRCA1 from chromatin in RAS-infected IMR90 cells (Figures 1F, 1L, 1M; Figures S1K–S1O). For example, as early as day 1, γH2AX had already accumulated in chromatin fractions (Figure 1F; Figure S1K), γH2AX and 53BP1 foci were increased, and the p53 expression levels were upregulated in RAS-infected IMR90 cells compared with controls (Figures 1L and 1M; Figures S1L–S1O). We conclude that RAS expression results in concomitant BRCA1 chromatin dissociation and DNA damage accumulation.

To determine whether BRCA1 chromatin dissociation is a RAS-specific effect, IMR90 cells were infected with control, RAS, BRAF, or myristylated AKT1 (myr-AKT1)-encoding retrovirus. Ectopic expression of RAS, BRAF, and myr-AKT1 was confirmed by western blot (data not shown). Notably, expression of RAS, BRAF, and myr-AKT1 all induced expression of markers of senescence in IMR90 cells (Figure S2A) (Krizhanovsky et al., 2008; Michaloglou et al., 2005; Xue et al., 2007; Zhang et al., 2005). Next, we examined BRCA1 protein levels in total cell lysates and chromatin fractions of control, RAS, BRAF, and myr-AKT1-infected IMR90 cells by western blot. Strikingly, compared with controls, BRCA1 levels decreased dramatically in the chromatin fractions of RAS and BRAF-infected IMR90 cells, but not in myr-AKT1-infected IMR90 cells (Figure 2A). These results suggest that BRCA1 chromatin dissociation is dependent upon specific oncogenic pathways and is not simply a consequence of senescence.

We next sought to determine whether BRCA1 chromatin dissociation coincides with DNA damage accumulation or is associated with SAHF formation. Toward this goal, control, RAS, BRAF, and myr-AKT1-infected IMR90 cells were stained with DAPI to visualize SAHF and with an antibody to mH2A, which is a component of SAHF (Zhang et al., 2005). Both RAS and BRAF, but not myr-AKT1, induced formation of SAHF and mH2A foci (Figure 2B). Additionally, compared with controls, both RAS and BRAF expression induced formation of γH2AX and 53BP1 foci and increased levels of chromatin-associated γH2AX and 53BP1 (Figures 2C–2E). In contrast, myr-AKT1, which did not induce BRCA1 chromatin dissociation, failed to induce formation of γH2AX and 53BP1 foci or increase the levels of chromatin-associated γH2AX and 53BP1 (Figures 2C–2E). Consistently, it has been recently reported that cell senescence induced by myr-AKT1 is not associated with SAHF formation or the DNA damage response (Kennedy et al., 2011). Similarly, PTEN knockdown induced expression of markers of senescence but had no effects on BRCA1 chromatin association and also failed to trigger formation of γH2AX foci or SAHF (Figures S2B–S2G). Likewise, it has been previously shown that senescence induced by loss of PTEN is not associated with the accumulation of DNA damage (Alimonti et al., 2010). The lack of both DNA damage and BRCA1 chromatin dissociation in the PTEN knockdown cells is consistent with the idea that BRCA1 chromatin dissociation contributes to DNA damage accumulation.

We next directly measured the extent of DNA damage in control, RAS, BRAF, and myr-AKT1-infected IMR90 cells using the comet assay. Compared with controls, there was a significant increase in DNA damage in RAS and BRAF-infected IMR90 cells ($p < 0.05$), whereas the difference between control and myr-AKT1-infected IMR90 cells was not significant ($p > 0.05$) (Figures 2F and 2G). The combined data suggest that dissociation of BRCA1 from chromatin coincides with DNA damage accumulation, correlates with SAHF formation, and is independent of PI3K/AKT signaling.

BRCA1 Knockdown Induces Senescence

We next sought to test whether BRCA1 knockdown is sufficient to drive SAHF formation and senescence in IMR90 cells. Toward this goal, three individual short hairpin RNA to the human *BRCA1* (shBRCA1) genes with different degrees of BRCA1 knockdown efficacy were utilized. BRCA1 knockdown efficiency was confirmed by IF staining and western blot (Figures 3A and 3B). Two individual shBRCA1s (#2 and #3), which efficiently knocked down BRCA1, induced SAHF formation and expression of SA-β-gal activity (Figures 3C–3F). Notably, an shBRCA1 (#1) that knocked down BRCA1 with ~40% efficacy at the total protein level had no effect on SAHF formation or expression of SA-β-gal activity (Figures 3A–3F). Interestingly, similar to the hyperproliferation observed in RAS-infected IMR90 cells prior to cell cycle exit (e.g., Figures 1G and 1H; Figure S5) (Di Micco et al., 2006), knockdown of BRCA1 in IMR90 cells also triggers a minor but statistically significant hyperproliferation prior to the cell cycle exit as demonstrated by increased BrdU incorporation (Figure S3A). Consistent with a previous report (Krum et al., 2010), we observed an increase in expression of γH2AX as well as formation of γH2AX foci following BRCA1 knockdown (Figures S3B and S3C). We conclude that knockdown of BRCA1 is sufficient to drive senescence.

Downregulation of BRIP1 Expression Triggers BRCA1 Chromatin Dissociation

Next, we investigated the molecular mechanism underlying BRCA1 chromatin dissociation. Notably, a fragment of the C terminus of BRCA1 (aa 1314–1863) containing two BRCT repeats was sufficient to be dissociated from chromatin in IMR90 cells infected with RAS (Figure S4A), suggesting that factors that interact with the BRCT repeats of BRCA1 may trigger BRCA1 chromatin dissociation.

BRCT repeats of BRCA1 bind to BRIP1, CtIP, and RAP80/Abraxas (Wang et al., 2007; Yu et al., 1998, 2003). Compared with controls, BRIP1 levels in both total cell lysates and the chromatin fractions of RAS-infected cells were dramatically decreased (Figures 4A and 4B; Figure S4B). In contrast, expression levels of CtIP and RAP80 did not overtly change in RAS-infected cells at the same time (Figure 4A). Notably, RAS-induced downregulation of BRIP1 occurred prior to the cell cycle exit, as reflected by the kinetics of cyclin A and pH3S10 expression (Figure 4B). Together, these results suggest that downregulation of BRIP1 may trigger BRCA1 chromatin dissociation in RAS-infected cells.

BRIP1 was first identified as a BRCA1 physiological binding partner (Cantor et al., 2001). We next sought to determine whether BRIP1 is downregulated at the mRNA level in

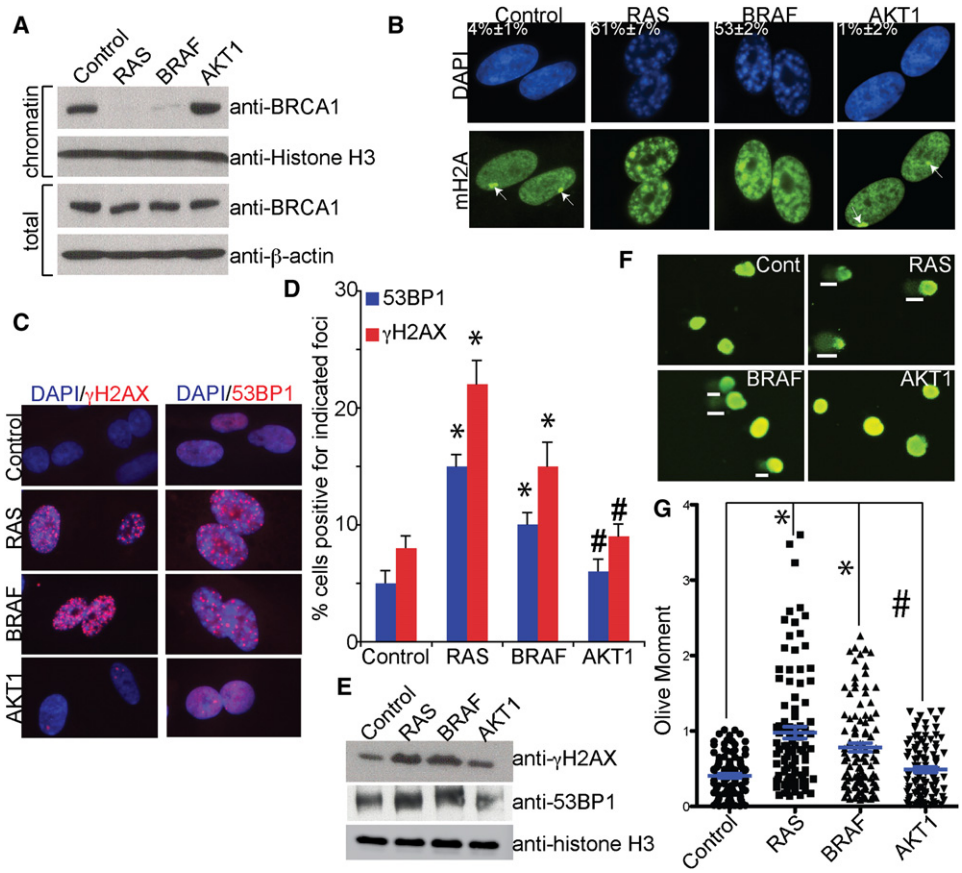

Figure 2. Oncogene-Induced BRCA1 Chromatin Dissociation Correlates with DNA Damage Accumulation and SAHF Formation

(A) IMR90 cells were infected with control or the indicated activated oncogene-encoding retrovirus. Expression of BRCA1, histone H3, and β-actin in the chromatin fractions and total cell lysates of indicated cells was assayed by western blot at day 4.

(B) Same as (A) but stained with DAPI and an antibody to mH2A, which is a component of SAHF. Percentage of SAHF-positive cells is indicated. Mean of three independent experiments with SD. Arrows point to mH2A-stained inactivated X chromosome (Costanzi and Pehrson, 1998).

(C) Same as (A) but stained with DAPI or antibodies against γH2AX or 53BP1.

(D) Quantitation of (C). A total of 200 cells were examined for formation of γH2AX foci and 53BP1 foci. Cells with more than five nuclear foci for γH2AX or 53BP1 were counted as positive. Mean of three independent experiments with SD. *$p < 0.05$ and #$p > 0.05$ as compared to controls.

(E) Expression of γH2AX, 53BP1, and histone H3 in the chromatin fractions of IMR90 cells infected with vector control or indicated activated oncogenes as determined by western blot.

(F) Same as (A). At day 2, drug-selected indicated cells were assayed for DNA damage by the comet assay. White bars indicate the examples of comet tails that resulted from damaged DNA.

(G) Quantitation of (F). DNA damage from the comet assay is calculated as artificial Olive Moment unit as described in Experimental Procedures. The Olive Moment in 100 cells from each group was measured. Mean of Olive Moment with SEM is shown in blue. *$p < 0.05$ and #$p > 0.05$ as compared to control.

See also Figure S2.

RAS-infected IMR90 cells. Expression of BRIP1 and BRCA1 mRNA in control and RAS-infected IMR90 cells was examined by quantitative reverse transcriptase-polymerase chain reaction (qRT-PCR). Compared with controls, BRIP1 mRNA levels were significantly decreased as early as day 1 in RAS-infected cells (Figure 4C). However, the BRCA1 mRNA expression level did not statistically change at the same time (Figure 4C). This is consistent with the idea that RAS-induced BRIP1 repression triggers BRCA1 chromatin dissociation prior to RAS-induced cell cycle exit.

We next sought to determine the mechanism underlying BRIP1 downregulation in RAS-infected cells. BRIP1 mRNA expression is downregulated in RAS-infected cells (Figure 4C), but the stability of BRIP1 mRNA is not decreased by RAS expression (data not shown), suggesting that BRIP1 may be regulated at the transcriptional level. Consistently, the activity of a 400 bp (−300 bp – +100 bp) fragment of the proximal human *BRIP1* gene promoter was significantly suppressed in RAS-infected cells (Figure S4C). Notably, deletion of a critical B-Myb binding site from the *BRIP1* promoter blocked the RAS-mediated suppression of promoter activity, suggesting that B-Myb plays a critical role in suppressing BRIP1 expression in response to RAS (Figure S4C). Interestingly, it has previously been demonstrated that B-Myb suppresses oncogenic RAS induced senescence (Masselink et al., 2001). Consistently, we observed downregulation of B-Myb in RAS-infected cells prior

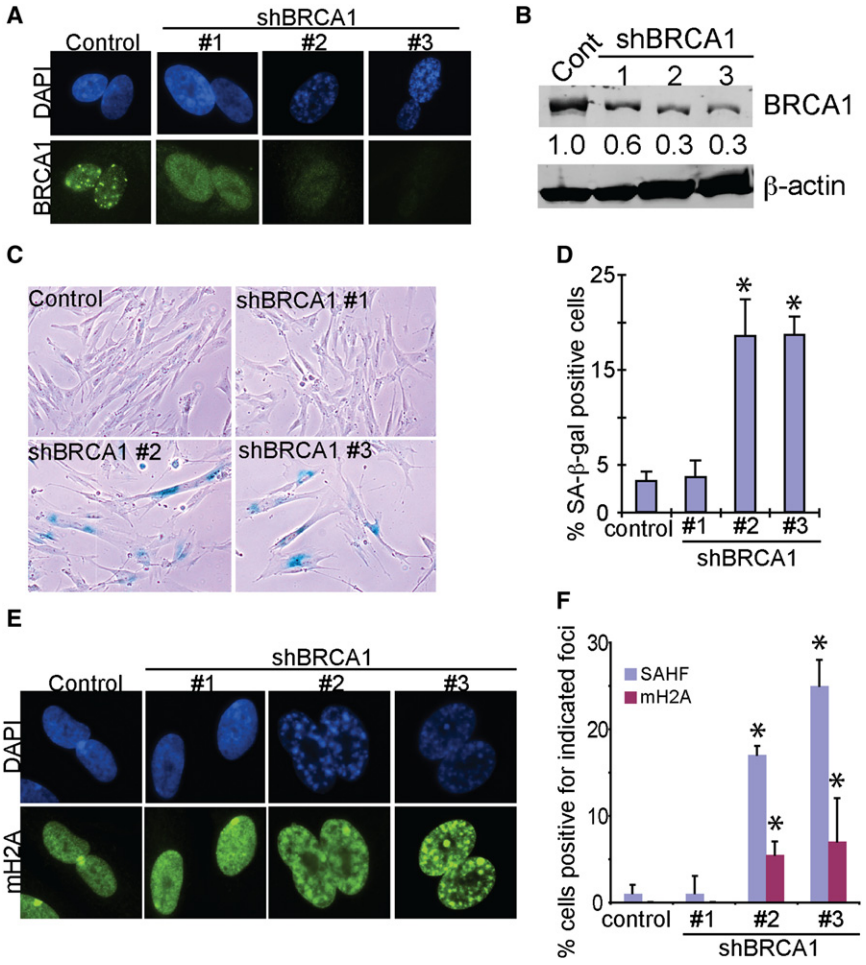

Figure 3. BRCA1 Knockdown Induces Senescence

(A) IMR90 cells were infected with lentivirus encoding three individual shRNAs to the human BRCA1 gene or a vector control and stained with an anti-BRCA1 antibody. Note that the BRCA1 nuclear foci in control cells are associated with the S/G2 phases of the cell cycle (Scully et al., 1997b), indicating that the BRCA1 staining is specific.

(B) Same as (A) but assayed for BRCA1 and β-actin expression by western blot. The levels of BRCA1 expression were quantified using the LI-COR Odyssey imaging system (normalized using β-actin as a loading control). Cont, control.

(C) Same as (A) but stained for SA-β-gal activity at day 5.

(D) Quantitation of (C). A total of 100 cells were examined for expression of SA-β-gal activity. Mean of three independent experiments with SD. *$p < 0.03$.

(E) Same as (C) but stained with DAPI to visualize SAHF and an antibody against mH2A.

(F) Quantitation of (E). A total of 100 cells were examined for SAHF and mH2A foci formation. Mean of three independent experiments with SD. *$p < 0.02$.

See also Figure S3.

to the RAS-induced cells cycle exit (i.e., as early as 12 hr) compared with controls (Figure S4D). Significantly, using an anti-B-Myb antibody, chromatin immunoprecipitation studies demonstrated that the binding of B-Myb to the promoter of the human *BRIP1* gene was significantly reduced in RAS-infected cells compared with controls (Figure 4D). Additionally, it has recently been demonstrated that B-Myb expression is suppressed by upregulation of microRNA 29 (mir29) during senescence (Lafferty-Whyte et al., 2009; Martinez et al., 2011). Consistently, expression of mir29 was upregulated in RAS-infected cells as early as 6 hr compared with controls (Figure S4E). We conclude that RAS-mediated inhibition of B-Myb contributes to the downregulation of BRIP1 during RAS-induced senescence.

Next, we asked whether knockdown of BRIP1 drives BRCA1 chromatin dissociation and senescence. Three individual *sh*RNAs to the human *BRIP1* gene (shBRIP1) were developed, and the efficacy of BRIP1 knockdown was confirmed by western blot (Figure 4E). BRCA1 levels in the chromatin fractions of shBRIP1-expressing cells were greatly reduced when compared to controls (Figure 4E). In addition, we observed an increase in expression of γH2AX in shBRIP1-expressing cells (Figure S4F). Notably, BRIP1 knockdown induced expression of markers of senescence, including SA-β-gal activity and SAHF formation (Figures 4F and 4G). Consistent with this, BRIP1 knockdown increased levels of p16, p21, p53, and hypophosphorylated pRB, demonstrating activation of both the p53 and the pRB pathways (Figure S4G). To limit off-target effects, we sought to determine whether BRIP1 restoration in shBRIP1-expressing cells could prevent senescence induced by BRIP1 knockdown. Indeed, ectopic expression of an shBRIP1-resistant wild-type BRIP1 significantly reduced the expression of markers of senescence induced by shBRIP1 (Figures 4H–4J), indicating the specificity of the senescence phenotype induced by BRIP1 knockdown. We conclude that BRIP1 knockdown is sufficient to dissociate BRCA1 from chromatin and induce senescence.

The interaction between BRIP1 and the BRCT repeats of BRCA1 depends on phosphorylation of BRIP1 at serine 990 (S990) (Yu et al., 2003). Thus, we determined whether rescuing of senescence by BRIP1 depends on the phosphorylation of BRIP1 at S990. For this purpose, we made a serine to alanine mutant (S990A) that mimics the nonphosphorylated state of BRIP1 (Yu et al., 2003). Compared with wild-type BRIP1, BRIP1 S990A failed to rescue the senescence induced by BRIP1 knockdown (Figures 4H–4J). This result suggests that the interaction between BRCA1 and BRIP1 plays a critical role in regulating senescence.

Ectopic BRIP1 Rescues BRCA1 Chromatin Dissociation and Suppresses RAS-Induced Senescence

We next asked whether ectopic BRIP1 might rescue BRCA1 chromatin dissociation and suppress oncogene-induced senescence. Toward this goal, IMR90 cells were cotransduced with a retrovirus encoding RAS to induce senescence and a retrovirus

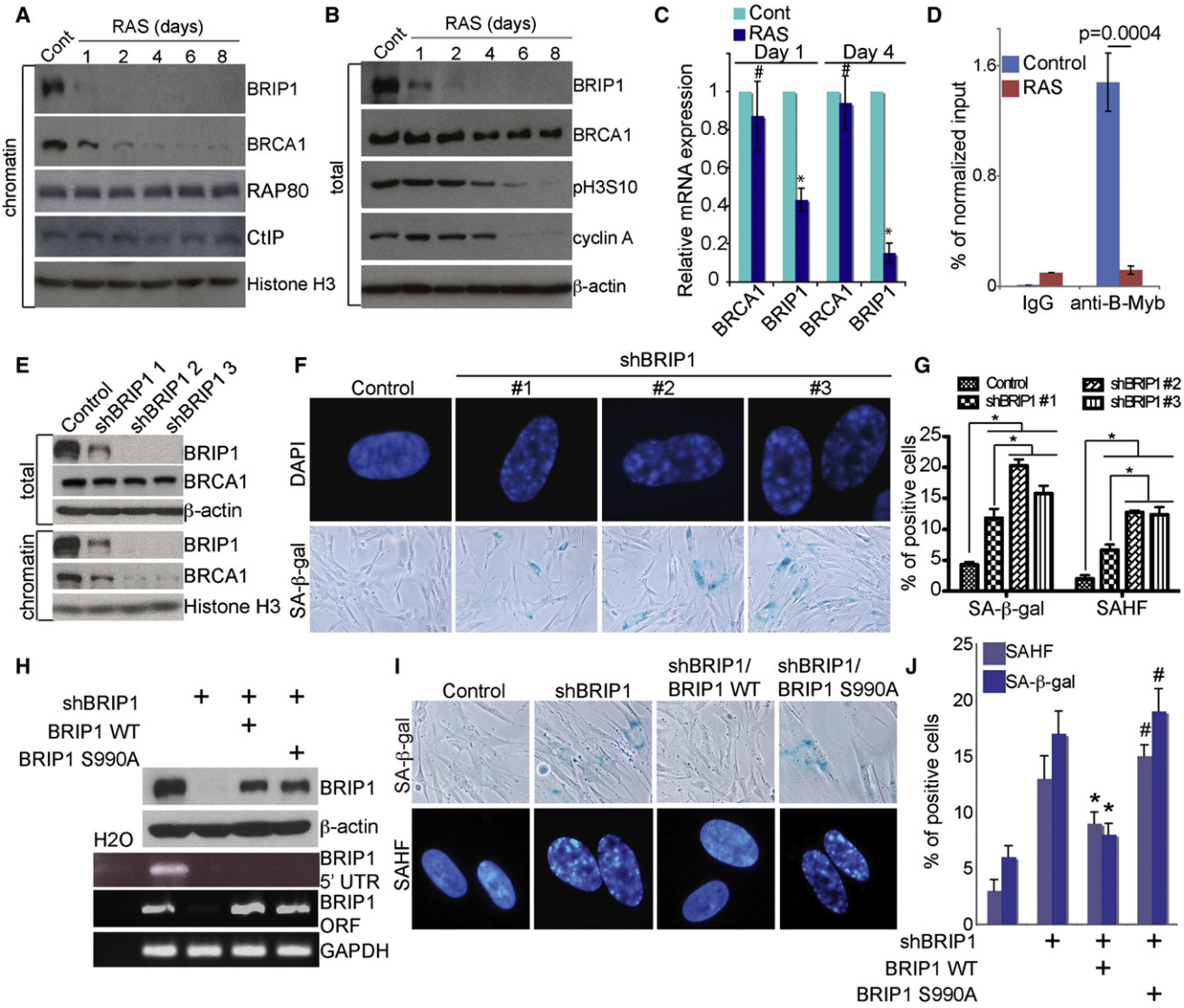

Figure 4. BRIP1 Repression Triggers BRCA1 Chromatin Dissociation

(A) IMR90 cells were infected with control (Cont) or RAS-encoding retrovirus. Expression of BRIP1, BRCA1, RAP80, CtIP, and histone H3 in the chromatin fractions of control and RAS-infected IMR90 cells was determined by western blot at the indicated time points.

(B) Same as (A). Expression of BRIP1, BRCA1, pH3S10, cyclin A, and β-actin was determined by western blot at the indicated time points in total cell lysates of control and RAS-infected IMR90 cells.

(C) Same as (A). Expression of BRCA1 and BRIP1 mRNA was determined by qRT-PCR at indicated time points in control and RAS-infected IMR90 cells. Mean of three independent experiments with SD. #$p > 0.05$ and *$p < 0.01$ versus controls.

(D) Same as (A). Control and RAS-infected cells were subjected to chromatin immunoprecipitation using an anti-B-Myb antibody as detailed in Experimental Procedures. The immunoprecipitated DNA was subjected to quantitative PCR analysis using primers that cover the B-Myb binding site in the promoter of human *BRIP1* gene.

(E) IMR90 cells were infected with lentivirus-encoding shBRIP1 or control. Expression of BRIP1, BRCA1, histone H3, and β-actin in total cell lysates and in chromatin fractions was determined by western blot.

(F) Same as (E) but stained for SA-β-gal activity or with DAPI to visualize SAHF.

(G) Quantitation of (F). Mean of four independent experiments with SEM. *$p < 0.05$.

(H) IMR90 cells were infected with a lentivirus-encoding shBRIP1 (#3) together with control, an shBRIP1-resistant wild-type BRIP1 (BRIP1 WT), or an shBRIP1-resistant S990A mutant as detailed in the Experimental Procedures. Expression of BRIP1 and β-actin in drug-selected cells was determined by western blot (top). In addition, expression of *BRIP1* mRNA was determined by RT-PCR using primers designed to its 5′ UTR region (only amplifies endogenous but not ectopic *BRIP1* mRNA) or its open reading frame (amplifies both endogenous and ectopic *BRIP1* mRNA) (bottom).

(I) Same as (H) but stained for SA-β-gal activity or with DAPI to visualize SAHF.

(J) Quantitation of (I). Mean of three independent experiments with SD. *$p < 0.05$ and #$p > 0.05$ compared with only shBRIP1-expressing cells.

See also Figure S4.

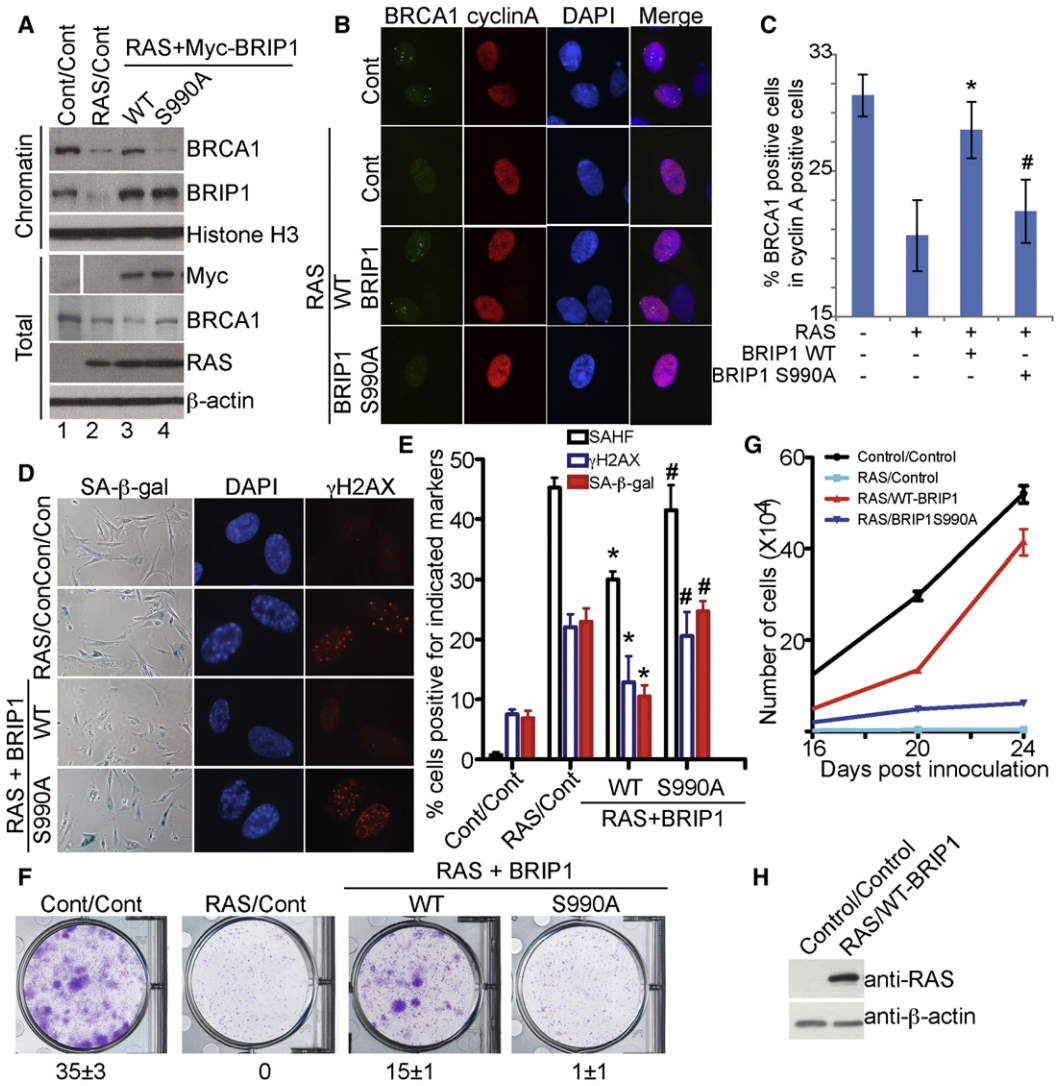

Figure 5. Ectopic BRIP1 Rescues BRCA1 Chromatin Dissociation and Suppresses Oncogene-Induced Senescence and DNA Damage Response

(A) IMR90 cells were infected with retroviruses encoding RAS together with control (Cont), Myc-tagged wild type (WT) BRIP1, or BRIP1 S990A mutant. At day 4, drug-selected cells were examined for expression of BRCA1, BRIP1, and histone H3 in the chromatin fractions and for expression of Myc-tagged ectopic BRIP1, BRCA1, RAS, and β-actin in total cell lysates.

(B) Same as (A) but stained with antibodies against BRCA1 and cyclin A.

(C) Quantitation of (B). A total of 100 cyclin A-positive cells were examined for BRCA1 foci formation. Mean of three independent experiments with SD. *$p < 0.05$ and #$p > 0.05$ compared with RAS-infected controls.

(D) Same as (A) but stained for SA-β-gal activity or DAPI to visualize SAHF or an antibody against γH2AX to detect DNA damage.

(E) Quantitation of (D). Mean of four independent experiments with SD. *$p < 0.015$ and #$p > 0.12$ versus RAS-infected control cells.

(F) Same as (A) but equal numbers of cells (3×10^3 cells/well) were plated in 6-well plates in triplicate for focus formation assays. After 2 weeks in culture, the plates were stained with 0.05% crystal violet in PBS to visualize foci. Shown are representative images of four independent experiments. Number of foci is indicated as mean with SD.

(G) Same as (F), but the number of cells was counted at indicated time points. Mean of three independent experiments with SD.

(H) Control and the senescence-bypassed cells isolated from (G) were examined for RAS and β-actin expression by western blot.

See also Figure S5.

encoding a Myc-tagged wild-type BRIP1 or control. Compared with controls, BRIP1 expression notably rescued the levels of BRCA1 in the chromatin fractions of RAS-infected cells (Figure 5A, lane 2 versus lane 3). This was not due to a lower RAS expression level because RAS was expressed at a higher level in ectopic BRIP1-expressing cells compared to controls (Figure 5A, lane 2 versus lane 3). In addition, the total BRCA1 protein level was not increased by ectopic BRIP1 (Figure 5A, lane 2 versus lane 3), implying that the increased level of chromatin-associated BRCA1 was not due to increased levels of total BRCA1.

Notably, ectopic BRIP1 restored BRCA1 foci formation in cyclin A-positive RAS-infected cells (Figures 5B and 5C). Interestingly, ectopic BRIP1 did not affect RAS-induced hyperproliferation (Figure S5), a trigger of the DNA damage response (Di Micco et al., 2006), suggesting that ectopic BRIP1 may instead affect DNA repair. In addition, expression of ectopic BRIP1 in RAS-infected cells suppressed expression of markers of senescence including SA-β-gal activity, SAHF formation, and senescence-induced cell growth arrest, and inhibited DNA damage response revealed by decreased γH2AX foci formation when compared to controls (Figures 5D–5H). These data further support the conclusion that BRIP1 plays a major role in BRCA1 chromatin association during RAS-induced senescence.

We next sought to determine whether suppression of BRCA1 chromatin dissociation by BRIP1 depends on the phosphorylation of BRIP1 at S990. Compared with wild-type BRIP1, the BRIP1 S990A mutant failed to rescue BRCA1 chromatin dissociation in RAS-infected cells (Figure 5A, lane 3 versus lane 4) and was also impaired in restoring BRCA1 foci in cyclin A-positive RAS-infected cells (Figures 5B and 5C). These results imply that the interaction between BRIP1 and BRCA1 is necessary for suppression of BRCA1 chromatin dissociation by BRIP1. Notably, the BRIP1 S990A mutant failed to suppress senescence and its associated DNA damage accumulation in RAS-infected IMR90 cells (Figures 5D–5G). We conclude that suppression of senescence by ectopic BRIP1 is dependent on its interaction with BRCA1.

Oncogenic RAS Impairs the BRCA1-Mediated DNA Repair Response prior to RAS-Induced Cell Cycle Exit during Senescence

We next asked whether oncogene-induced BRCA1 chromatin dissociation inactivates the BRCA1-mediated DNA repair response. Upon DNA damage BRCA1 foci largely disappear in normal cycling cells, although new damage-induced foci form hours after DNA damage during the S/G2 phase of the cell cycle (Chen et al., 1998; Durant and Nickoloff, 2005; Scully et al., 1997a; Xu et al., 2001). To determine the effects of oncogenic RAS expression on the BRCA1-mediated DNA repair response, at day 2, control and RAS-infected IMR90 cells were treated with 2 Gy of IR to induce DNA DSBs. Notably, IR did not prevent BRCA1 chromatin dissociation in RAS-infected cells (Figure 6A). This was not due to a lack of DNA damage induction by IR in RAS-infected cells because nearly 100% of both control and RAS-infected cells were positive for γH2AX foci (Figure 6B). We next examined formation of damage-induced BRCA1 foci in the S/G2 phases of cycling cells by costaining cells with antibodies against BRCA1 and cyclin A 5 hr after IR treatment (Peng et al., 2006; Zhang et al., 2009). As expected, BRCA1 foci were significantly induced upon IR treatment in controls (Figures 6C and 6D). However, formation of damage-induced BRCA1 foci was severely impaired in RAS-infected IMR90 cells when exposed to IR (Figures 6C and 6D).

Functional BRCA1 is required for relocating/sustaining BRCA2 and its partner protein PALB2 at damage-induced foci (Sy et al., 2009; Zhang et al., 2009), which are critical for BRCA1-mediated DNA DSB repair (Huen et al., 2010). Consistently, formation of damage-induced BRCA2 and PALB2 foci was also significantly impaired in RAS-infected cells upon IR treatment compared to controls (Figures 6E–6G). Based on these results, we conclude that oncogenic RAS impairs the BRCA1-mediated DNA repair response prior to the RAS-induced cell cycle exit during senescence.

DNA Damage Promotes Senescence Bypass in RAS-Infected Cells

The impaired ability of BRCA1 to repair DNA damage promotes genomic instability, facilitates acquisition of oncogenic alterations, and ultimately drives tumorigenesis (Turner et al., 2004). Thus, we anticipated that impaired BRCA1-mediated DNA repair might lead to DNA damage accumulation and allow for accumulation of secondary hits that might promote senescence bypass. Consistently, we reproducibly observed rare foci of senescence-bypassed cells in RAS-infected IMR90 cells (Figure S6A). RAS remains overexpressed in those cells (Figure S6B), suggesting that senescence bypass is not due to loss of ectopic RAS expression. To directly test our hypothesis, control and RAS-infected IMR90 cells were treated with 2 Gy IR at day 2, and the extent of DNA damage was measured by the comet assay. At this time point, BRCA1 was largely dissociated from chromatin in RAS-infected proliferative cells (Figure 1F). There was increased DNA damage in IR-treated RAS-infected cells, which was significantly greater than either IR-treated control cells or RAS-infected cells without IR treatment ($p < 0.05$) (Figures 7A and 7B). Notably, ectopic expression of wild-type BRIP1, but not the BRIP1 S990A mutant, suppressed the DNA damage accumulation in IR-treated RAS-infected cells (Figures 7C and 7D).

We next sought to determine whether this decreased ability to repair DNA might lead to senescence bypass. We tested this by focus formation and cell growth assays. Indeed, IR treatment consistently induced senescence bypass as evidenced by both focus formation and apparent cell growth in IR-treated cells compared to controls (Figures 7E and 7F). Notably, senescence-bypassed cells formed colonies under anchorage-independent growth condition in soft agar (Figures 7G and 7H). As a negative control, IR did not promote the proliferation of control cells (Figure 7E; Figures S6D and S6E). To eliminate the possibility that senescence bypass observed in IR-treated cells was due to loss of ectopic RAS, these cells were isolated and analyzed by western blot for exogenous RAS expression. Compared with controls, RAS remained greatly overexpressed in the senescence-bypassed cells (Figure 7I). In addition, pRB was hyperphosphorylated, and p53 expression was reduced in the senescence-bypassed cells (Figure 7J), suggesting that inactivation of the key senescence-promoting pRB and p53 pathways contributes to the senescence bypass induced by IR treatment. Notably, IR treatment has no effect on senescence-associated cell growth arrest once RAS-infected cells have exited from cell cycle (e.g., at day 7) (Figures S6C–S6E). This result suggests that the senescence bypass observed in IR-treated RAS-infected cells is not due to the preexistence of senescence-resistant cells. Ectopic BRIP1 suppresses senescence (Figures 5D–5H), which prevented us from determining whether rescuing BRCA1 chromatin dissociation by ectopic BRIP1 inhibits IR treatment-induced senescence bypass in RAS-infected cells.

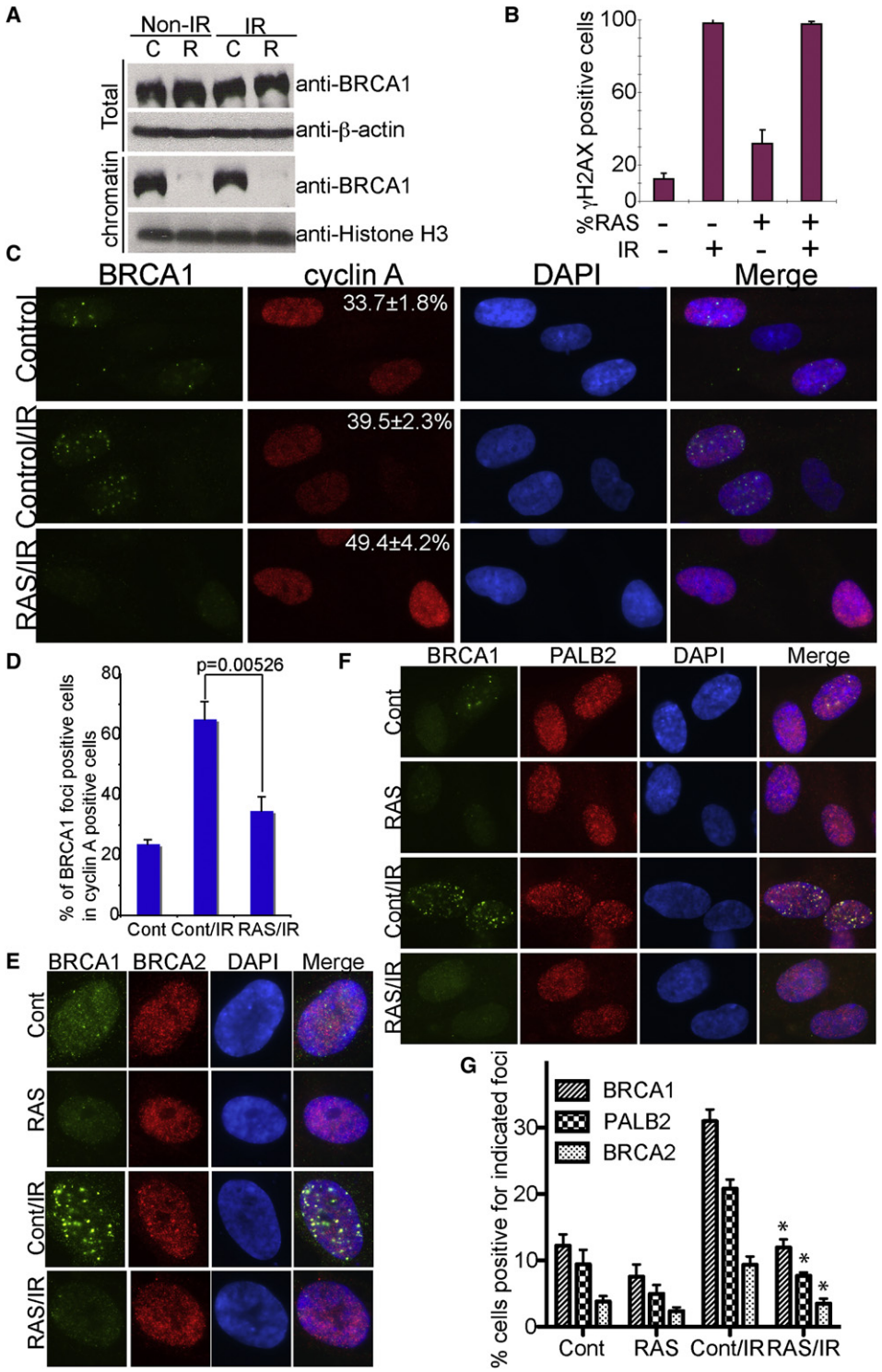

Figure 6. BRCA1-Mediated DNA Repair Response Is Impaired prior to the Oncogene-Induced Cell Cycle Exit

(A) IMR90 cells were infected with control (C) or RAS (R)-encoding retrovirus. At day 2, drug-selected cells were treated with or without 2 Gy IR. After 5 hr of recovery, expression of BRCA1, histone H3, and β-actin in total cell lysates and in the chromatin fractions was determined by western blot.

(B) Same as (A) but quantified for γH2AX foci formation in the indicated groups. Mean of three independent experiments with SD.

(C) Same as (A) but stained with antibodies against BRCA1 and cyclin A (using a rabbit anti-cyclin A antibody). Percentage of cyclin A-positive cells is indicated as mean of three independent experiments with SD.

(D) Quantitation of (C). A total of 100 cyclin A-positive cells from each of the indicated groups were examined for BRCA1 foci formation. Mean of three independent experiments with SD.

If senescence bypass in IR-treated cells is achieved through accumulation of DNA damage and acquisition of secondary hits due to BRCA1 chromatin dissociation induced by BRIP1 repression, we anticipated that BRIP1 might remain downregulated, and BRCA1 might remain dissociated from chromatin in the senescence-bypassed cells. Indeed, compared with controls, BRIP1 remained downregulated, and BRCA1 remained dissociated from chromatin in the senescence-bypassed cells (Figure 7K). These results further support the idea that BRCA1 chromatin dissociation is not merely a consequence of senescence-associated cell cycle exit because the senescence-bypassed cells are highly proliferative. In addition, markers of DNA damage (such as γH2AX and 53BP1 foci) were expressed at higher levels in the senescence-bypassed cells compared to controls (Figures 7L–7N). This is consistent with the idea that BRCA1 chromatin dissociation contributes to DNA damage accumulation in those cells. Together, these results suggest that the loss of BRCA1-mediated DNA repair may also allow for subsequent hits that ultimately enable a small fraction of Ras-induced cells to bypass senescence.

DISCUSSION

Our study reveals that oncogenic RAS induces dissociation of BRCA1 from chromatin prior to the cell cycle exit during RAS-induced senescence. This dissociation of BRCA1 from chromatin coincides with DNA damage accumulation. Downregulation of BRIP1, a BRCA1-binding partner, contributes to BRCA1 chromatin dissociation. Conversely, ectopic BRIP1 rescues BRCA1 chromatin dissociation and suppresses RAS-induced senescence. Significantly, the BRCA1-mediated DNA repair response is impaired prior to the RAS-induced cell cycle exit, which renders cells susceptible to the accumulation of secondary hits. In some instances this may ultimately allow for senescence bypass.

The Role of BRCA1 Chromatin Dissociation during Oncogene-Induced Senescence

DNA damage persists in senescent cells (Rodier et al., 2009), suggesting that defects in DNA repair may contribute to the accumulation of DNA damage observed during senescence. Our data reveal that BRCA1 chromatin dissociation coincides with DNA damage accumulation, which occurs as early as the hyperproliferation phase in RAS-infected cells (Figures 1F–1H, 1L, and 1M). A previous report by Di Micco et al. (2006) showed that the accumulation of DNA damage closely follows the hyperproliferation phase in RAS-infected cells during senescence. The basis for this minor discrepancy between these two reports remains to be determined. It could be due to quantitative approaches used in the current study, which make it easier to reveal subtle differences at early stages (Figures 1L and 1M). We showed that BRCA1 chromatin dissociation correlates with the DNA damage response in both RAS and BRAF-infected cells (Figure 2). Furthermore, BRCA1 knockdown in primary human cells triggers the DNA damage response and induces senescence (Figure 3; Figure S3B and S3C). Finally, suppression of BRCA1 chromatin dissociation by ectopic BRIP1 suppresses the DNA damage induced by oncogenic RAS (Figures 5B–5E). Together, these results support the notion that BRCA1 chromatin dissociation contributes to the accumulation of DNA damage during oncogene-induced senescence.

Herein, we demonstrated that RAS-induced dissociation of BRCA1 from chromatin precedes SAHF formation (Figures 1C–1F), and BRCA1 knockdown drives SAHF formation (Figure 3). Furthermore, BRCA1 chromatin dissociation correlates with SAHF formation in IMR90 cells expressing RAS and BRAF oncogenes (Figures 2A and 2B). Consistent with this idea that BRCA1 antagonizes heterochromatin formation and/or maintenance, it has been previously demonstrated that targeting BRCA1 to an amplified lac operator-containing chromosome region in the mammalian genome results in large-scale chromatin unfolding (Ye et al., 2001). We were unable to ectopically express wild-type BRCA1 in primary human cells (data not shown), which prevented us from determining whether ectopically expressed BRCA1 might suppress SAHF formation. However, ectopic BRIP1 was able to rescue BRCA1 chromatin dissociation and suppress SAHF formation (Figures 5D and 5E). Together, these findings support the idea that BRCA1 chromatin dissociation promotes senescence by contributing to SAHF formation.

Suppression of the DNA damage response by ectopic BRIP1 inhibits SAHF formation (Figures 5B–5E). Conversely, knockdown of BRCA1, which induces DNA damage, drives SAHF formation (Figure 3; Figure S3). In addition, AKT or shPTEN, neither of which dissociates BRCA1 from chromatin, also fails to induce a DNA damage response or SAHF formation (Figure 2; Figure S2). Together, these data suggest that DNA damage response triggered by BRCA1 chromatin dissociation is required for SAHF formation. Indeed, there is evidence to suggest that formation of SAHF limits the degree of DNA damage response during oncogene-induced senescence (Di Micco et al., 2011). However, the DNA damage response is not sufficient for SAHF formation, which also requires activation of p16/pRB and HIRA/PML pathways (Narita et al., 2003; Ye et al., 2007; Zhang et al., 2005, 2007a). Overall, these results support the notion that DNA damage is necessary but not sufficient for SAHF formation.

The Role of BRIP1 Repression during Oncogene-Induced Senescence

Stable BRIP1 knockdown reduces damage-induced BRCA1 foci formation, and BRIP1-deficient cells demonstrate defects in the number and intensity of BRCA1 foci (Peng et al., 2006). This suggests that BRIP1 plays an important role in BRCA1-mediated DNA repair. BRIP1 has been shown to be significantly downregulated in response to RAS expression in primary human fibroblasts based on gene expression microarray analysis, while

(E) Same as (C) but stained with antibodies against BRCA1 and BRCA2.
(F) Same as (C) but stained with antibodies against BRCA1 and PALB2.
(G) Quantitation of results from (E) and (F). A total of 100 cells from each of the indicated group were examined for BRCA1, BRCA2, and PALB2 foci formation. Mean of three independent experiments with SD. *$p < 0.02$ versus control IR-treated cells. Cont, control.

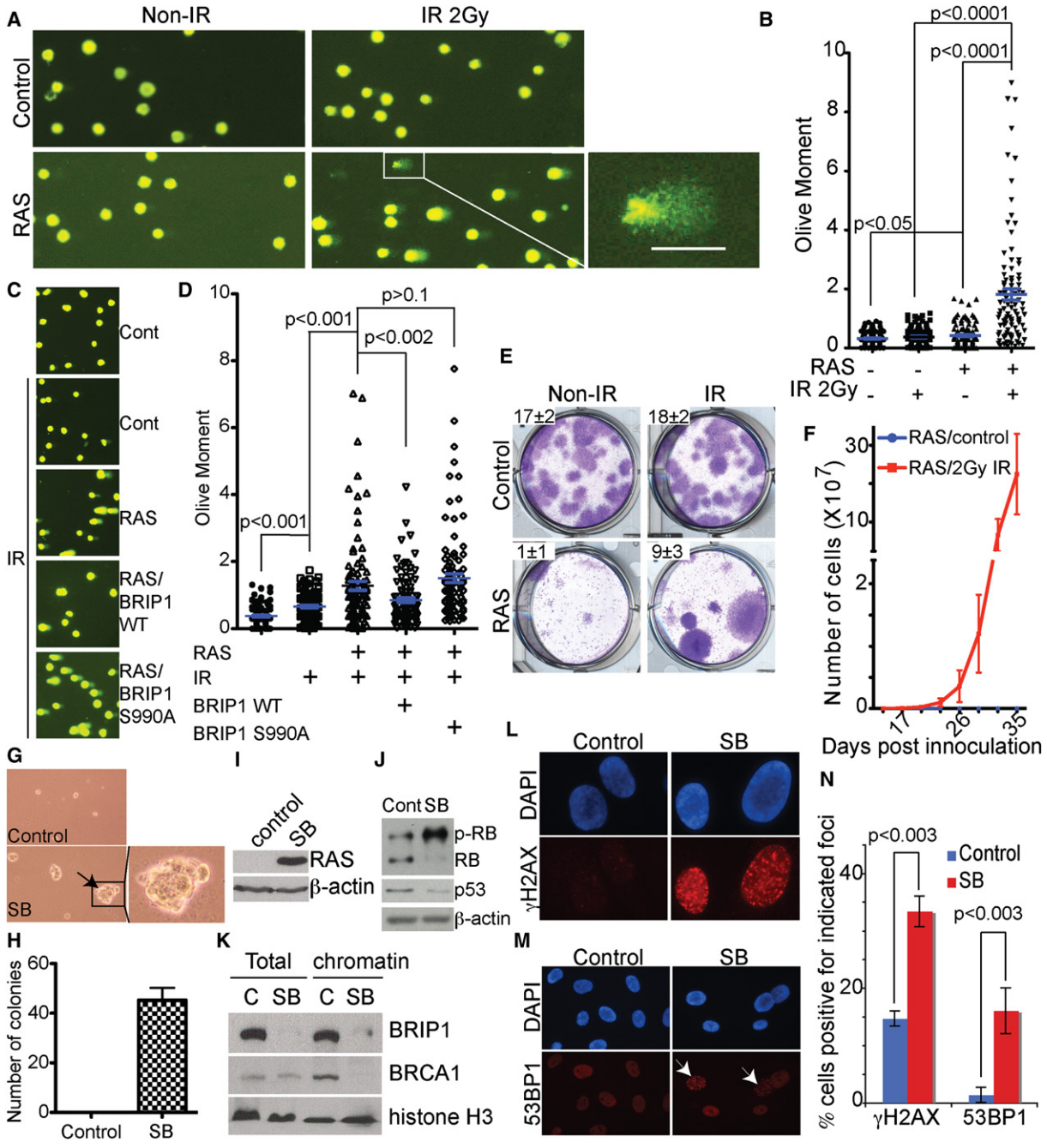

Figure 7. DNA Damage Promotes Senescence Bypass

(A) IMR90 cells were infected with control or RAS-encoding retrovirus, and drug-selected cells were treated with or without 2 Gy IR at day 2. After 5 hr of recovery, comet assays were performed to detect DNA damage. Shown are representative images of six independent experiments. The white bar indicates an example of the comet tails that reflect the extent of DNA damage. Note that a shorter exposure time was used here compared with Figure 2F to avoid saturation of comet tail signal in IR-treated RAS-infected cells.

(B) Quantitation of results from (A). A total of 120 cells from each of the indicated groups were measured for Olive Moment. Means of Olive Moment with SEM are indicated in blue. Note that there was a significant increase in DNA damage in RAS-infected cells without IR treatment compared with controls ($p < 0.05$).

(C) Same as (A). Comet assays were performed to detect DNA damage in the indicated cells. Shown are representative images of three independent experiments. Cont, control.

(D) Quantitation of results from (C). A total of 100 cells from each of the indicated groups were measured for Olive Moment. Means of Olive Moment with SEM are indicated in blue.

(E) At day 2, control and RAS-infected BJ-hTERT cells were treated with or without 2 Gy IR. Equal numbers of the indicated cells (3×10^3 cells/well) were plated in 6-well plates for focus formation assays. After 2 weeks of culture, the plates were stained with 0.05% crystal violet in PBS to visualize foci. Shown are representative images of four independent experiments. The number of foci is indicated as mean with SD.

CtIP and RAP80 are not among the list of genes whose expression is significantly changed in the same analysis (Mason et al., 2004). Interestingly, BRIP1, but not CtIP or RAP80/Abraxas, regulates DNA replication and is required for timely S phase progression (Huen et al., 2010; Kumaraswamy and Shiekhattar, 2007), implying that the BRCA1/BRIP1 complex may regulate senescence by altering DNA replication. In support of this idea, RAS-induced senescence is characterized as a DNA damage response triggered by aberrant DNA replication (Di Micco et al., 2006). Furthermore, B-Myb, a key regulator of BRIP1 expression (Figure 4D; Figures S4C and S4D), is critical for proper DNA replication and regulates the DNA damage response (Ahlbory et al., 2005; Lorvellec et al., 2010). Notably, BRIP1 is expressed at higher levels in advanced breast carcinomas, and its overexpression correlates with a higher cell proliferation index (Eelen et al., 2008), supporting the notion that high levels of BRIP1 may contribute to cell proliferation by suppressing senescence (Figure 5). Taken together, these data imply a key role for BRIP1 in accumulation of DNA damage during oncogene-induced senescence.

The Role of BRCA1 Chromatin Dissociation in Senescence Bypass

Oncogene-induced BRCA1 chromatin dissociation precedes the cell cycle exit during senescence (Figure 1). Significantly, oncogenic RAS impairs BRCA1-mediated DNA repair response prior to the cell cycle exit during senescence (Figures 6 and 7). This allows for the creation of a large time window for cells to accumulate secondary oncogenic hits prior to the senescence-associated cell cycle exit, which ultimately leads to senescence bypass in a minority of cells while the vast majority of cells eventually exit from the cell cycle and become senescent. Consistent with this model, RAS-expressing cells accumulate significantly greater DNA damage after IR treatment, and IR treatment promotes senescence bypass in RAS-infected cells (Figure 7). The mechanism we uncovered here may help explain the paradox of why activation of oncogenes (such as RAS) promotes senescence but at the same time predisposes cells to transformation.

EXPERIMENTAL PROCEDURES

Chromatin Isolation and Chromatin Immunoprecipitation

Chromatin was prepared according to published methods (Méndez and Stillman, 2000; Narita et al., 2006). Soluble proteins in supernatant 1 (SN1, cytoplasmic) and 2 (SN2, nuclear) and chromatin-bound proteins in the chromatin fraction were detected by western blot.

Chromatin immunoprecipitation in control and RAS-infected IMR90 cells was performed at day 6 as previously described (Zhang et al., 2007b) using a monoclonal anti-B-Myb antibody (Santa Cruz Biotechnology) or an isotype-matched IgG control. Immunoprecipitated DNA was analyzed using SYBR Green quantitative PCR (SABiosciences) against the human *BRIP1* gene promoter region containing the B-Myb binding site using the following primers: forward, 5′-ATAAAGCGGAGCCCTGGAAGAGAA-3′; reverse, 5′-ATTCGTCTCGGGTTGTGTG-GTTGA-3′.

Comet Assay

The comet assay was performed with the CometAssay (Trevigen) kit following the manufacturer's instructions. DNA damage was measured as the artificial Olive Moment using CometScore software downloaded from http://www.tritekcorp.com. To determine significance, the t test was performed using GraphPad Prism software (http://www.graphpad.com).

Anchorage-Independent Growth in Soft Agar and Focus Formation Assay

Anchorage-independent growth in soft agar was performed as previously described (Li et al., 2010). For focus formation, 4 days after initial infection, control or oncogenic H-RAS^{G12V}-encoding retrovirus-infected BJ-hTERT cells were treated with 2 Gy IR. Cells were cultured for 6 days to eliminate the apoptotic cells induced by IR. Then, control and H-RAS^{G12V}-expressing cells with or without IR treatment were seeded into 6-well plates at a density of 3000 cells/well in triplicate. Two weeks later, the plates were stained with 0.05% crystal violet in PBS (Kuilman et al., 2008).

Retrovirus and Lentivirus Infections

Retrovirus production and transduction were performed as described previously (Ye et al., 2007; Zhang et al., 2005) using Phoenix cells to package the infection viruses (Dr. Gary Nolan, Stanford University). Lentivirus was packaged using the ViraPower Kit from Invitrogen following the manufacturer's instructions and as described previously (Li et al., 2010; Ye et al., 2007). Cells infected with viruses encoding a drug-resistant gene to puromycin or neomycin were selected in 1 and 500 μg/ml, respectively, of the corresponding agent.

Immunofluorescence, BrdU Labeling, FACS, and SA-β-gal Staining

Immunofluorescence staining and BrdU labeling for cultured cells were performed as described previously using antibodies described above (Zhang et al., 2005, 2007a, 2007b). Soluble protein pre-extraction with detergent was carried out as described previously (Taddei et al., 2001). Briefly, cells were incubated with PBS supplemented with 0.5% Triton X-100 for 5 min at room temperature, followed by fixation in 4% paraformaldehyde (Sigma-Aldrich) for 10 min. Fixed cells were incubated with a rabbit anti-BRCA1 antibody for 1 hr at room temperature and visualized by incubating the cells with goat anti-rabbit Cy3 (Jackson ImmunoResearch; 1:5000) secondary antibody followed by detection of BrdU using a FITC-labeled anti-BrdU antibody (BD Biosciences). FACS was performed as previously described (Ye et al., 2007), and FlowJo software was used to analyze cell cycle distribution. SA-β-gal staining was performed as previously described (Dimri et al., 1995).

For additional information about cell culture methods, RT-PCR, and luciferase assays, as well as antibodies and plasmids used in this study, please see the Supplemental Experimental Procedures.

(F) Same as (E), but an equal number (1×10^4) of indicated cells were inoculated and cultured. The number of cells from each group was counted at indicated time points. Mean of three independent experiments with SD.
(G) Equal numbers of parental and senescence-bypassed cells were grown under anchorage-independent conditions in soft agar. Arrow points to an example of colonies formed by the senescence-bypassed cells.
(H) Quantitation of (G). Mean of three independent experiments with SD.
(I) Expression of RAS and β-actin in control (C) and the senescence-bypassed (SB) cells isolated from (F) was determined by western blot.
(J) Same as (I) but assayed for pRB, p53, and β-actin expression by western blot.
(K) Same as (I) but examined for expression of BRIP1, BRCA1, and histone H3 in total cell lysates and in the chromatin fractions by western blot.
(L) Same as (I) but stained with an anti-γH2AX antibody.
(M) Same as (L) but stained with an anti-53BP1 antibody. Arrows point to examples of 53BP1 foci-positive cells.
(N) Quantitation of (L) and (M). A total of 100 cells from each indicated group were examined for γH2AX and 53BP1 foci formation. Mean of three independent experiments with SD.
See also Figure S6.

SUPPLEMENTAL INFORMATION

Supplemental Information includes six figures and Supplemental Experimental Procedures and can be found with this article online at doi:10.1016/j.devcel.2011.10.010.

ACKNOWLEDGMENTS

We thank Dr. Kathy Wilson and Igor Makhlin for reagents, other laboratory members for critical discussion, and Dr. Xinying Zhuang for technical assistance. We thank Drs. Hua-Ying Fan, Erica Golemis, and Maureen Murphy for critical reading of the manuscript. Z.T. performed most of the experiments, designed the experiments, and drafted the manuscript. K.M.A. contributed to Figure 4H and Figures S2C, S2D, S2F, S2G, and S4C. B.G.B. contributed to Figure 4D. J.P.N. contributed to initial observations that led to Figure 1A. N.B., B.X., and T.J.Y. provided critical materials and/or reagents. R.Z. conceived the study, designed experiments, and wrote the manuscript. R.Z. is an Ovarian Cancer Research Fund (OCRF) Liz Tilberis Scholar. This work was supported in part by an NCI FCCC-UPenn ovarian cancer SPORE (P50 CA083638) pilot project and SPORE career development award (to R.Z.), a DOD ovarian cancer academy award (OC093420 to R.Z.), and an OCRF program project (to R.Z.). B.G.B. is supported by an NCI postdoctoral training grant (CA-009035-35). We would like to acknowledge Anna Pecherskaya and Margret Einarson for help with quantitative image analysis and Emmanuelle Nicolas for help with microRNA qRT-PCR analysis.

Received: October 7, 2010
Revised: June 29, 2011
Accepted: October 11, 2011
Published online: December 1, 2011

REFERENCES

Ahlbory, D., Appl, H., Lang, D., and Klempnauer, K.H. (2005). Disruption of B-myb in DT40 cells reveals novel function for B-Myb in the response to DNA-damage. Oncogene *24*, 7127–7134.

Alimonti, A., Nardella, C., Chen, Z., Clohessy, J.G., Carracedo, A., Trotman, L.C., Cheng, K., Varmeh, S., Kozma, S.C., Thomas, G., et al. (2010). A novel type of cellular senescence that can be enhanced in mouse models and human tumor xenografts to suppress prostate tumorigenesis. J. Clin. Invest. *120*, 681–693.

Bartkova, J., Rezaei, N., Liontos, M., Karakaidos, P., Kletsas, D., Issaeva, N., Vassiliou, L.V., Kolettas, E., Niforou, K., Zoumpourlis, V.C., et al. (2006). Oncogene-induced senescence is part of the tumorigenesis barrier imposed by DNA damage checkpoints. Nature *444*, 633–637.

Braig, M., Lee, S., Loddenkemper, C., Rudolph, C., Peters, A.H., Schlegelberger, B., Stein, H., Dörken, B., Jenuwein, T., and Schmitt, C.A. (2005). Oncogene-induced senescence as an initial barrier in lymphoma development. Nature *436*, 660–665.

Campisi, J. (2005). Senescent cells, tumor suppression, and organismal aging: good citizens, bad neighbors. Cell *120*, 513–522.

Cantor, S.B., Bell, D.W., Ganesan, S., Kass, E.M., Drapkin, R., Grossman, S., Wahrer, D.C., Sgroi, D.C., Lane, W.S., Haber, D.A., and Livingston, D.M. (2001). BACH1, a novel helicase-like protein, interacts directly with BRCA1 and contributes to its DNA repair function. Cell *105*, 149–160.

Cao, L., Li, W., Kim, S., Brodie, S.G., and Deng, C.X. (2003). Senescence, aging, and malignant transformation mediated by p53 in mice lacking the Brca1 full-length isoform. Genes Dev. *17*, 201–213.

Chen, J., Silver, D.P., Walpita, D., Cantor, S.B., Gazdar, A.F., Tomlinson, G., Couch, F.J., Weber, B.L., Ashley, T., Livingston, D.M., and Scully, R. (1998). Stable interaction between the products of the BRCA1 and BRCA2 tumor suppressor genes in mitotic and meiotic cells. Mol. Cell *2*, 317–328.

Costanzi, C., and Pehrson, J.R. (1998). Histone macroH2A1 is concentrated in the inactive X chromosome of female mammals. Nature *393*, 599–601.

Di Micco, R., Fumagalli, M., Cicalese, A., Piccinin, S., Gasparini, P., Luise, C., Schurra, C., Garre', M., Nuciforo, P.G., Bensimon, A., et al. (2006). Oncogene-induced senescence is a DNA damage response triggered by DNA hyper-replication. Nature *444*, 638–642.

Di Micco, R., Sulli, G., Dobreva, M., Liontos, M., Botrugno, O.A., Gargiulo, G., dal Zuffo, R., Matti, V., d'Ario, G., Montani, E., et al. (2011). Interplay between oncogene-induced DNA damage response and heterochromatin in senescence and cancer. Nat. Cell Biol. *13*, 292–302.

Dimri, G.P., Lee, X., Basile, G., Acosta, M., Scott, G., Roskelley, C., Medrano, E.E., Linskens, M., Rubelj, I., Pereira-Smith, O., et al. (1995). A biomarker that identifies senescent human cells in culture and in aging skin in vivo. Proc. Natl. Acad. Sci. USA *92*, 9363–9367.

Durant, S.T., and Nickoloff, J.A. (2005). Good timing in the cell cycle for precise DNA repair by BRCA1. Cell Cycle *4*, 1216–1222.

Eelen, G., Vanden Bempt, I., Verlinden, L., Drijkoningen, M., Smeets, A., Neven, P., Christiaens, M.R., Marchal, K., Bouillon, R., and Verstuyf, A. (2008). Expression of the BRCA1-interacting protein Brip1/BACH1/FANCJ is driven by E2F and correlates with human breast cancer malignancy. Oncogene *27*, 4233–4241.

Erlandsson, F., Linnman, C., Ekholm, S., Bengtsson, E., and Zetterberg, A. (2000). A detailed analysis of cyclin A accumulation at the G(1)/S border in normal and transformed cells. Exp. Cell Res. *259*, 86–95.

Halazonetis, T.D., Gorgoulis, V.G., and Bartek, J. (2008). An oncogene-induced DNA damage model for cancer development. Science *319*, 1352–1355.

Huen, M.S., Sy, S.M., and Chen, J. (2010). BRCA1 and its toolbox for the maintenance of genome integrity. Nat. Rev. Mol. Cell Biol. *11*, 138–148.

Hurlin, P.J., Maher, V.M., and McCormick, J.J. (1989). Malignant transformation of human fibroblasts caused by expression of a transfected T24 HRAS oncogene. Proc. Natl. Acad. Sci. USA *86*, 187–191.

Kennedy, A.L., Morton, J.P., Manoharan, I., Nelson, D.M., Jamieson, N.B., Pawlikowski, J.S., McBryan, T., Doyle, B., McKay, C., Oien, K.A., et al. (2011). Activation of the PIK3CA/AKT pathway suppresses senescence induced by an activated RAS oncogene to promote tumorigenesis. Mol. Cell *42*, 36–49.

Krizhanovsky, V., Xue, W., Zender, L., Yon, M., Hernando, E., and Lowe, S.W. (2008). Implications of cellular senescence in tissue damage response, tumor suppression, and stem cell biology. Cold Spring Harb. Symp. Quant. Biol. *73*, 513–522.

Krum, S.A., la Rosa Dalugdugan, E., Miranda-Carboni, G.A., and Lane, T.F. (2010). BRCA1 forms a functional complex with γ-H2AX as a late response to genotoxic stress. J Nucleic Acids *2010*, 801594.

Kuilman, T., Michaloglou, C., Vredeveld, L.C., Douma, S., van Doorn, R., Desmet, C.J., Aarden, L.A., Mooi, W.J., and Peeper, D.S. (2008). Oncogene-induced senescence relayed by an interleukin-dependent inflammatory network. Cell *133*, 1019–1031.

Kumaraswamy, E., and Shiekhattar, R. (2007). Activation of BRCA1/BRCA2-associated helicase BACH1 is required for timely progression through S phase. Mol. Cell. Biol. *27*, 6733–6741.

Lafferty-Whyte, K., Cairney, C.J., Jamieson, N.B., Oien, K.A., and Keith, W.N. (2009). Pathway analysis of senescence-associated miRNA targets reveals common processes to different senescence induction mechanisms. Biochim. Biophys. Acta *1792*, 341–352.

Li, H., Cai, Q., Godwin, A.K., and Zhang, R. (2010). Enhancer of zeste homolog 2 promotes the proliferation and invasion of epithelial ovarian cancer cells. Mol. Cancer Res. *8*, 1610–1618.

Livingston, D.M. (2009). Cancer. Complicated supercomplexes. Science *324*, 602–603.

Lorvellec, M., Dumon, S., Maya-Mendoza, A., Jackson, D., Frampton, J., and García, P. (2010). B-Myb is critical for proper DNA duplication during an unperturbed S phase in mouse embryonic stem cells. Stem Cells *28*, 1751–1759.

Manke, I.A., Lowery, D.M., Nguyen, A., and Yaffe, M.B. (2003). BRCT repeats as phosphopeptide-binding modules involved in protein targeting. Science *302*, 636–639.

Martinez, I., Cazalla, D., Almstead, L.L., Steitz, J.A., and DiMaio, D. (2011). miR-29 and miR-30 regulate B-Myb expression during cellular senescence. Proc. Natl. Acad. Sci. USA *108*, 522–527.

Mason, D.X., Jackson, T.J., and Lin, A.W. (2004). Molecular signature of oncogenic ras-induced senescence. Oncogene *23*, 9238–9246.

Masselink, H., Vastenhouw, N., and Bernards, R. (2001). B-myb rescues ras-induced premature senescence, which requires its transactivation domain. Cancer Lett. *171*, 87–101.

Méndez, J., and Stillman, B. (2000). Chromatin association of human origin recognition complex, cdc6, and minichromosome maintenance proteins during the cell cycle: assembly of prereplication complexes in late mitosis. Mol. Cell. Biol. *20*, 8602–8612.

Michaloglou, C., Vredeveld, L.C., Soengas, M.S., Denoyelle, C., Kuilman, T., van der Horst, C.M., Majoor, D.M., Shay, J.W., Mooi, W.J., and Peeper, D.S. (2005). BRAFE600-associated senescence-like cell cycle arrest of human naevi. Nature *436*, 720–724.

Narita, M., Nũnez, S., Heard, E., Narita, M., Lin, A.W., Hearn, S.A., Spector, D.L., Hannon, G.J., and Lowe, S.W. (2003). Rb-mediated heterochromatin formation and silencing of E2F target genes during cellular senescence. Cell *113*, 703–716.

Narita, M., Narita, M., Krizhanovsky, V., Nuñez, S., Chicas, A., Hearn, S.A., Myers, M.P., and Lowe, S.W. (2006). A novel role for high-mobility group a proteins in cellular senescence and heterochromatin formation. Cell *126*, 503–514.

Peng, M., Litman, R., Jin, Z., Fong, G., and Cantor, S.B. (2006). BACH1 is a DNA repair protein supporting BRCA1 damage response. Oncogene *25*, 2245–2253.

Rodier, F., Coppé, J.P., Patil, C.K., Hoeijmakers, W.A., Muñoz, D.P., Raza, S.R., Freund, A., Campeau, E., Davalos, A.R., and Campisi, J. (2009). Persistent DNA damage signalling triggers senescence-associated inflammatory cytokine secretion. Nat. Cell Biol. *11*, 973–979.

Sartori, A.A., Lukas, C., Coates, J., Mistrik, M., Fu, S., Bartek, J., Baer, R., Lukas, J., and Jackson, S.P. (2007). Human CtIP promotes DNA end resection. Nature *450*, 509–514.

Scully, R., and Livingston, D.M. (2000). In search of the tumour-suppressor functions of BRCA1 and BRCA2. Nature *408*, 429–432.

Scully, R., Chen, J., Ochs, R.L., Keegan, K., Hoekstra, M., Feunteun, J., and Livingston, D.M. (1997a). Dynamic changes of BRCA1 subnuclear location and phosphorylation state are initiated by DNA damage. Cell *90*, 425–435.

Scully, R., Chen, J., Plug, A., Xiao, Y., Weaver, D., Feunteun, J., Ashley, T., and Livingston, D.M. (1997b). Association of BRCA1 with Rad51 in mitotic and meiotic cells. Cell *88*, 265–275.

Sy, S.M., Huen, M.S., and Chen, J. (2009). PALB2 is an integral component of the BRCA complex required for homologous recombination repair. Proc. Natl. Acad. Sci. USA *106*, 7155–7160.

Taddei, A., Maison, C., Roche, D., and Almouzni, G. (2001). Reversible disruption of pericentric heterochromatin and centromere function by inhibiting deacetylases. Nat. Cell Biol. *3*, 114–120.

Turner, N., Tutt, A., and Ashworth, A. (2004). Hallmarks of 'BRCAness' in sporadic cancers. Nat. Rev. Cancer *4*, 814–819.

Wang, B., Matsuoka, S., Ballif, B.A., Zhang, D., Smogorzewska, A., Gygi, S.P., and Elledge, S.J. (2007). Abraxas and RAP80 form a BRCA1 protein complex required for the DNA damage response. Science *316*, 1194–1198.

Xia, B., Sheng, Q., Nakanishi, K., Ohashi, A., Wu, J., Christ, N., Liu, X., Jasin, M., Couch, F.J., and Livingston, D.M. (2006). Control of BRCA2 cellular and clinical functions by a nuclear partner, PALB2. Mol. Cell *22*, 719–729.

Xu, B., Kim St, and, and Kastan, M.B. (2001). Involvement of Brca1 in S-phase and G(2)-phase checkpoints after ionizing irradiation. Mol. Cell. Biol. *21*, 3445–3450.

Xue, W., Zender, L., Miething, C., Dickins, R.A., Hernando, E., Krizhanovsky, V., Cordon-Cardo, C., and Lowe, S.W. (2007). Senescence and tumour clearance is triggered by p53 restoration in murine liver carcinomas. Nature *445*, 656–660.

Ye, Q., Hu, Y.F., Zhong, H., Nye, A.C., Belmont, A.S., and Li, R. (2001). BRCA1-induced large-scale chromatin unfolding and allele-specific effects of cancer-predisposing mutations. J. Cell Biol. *155*, 911–921.

Ye, X., Zerlanko, B., Zhang, R., Somaiah, N., Lipinski, M., Salomoni, P., and Adams, P.D. (2007). Definition of pRB- and p53-dependent and -independent steps in HIRA/ASF1a-mediated formation of senescence-associated heterochromatin foci. Mol. Cell. Biol. *27*, 2452–2465.

Yu, X., Wu, L.C., Bowcock, A.M., Aronheim, A., and Baer, R. (1998). The C-terminal (BRCT) domains of BRCA1 interact in vivo with CtIP, a protein implicated in the CtBP pathway of transcriptional repression. J. Biol. Chem. *273*, 25388–25392.

Yu, X., Chini, C.C., He, M., Mer, G., and Chen, J. (2003). The BRCT domain is a phospho-protein binding domain. Science *302*, 639–642.

Zhang, R., Poustovoitov, M.V., Ye, X., Santos, H.A., Chen, W., Daganzo, S.M., Erzberger, J.P., Serebriiskii, I.G., Canutescu, A.A., Dunbrack, R.L., et al. (2005). Formation of MacroH2A-containing senescence-associated heterochromatin foci and senescence driven by ASF1a and HIRA. Dev. Cell *8*, 19–30.

Zhang, R., Chen, W., and Adams, P.D. (2007a). Molecular dissection of formation of senescence-associated heterochromatin foci. Mol. Cell. Biol. *27*, 2343–2358.

Zhang, R., Liu, S.T., Chen, W., Bonner, M., Pehrson, J., Yen, T.J., and Adams, P.D. (2007b). HP1 proteins are essential for a dynamic nuclear response that rescues the function of perturbed heterochromatin in primary human cells. Mol. Cell. Biol. *27*, 949–962.

Zhang, F., Ma, J., Wu, J., Ye, L., Cai, H., Xia, B., and Yu, X. (2009). PALB2 links BRCA1 and BRCA2 in the DNA-damage response. Curr. Biol. *19*, 524–529.

Published OnlineFirst December 5, 2011; DOI:10.1158/1940-6207.CAPR-11-0414

Cancer Prevention Research

ALDH1A1 Is a Novel EZH2 Target Gene in Epithelial Ovarian Cancer Identified by Genome-Wide Approaches

Hua Li, Benjamin G. Bitler, Vinod Vathipadiekal, et al.

Cancer Prev Res 2012;5:484-491. Published OnlineFirst December 5, 2011.

Published OnlineFirst December 5, 2011; DOI:10.1158/1940-6207.CAPR-11-0414

Research Article

Cancer Prevention Research

ALDH1A1 Is a Novel EZH2 Target Gene in Epithelial Ovarian Cancer Identified by Genome-Wide Approaches

Hua Li[1], Benjamin G. Bitler[1], Vinod Vathipadiekal[4], Marie E. Maradeo[2], Michael Slifker[3], Caretha L. Creasy[5], Peter J. Tummino[5], Paul Cairns[2], Michael J. Birrer[4], and Rugang Zhang[1]

Abstract

Epithelial ovarian cancer (EOC) remains the most lethal gynecologic malignancy in the United States. EZH2 silences gene expression through trimethylating lysine 27 on histone H3 (H3K27Me3). EZH2 is often overexpressed in EOC and has been suggested as a target for EOC intervention. However, EZH2 target genes in EOC remain poorly understood. Here, we mapped the genomic loci occupied by EZH2/H3K27Me3 using chromatin immunoprecipitation followed by next-generation sequencing (ChIP-seq) and globally profiled gene expression in EZH2-knockdown EOC cells. Cross-examination of gene expression and ChIP-seq revealed a list of 60 EZH2 direct target genes whose expression was upregulated more than 1.5-fold upon EZH2 knockdown. For three selected genes (*ALDH1A1*, *SSTR1*, and *DACT3*), we validated their upregulation upon EZH2 knockdown and confirmed the binding of EZH2/H3K27Me3 to their genomic loci. Furthermore, the presence of H3K27Me3 at the genomic loci of these EZH2 target genes was dependent upon EZH2. Interestingly, expression of ALDH1A1, a putative marker for EOC stem cells, was significantly downregulated in high-grade serous EOC ($n = 53$) compared with ovarian surface epithelial cells ($n = 10$, $P < 0.001$). Notably, expression of ALDH1A1 negatively correlated with expression of EZH2 ($n = 63$, Spearman $r = -0.41$, $P < 0.001$). Thus, we identified a list of 60 EZH2 target genes and established that *ALDH1A1* is a novel EZH2 target gene in EOC cells. Our results suggest a role for EZH2 in regulating EOC stem cell equilibrium via regulation of ALDH1A1 expression. *Cancer Prev Res; 5(3); 484–91. ©2011 AACR.*

Introduction

Epithelial ovarian cancer (EOC) accounts for more deaths than any other gynecologic malignancy in the United States. EOCs are classified into distinct histologic types including serous, mucinous, endometrioid, and clear cell (1). The most common histology of EOC is serous (~60% of all cancers) and less common histologies include endometrioid, clear cell, and mucinous (1). Recently, an alternative classification has been proposed, in which EOC is broadly divided into 2 types (2). Type I EOC includes mucinous, low-grade serous, low-grade endometrioid, and clear cell carcinomas, and type II EOC includes high-grade serous carcinomas, which is the most lethal histosubtype (2).

Enhancer of zeste homology 2 (EZH2) is a histone methyltransferase that mediates gene silencing by catalyzing the trimethylation on lysine 27 of histone H3 (H3K27Me3; ref. 3). EZH2 is often expressed at higher levels in human EOC cells, and its expression positively correlates with cell proliferation in these cells (4). Further underscoring the importance of EZH2 in EOC, EZH2 knockdown triggers apoptosis and inhibits the invasion of human EOC cells (4). In addition, EZH2 is overexpressed in ovarian tumor–associated endothelial cells, which promotes angiogenesis (5). Finally, there is evidence to suggest that EZH2 is overexpressed in ovarian cancer stem cell–like populations enriched by chemotherapy (6). Accordingly, EZH2 has been suggested as a putative target for developing EOC therapeutics. Thus, it is important to identify EZH2 target genes in EOC to gain insights into the biology of the disease and to facilitate translational EOC research related to EZH2. Although a number of EZH2 target genes have been characterized in a few cancer types, including prostate and breast, using chromatin immunoprecipitation (ChIP)-on-chip analysis (7, 8), studies that aim to globally identify EZH2 target genes in EOC cells have yet to be conducted.

Here, we report the identification of direct EZH2 target genes in human EOC cells using a combination of genome-wide approaches. Specifically, we identified the genomic loci occupied by EZH2/H3K27Me3 using ChIP followed by next-generation sequencing (ChIP-seq). In addition, we discovered a list of genes whose expression was upregulated

Authors' Affiliations: [1]Women's Cancer Program and Epigenetics and Progenitor Cell Keystone Program, [2]Cancer Biology Program, [3]Biostatistics and Bioinformatics Facility, Fox Chase Cancer Center, Philadelphia, Pennsylvania; [4]Massachusetts General Hospital Cancer Center and Harvard Medical School, Boston, Massachusetts; and [5]Cancer Epigenetics Discovery Performance Unit, Oncology R&D, GlaxoSmithKline Pharmaceuticals, Inc., Collegeville, Pennsylvania

Note: Supplementary data for this article are available at Cancer Prevention Research Online (http://cancerprevres.aacrjournals.org/).

Corresponding Author: Rugang Zhang, Fox Chase Cancer Center, W446, 333 Cottman Avenue, Philadelphia, PA 19111. Phone: 215-728-7108; Fax: 215-728-3616; E-mail: rugang.zhang@fccc.edu

doi: 10.1158/1940-6207.CAPR-11-0414

Published OnlineFirst December 5, 2011; DOI:10.1158/1940-6207.CAPR-11-0414

more than 1.5-fold in EZH2-knockdown EOC cells compared with controls using gene expression microarray analysis. Cross-examination of gene expression profiling and ChIP-seq analysis revealed a list of 60 genes that are direct EZH2/H3K27Me3 target genes, including 56 novel putative EZH2 target genes. For validation, we selected 3 genes that are implicated in regulating stem cells, apoptosis, cell growth, or invasion. We validated their upregulation upon EZH2 knockdown in EOC cells and confirmed the binding of EZH2/H3K27Me3 by ChIP analysis. Interestingly, expression of ALDH1A1, a putative marker for EOC stem cells (9–11), was expressed at significantly lower levels in high-grade serous EOC than in normal human ovarian surface epithelial (HOSE) cells and negatively correlated with expression of EZH2.

Materials and Methods

Cell culture, short hairpin RNA, lentivirus packaging and infection

The SKOV3 human EOC cell line was cultured according to the American Type Culture Collection and as previously described (4, 12). SKOV3 cell line identification was further confirmed by DNA Diagnostic Center. The sense sequences of 2 individual short hairpin RNAs (shRNA) to the human *EZH2* genes are as we have previously published (4). Lentivirus packaging was conducted using ViraPower system (Invitrogen) according to the manufacturer's instruction and as previously described (4). Briefly, SKOV3 cells at 40% to 50% confluency were infected with lentivirus expressing shRNA to EZH2 or vector control. The infected cells were drug selected with 3 μg/mL of puromycin to eliminate noninfected cells.

Antibodies, Western blot analysis, RNA isolation, and quantitative reverse-transcriptase PCR

The following antibodies were used for Western blot analysis: mouse anti-EZH2 (1:2,500; BD Bioscience), rabbit anti-H3K27Me3 (1:1,000; Cell Signaling), and mouse anti-GAPDH (1:10,000; Millipore). RNA from cultured human SKOV3 EOC cells was isolated using TRIzol (Invitrogen) according to the manufacturer's instruction. For quantitative reverse-transcriptase PCR (qRT-PCR), TRIzol-isolated RNA was further purified using an RNeasy kit (Qiagen) following the manufacturer's instruction. The primers for *ALDH1A1*, *SSTR1*, and *DACT3* genes used for qRT-PCR were purchased from Applied Biosystems. Expression of the housekeeping gene *β-2-microglobulin* was used to normalize mRNA expression.

ChIP-seq analysis and ChIP validation for selected EZH2 target genes

Briefly, SKOV3 cells were fixed with 1% formaldehyde for 15 minutes and quenched with 0.125 mol/L glycine. Chromatin was isolated by adding lysis buffer (1% SDS, 10 mmol/L EDTA, 50 mmol/L Tris-HCl, pH 8.1, 1 mmol/L phenylmethylsulfonylfluoride) followed by disruption with a Dounce homogenizer. Lysates were sonicated using a Misonix Sonicator 3000 to shear the DNA to an average length of 300 to 500 bp. Lysates were cleared by centrifugation to collect chromatin suspensions. Prior to their use in the ChIP protocol, protein A agarose beads (Invitrogen) were preblocked using blocking proteins and nucleic acids for 3 hours. For each ChIP reaction, an aliquot of chromatin (20–30 μg) was precleared with 30 μL preblocked protein A agarose beads for 1 to 2 hours. ChIP reactions were set up using precleared chromatin and antibody (anti-H3K27Me3, Millipore 07-449; anti-EZH2, Millipore 07-689) and incubated overnight at 4°C. Preblocked protein A agarose beads were added and incubation at 4°C was continued for another 3 hours. Agarose beads containing the immune complexes were washed, and the immune complexes eluted from the beads were subjected to RNase treatment at 37°C for 20 minutes and proteinase K treatment at 37°C for 3 hours. Cross-links were reversed, and ChIP DNAs were purified by phenol–chloroform extraction and ethanol precipitation.

ChIP DNA was amplified using the Illumina ChIP-Seq DNA Sample Prep Kit. In brief, DNA was resonicated and ends were polished and 5′-phosphorylated using T4 DNA polymerase, Klenow polymerase, and T4 polynucleotide kinase. After addition of 3′-A to the ends using Klenow fragment (3′–5′ exo minus), Illumina genomic adapters were ligated and the sample was size-fractionated (300–400 bp) on a 2% agarose gel. After a final PCR amplification step (18 cycles, Phusion polymerase), the resulting DNA libraries were quantified and tested by qPCR at the same specific genomic regions as the original ChIP DNA to assess quality of the amplification reactions. DNA libraries were sequenced on a Genome Analyzer II. Sequences (36-nucleotide reads) were aligned to the human genome (NCBI Build 37.1/hg19) using Eland software (Illumina). Aligned sequences were extended *in silico* at their 3′-ends to a length of 240 bp, which is the average genomic fragment length in the size-selected library, and assigned to 32-nucleotide bins along the genome. The resulting histograms were stored in BAR (Binary Analysis Results) files. Peak locations were determined using the MACS algorithm.

For validation of binding of EZH2/H3K27Me3 to the genomic loci of the selected EZH2/H3K27Me3 target genes, SKOV3 EOC cells were transduced with lentivirus encoding control or shEZH2. Drug-selected cells were subjected to ChIP analysis as previously described (13, 14). The following antibodies were used to conduct ChIP: anti-EZH2 (C11, BD Biosciences), anti-H3K27Me3 (C36B11, Cell Signalling), and anti-histone H3 (05-928, Millipore). An isotype-matched IgG was used a negative control. Immunoprecipitated DNA was analyzed with PCR against the genomic regions of *ALDH1A1* (forward: 5′-TGGCACTGGTTATTCAACGTGGTC-3′ and reverse: 5′-GAGGGTGGAAGCTCTTGTAGGTTT-3′), *DACT3* (forward: 5′-CACACACACACACAAACAGTGCCT-3′ and reverse: 5′-TTCCTCCAACTAGGCTGGCAGTTT-3′) and *SSTR1* (forward: 5′-TAGCCTAAGCTGCCTGCTGTGTTA-3′ and reverse: 5′-AAAGTGCATGTGCGGTCTGTTAGC-3′). PCR products were visualized on a 2% agarose gel.

Published OnlineFirst December 5, 2011; DOI:10.1158/1940-6207.CAPR-11-0414

Gene expression microarray analysis

For gene expression microarray analysis in SKOV3 cells, 500 ng of total RNA was amplified and labeled using Agilent QuickAmp labeling kit following the manufacturer's protocol. A total of 1.65 μg of Cy-3–labeled cRNA targets were hybridized onto Agilent 4 × 44 k whole genome arrays for 17 hours at 65°C and washed according to procedure described by Agilent. The hybridized slides were scanned at 5-μm resolution on an Agilent scanner (Agilent), and fluorescent intensities of hybridization signals are extracted using Agilent Feature Extraction software.

Data sets

Gene expression microarray data sets for 53 cases of laser capture and microdissected (LCM) high-grade serous EOC and 10 individual isolations of normal HOSE cells were obtained from Gene Expression Omnibus (GEO; http://www.ncbi.nlm.nih.gov/geo/; GEO accession number: GSE18521).

Statistical analysis

Quantitative data are expressed as mean ± SD unless otherwise stated. ANOVA with Fisher least significant difference (LSD) was used to identify significant differences in multiple comparisons. Spearman test was used to measure statistical dependence between EZH2 mRNA levels and ALDH1A1 mRNA levels. For all statistical analyses, the level of significance was set at 0.05.

Results and Discussion

Genome-wide mapping of EZH2/H3K27Me3 direct target genes in human EOC cells

To identify genes whose expression was suppressed by EZH2, we conducted gene expression microarray analysis in control and EZH2-knockdown SKOV3 human EOC cells. Two individual shRNAs to the human *EZH2* gene (shEZH2) were used to limit potential off-target effects. Knockdown efficacy was confirmed by immunoblotting analysis (Fig. 1A). EZH2 knockdown notably decreased the levels of H3K27Me3, which is consistent with the idea that EZH2 plays a major role in regulating the levels of H3K27Me3 in human EOC cells (Fig. 1A). A list of 148 genes and 501 genes were upregulated more than 1.5-fold by shEZH2#1 and shEZH2#2, respectively, whereas 128 genes overlapped between the 2 different shEZH2s (Fig. 1B). Further data can be found at GEO database upon publication (GEO access number: GSE31433). The difference in the number of the genes altered by 2 individual shEZH2s may be due to different degrees of EZH2 knockdown. Consistent with this possibility, shEZH2#2, which decreases EZH2 levels with better efficacy than shEZH2#1, resulted in a greater number of upregulated genes (Fig. 1A and B). Alternatively, the differences in gene upregulation observed with individual EZH2 shRNAs may be due to off-target effects. To avoid this potential issue, we chose to analyze the genes that are upregulated by both shEZH2s. Of note, some of the known EZH2 target genes were approaching the 1.5-fold upregulation cutoff point but were not included in further analysis, including *VASH1* (5) and *E-cadherin* (ref. 15; data not shown). Although the conservative approach we implemented may lead to missing certain EZH2 target genes, we felt these rigorous methods allowed us to minimize false-positive EZH2 target genes in human EOCs.

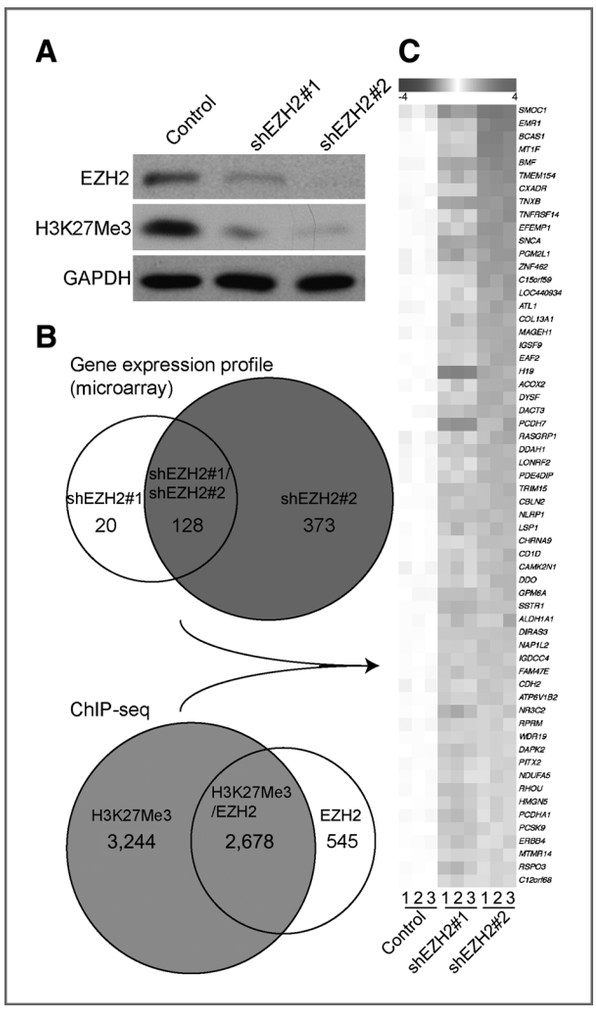

Figure 1. Identification of EZH2 target genes in human SKOV3 EOC cells. A, SKOV3 cells were infected with indicated lentivirus encoding shEZH2 or control. Drug-selected cells were examined for expression of EZH2, H3K27Me3, and GAPDH by immunoblotting analysis using indicated antibodies. B, schematic of experimental strategies used to identify EZH2 target genes. Genes whose expression was upregulated more than 1.5-fold upon EZH2 knockdown by 2 individual shEZH2 were identified by global gene expression microarray analysis. Genomic loci occupied by EZH2/H3K27Me3 were profiled by ChIP-seq analysis. C, cross-examination of gene expression profiling and ChIP-seq analysis as illustrated in (B) revealed a list of 60 putative EZH2 target genes in human SKOV3 EOC cells. GAPDH, glyceraldehyde-3-phosphate dehydrogenase.

We next sought to identify genomic loci that are directly bound by EZH2/H3K27Me3. Toward this goal, we conducted ChIP-seq analysis in SKOV3 human EOC cells using antibodies specific to EZH2 or H3K27Me3. EZH2 and H3K27Me3 occupancy was mapped to the genomic loci of

Published OnlineFirst December 5, 2011; DOI:10.1158/1940-6207.CAPR-11-0414

3,223 and 5,922 genes, respectively, and 2,678 genes were associated with both EZH2 and H3K27Me3 (Fig. 1B and Supplementary Table S1). The difference between the number of genes whose locus was occupied by EZH2 and H3K27Me3 may reflect the difference in affinity of the antibodies used for ChIP. Alternatively, for methylated sites not bound by EZH2, it is possible that other epigenetic regulators in addition to EZH2 can also generate H3K27Me3. Consistently, EZH1, a homolog of EZH2 in human cells, is also capable of catalyzing H3K27Me3 epigenetic modifications, albeit at a lower rate than EZH2 (16). Furthermore, genes bound by EZH2, but not H3K27Me3, may reflect an H3K27Me3-independent function for EZH2 as previous reports have suggested (for example, see ref. 17).

To identify the genes that are directly silenced by EZH2, we cross-examined the gene expression and ChIP-seq data. As a result, we identified a list of 60 EZH2/H3K27Me3 target genes whose expression was upregulated more than 1.5-fold upon EZH2 knockdown in SKOV3 human EOC cells (Fig. 1C). Further confirming our approach, 4 of the 60 identified genes have previously been shown as EZH2/H3K27Me3 target genes, namely, *SNAC* (18), *H19* (19), *DIRAS3* (20), and *DACT3* (21). Notably, Ingenuity networks analysis revealed that the networks enriched by the identified genes included (i) cell death, growth, and proliferation (e.g., *BMF*, *DAPK2*, *NLRP1*, and *DIRAS3*) and (ii) reproductive system development and cancer (e.g., *EAF2*, *ALDH1A1*, *SSTR1*, and *MAGEH1*; data not shown). This is consistent with the proliferation-promoting and apoptosis-suppressing function of EZH2, which we have previously reported in human EOC cells (4).

Interestingly, the number of genes upregulated more than 1.5-fold upon EZH2 knockdown is notably lower than the number of genes whose genomic loci are directly occupied by EZH2/H3K27Me3 (Fig. 1B). This result suggests that additional mechanisms may cooperate with EZH2/H3K27Me3 in silencing or reactivating EZH2 target genes. Consistent with this idea, previous reports have shown that EZH2 target genes are also subject to epigenetic silencing by H3K9Me3 (22) or histone deacetylase (23). This implies that to achieve maximum reactivation of EZH2/H3K27Me3-silenced target genes in human EOC cells, additional epigenetic gene silencing mechanisms may be considered for simultaneous targeting together with EZH2 inhibition. Alternatively, this result may be due to the bivalent modification (i.e., H3K27Me3 and H3K4Me3) at the genomic loci of those upregulated genes, which primes those genes for activation while keeping them silenced (24). Further studies are warranted to differentiate these possibilities.

Validation of the selected EZH2 target genes in human EOC cells

The list of upregulated genes was prioritized for validation by examining their expression in the newly released the Cancer Genomics Atlas (TCGA) ovarian database (25). We first chose those genes whose expression was downregulated more than 2-fold in more than 75% of EOC cases in TCGA ovarian database. In addition, known imprinted genes such as *H19* (19) and *DIRAS3* (20) or poorly annotated genes were excluded. Given that EZH2 promotes proliferation and invasion, suppresses apoptosis, and regulates stem cell–like population in human EOCs (4, 6), we selected 3 identified EZH2/H3K27Me3 target genes with one or more of these roles for validation studies. Those genes are *ALDH1A1* (11), *SSTR1* (26), and *DACT3* (ref. 21; Table 1).

We first validated the upregulation of the selected 3 genes in EZH2-knockdown SKOV3 human EOC cells by qRT-PCR. Indeed, all 3 selected genes were significantly upregulated in shEZH2-expressing SKOV3 cells compared with controls (Fig. 2, $P < 0.05$ vs. controls.). In addition, all 3 genes were upregulated by both shEZH2s, and there was a correlation between the degree of EZH2 knockdown and the levels of upregulation of these genes (Figs. 1A and 2). We conclude that EZH2 knockdown upregulates the expression of *ALDH1A1*, *SSTR1*, and *DACT3* in SKOV3 human EOC cells.

Next, we sought to validate the binding of EZH2/H3K27Me3 to the genomic loci of the selected genes. Toward this goal, we conducted ChIP analysis using antibodies specific to EZH2 or H3K27Me3, respectively. An isotype-matched IgG was used as a negative control, and an antibody to the core histone H3 was used as a positive control for ChIP analysis. Indeed, we observed the binding of both EZH2 and H3K27Me3 to the genomic loci of the selected EZH2 target genes in SKOV3 human EOC cells as determined by ChIP analysis (Fig. 3).

Table 1. Three putative EZH2 target genes identified by genome-wide approaches selected for further validation

Gene name	Location	Function	% TCGA cases downregulated >2-fold
NM_000689 ALDH1A1	9q21.13	Cancer stem cell marker	96
NM_001049 SSTR1	14q13	Proliferation and invasion inhibitor, cell signaling	95
NM_145056 DACT3	19q13.32	Apoptosis inducer, Wnt signaling antagonist	76

Published OnlineFirst December 5, 2011; DOI:10.1158/1940-6207.CAPR-11-0414

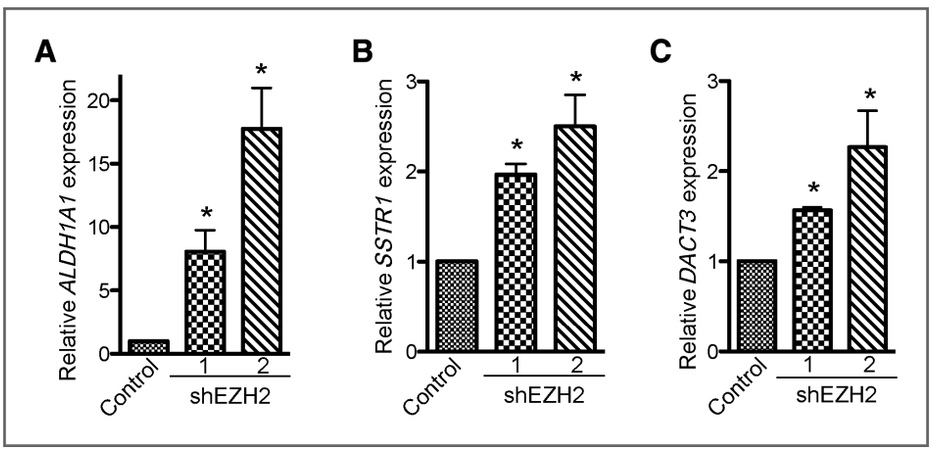

Figure 2. Validation of upregulation of the selected EZH2-silenced target genes in SKOV3 human EOC cells upon EZH2 knockdown by qRT-PCR. SKOV3 cells were infected with lentivirus encoding the indicated shEZH2s or control. After drug selection, mRNA was extracted and examined for expression of (A) *ALDH1A1* mRNA, (B) *SSTR1* mRNA, and (C) *DACT3* mRNA by qRT-PCR. Expression of *β-2-microglobulin* was used to normalize the expression of ALDH1A1, SSTR1 and DACT3 mRNA. *, $P < 0.05$ compared with controls.

We next sought to determine whether the occupancy of H3K27Me3 on the genomic loci of EZH2 target genes depends upon EZH2. Toward this goal, we conducted the ChIP analysis in EZH2-knockdown SKOV3 EOC cells. Indeed, knockdown of EZH2 severely weakened the association of both EZH2 and H3K27Me3 to the genomic loci of the selected EZH2 target genes (Fig. 3). This result suggests that EZH2 plays a major role in regulating H3K27Me3 modification on the genomic loci of these genes in human EOC cells. This result also implies that the binding of EZH2/H3K27Me3 to the genomic loci of these genes we observed here is specific.

Expression of EZH2 inversely correlates with expression of ALDH1A1

We next sought to determine whether there is an inverse correlation between expression of EZH2 and expression of the EZH2 target genes that we have identified and validated in this study. In addition to EOC cells, EZH2 is upregulated

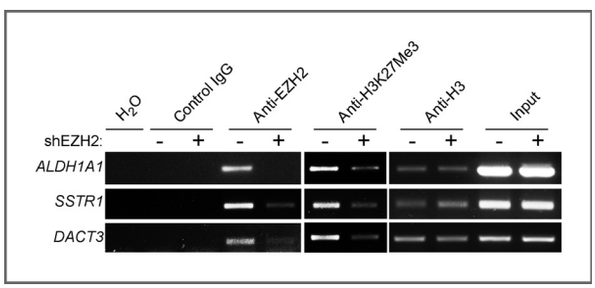

Figure 3. Validation of occupancy of the genomic loci of the selected EZH2 target genes by EZH2 and H3K27Me3 in SKOV3 human EOC cells using ChIP analysis. Control and shEZH2#2-expressing SKOV3 cells were subjected to ChIP analysis using antibodies specific to EZH2 or H3K27Me3, respectively. An isotype-matched IgG was used as a negative control, and an antibody specific to core histone H3 was used as a positive control. After ChIP analysis, the genomic loci of the indicated genes were subjected to PCR amplification using primers detailed in Materials and Methods. Please see Fig. 1A for shEZH2 knockdown efficacy. Shown are representative images of 3 independent experiments. Note that for H3K27Me3 ChIP, a low number of PCR cycles were used compared with EZH2 or histone H3 ChIP to avoid oversaturation of signals.

in ovarian tumor–associated endothelial cells (5). To limit the confounding effects of EOC-associated stromal cells (including EOC-associated endothelial cells), we chose to analyze the correlation between expression of EZH2 and its target genes in specimens from LCM high-grade serous subtype EOC, which accounts for the majority of EOC-associated mortalities (27).

EZH2 is expressed at higher levels in human EOC cells than in normal HOSE cells (4). Therefore, we hypothesized that EZH2 target genes that are silenced by EZH2 would be expressed at lower levels in human EOC cells. Toward testing this hypothesis, we examined the expression of EZH2 and the 3 validated EZH2 target genes in a published microarray database, which compares the gene expression profile in 53 cases of LCM high-grade serous EOCs and 10 individual isolations of primary HOSE cells (28). Consistent with our previous report (4), EZH2 was expressed at significantly higher levels in human EOCs than in primary HOSE cells ($P < 0.001$; Fig. 4A and B). Notably, the EZH2 target gene *ALDH1A1* was expressed at significantly lower levels in human EOCs than in normal HOSE cells ($P < 0.001$; Fig. 4C and D). Indeed, there was a negative correlation between expression of *EZH2* and its target gene *ALDH1A1* in a Spearman statistical analysis of the cases including both EOC and primary HOSE cells ($P < 0.001$ and $r = -0.41$; Fig. 4E, including both open circles and solid dots). However, the coefficiency Spearman r is 0.41. This result indicates that other factors may also play a role in the expression relation. Consistently, there is evidence to suggest that Notch signaling also regulates ALDH1A1 expression (29). In addition, the correlation between expression of EZH2 and ALDH1A1 is not significant among EOC cases ($P = 0.81$; Fig. 4E, solid dots only). This may be due to the fact the ALDH1A1 is expressed at very low levels in the vast majority of EOC cases, and thus, the variation in expression may simply be a reflection of experimental variations.

Comparing EOCs with normal HOSE cells, *ALDH1A1* showed a high fold change in expression (>8-fold), whereas *SSTR1* (~3.5-fold) or *DACT3* (<1.5-fold) only showed a moderate to minimal fold change in expression (Fig. 4D and Supplementary Fig. S1). It is possible that EZH2 is the

Published OnlineFirst December 5, 2011; DOI:10.1158/1940-6207.CAPR-11-0414

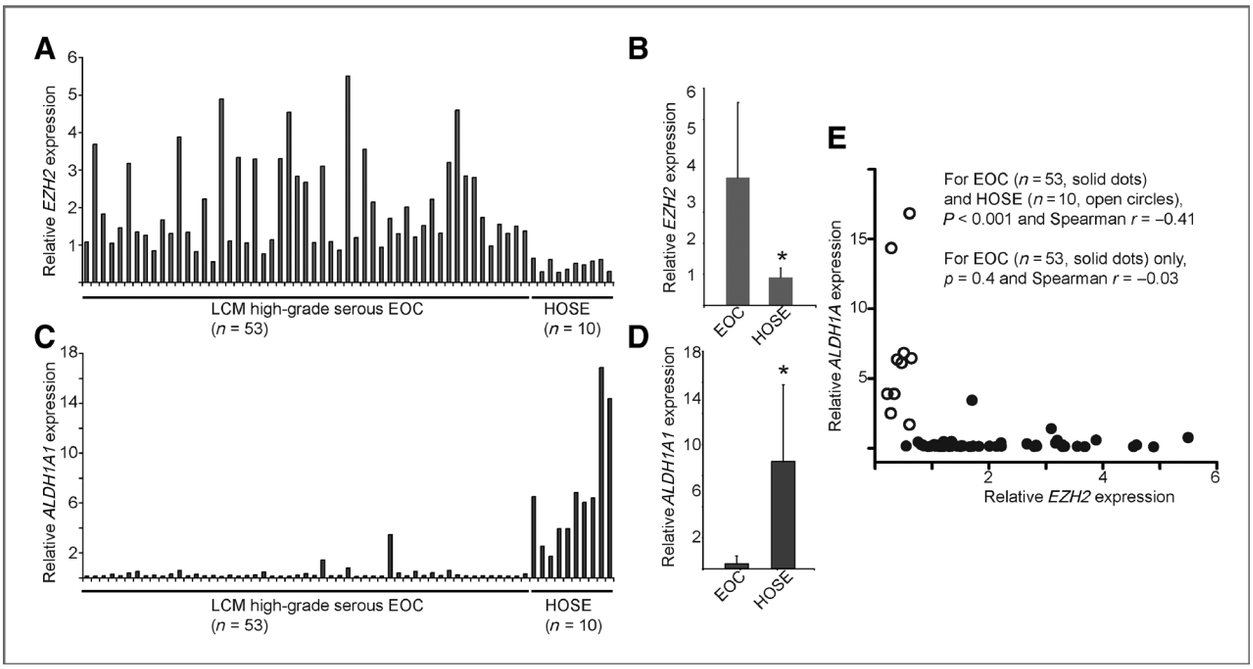

Figure 4. EZH2 targets ALDH1A1 in high-grade serous subtype EOC. A, relative expression of *EZH2* mRNA in 53 cases of LCM high-grade serous EOC and 10 individual isolations of normal HOSE cells. B, quantitation of (A). *, $P < 0.001$ compared with high-grade serous EOC. C, same as (A), but for relative expression of *ALDH1A1* mRNA. D, quantitation of (C). *, $P < 0.001$ compared with high-grade serous EOC. E, correlation between expression of *ALDH1A1* and *EZH2* as determined by Spearman statistical analysis using GraphPad Prism version 5.0 software.

major epigenetic regulator of ALDH1A1, whereas additional epigenetic silencing mechanisms may contribute to suppression of the other 2 validated EZH2 target genes. In support of this possibility, EZH2 knockdown induced much greater levels of upregulation for ALDH1A1 (up to 22-fold) than the other 2 EZH2 target genes (Fig. 2).

Next, we sought to examine the correlation between expression of EZH2 or ALDH1A1 and survival of patients with high-grade serous EOC. Consistent with our previous report (4), the difference in overall survival between high and low EZH2 expression in patients with high-grade serous EOC was not significant ($P = 0.1684$; Supplementary Fig. S2). In addition, the difference in survival between low ALDH1A1 expression group and high ALDH1A1 group was not significant ($P = 0.7789$; Supplementary Fig. S2). In contrast to our results, high ALDH1A has previously been reported to be associated with poor prognosis in patients with EOC (10, 30). The basis for this discrepancy remains to be determined. However, the discrepancy could be due to different methods that were used in this study (microarray) versus the other 2 studies (immunohistochemical staining).

ALDH1A1 has been reported as a marker of cancer stem cells in certain types of cancers including breast and ovarian (10, 29, 31–33). Likewise, EZH2 plays an important role in stem cell biology (34). Our data suggest that EZH2 directly regulates the levels of ALDH1A1 in EOC cells, implying that EZH2 may regulate the EOC stem cell population by controlling the levels of ALDH1A1 expression. Similarly, it has been shown that EZH2 directly regulates the epigenetic status of Nanog, an important factor for both embryonic stem cell and induced pluripotent stem cells, to balance the equilibrium between self-renewal and differentiation of stem cells (35). Similarly, other putative markers of cancer stem cells [such as CD133 (ref. 36) and TACSTD2 (ref. 37)] have been also reported to be hypermethylated in cancerous cells. While the expression in stem cells will be masked by the vastly more abundant non–stem cell population in our or any similar analysis, it is nevertheless intriguing that differential expression of ALDH1A1 has been described as a marker of stemness in cancer, including in EOC (10, 33). Together, our data suggest that EZH2 may regulate the EOC stem cell population by controlling the levels of ALDH1A1 expression. Our future work will test this hypothesis.

In the present study, using a combination of global gene expression profiling and genome-wide ChIP-seq analysis, we identified a list of 60 EZH2 direct target genes, whose expression was upregulated more than 1.5-fold upon EZH2 knockdown in human EOC cells. These genes include 56 novel putative EZH2 target genes and 4 known EZH2 target genes. We validated 3 selected EZH2 target genes that are implicated in regulating cancer stem cells, cell proliferation, apoptosis, and cell invasion. We showed that ALDH1A1, a putative marker of EOC stem cells (11), was expressed at lower levels in high-grade serous EOCs than in normal HOSE cells, and there was a negative correlation between expression of EZH2 and expression of ALDH1A1. Further studies are warranted to mine the data presented here as well as functional characterization of the identified EZH2 target genes. These studies should provide important insights

Published OnlineFirst December 5, 2011; DOI:10.1158/1940-6207.CAPR-11-0414

into the biology of EOC development and the identification of potential candidate targets for prevention and intervention of EOC.

Disclosure of Potential Conflicts of Interest

C.L. Creasy and P.J. Tummino are employees and stockholders of GlaxoSmithKline Pharmaceuticals. No potential conflicts of interests were disclosed by other authors.

Acknowledgments

The authors thank Dr. Katherine Aird for critical reading of the manuscript, members of laboratory of R. Zhang for discussion, and Dr. Yue-Sheng Li at the genomics facility of Fox Chase Cancer Center for technical assistance.

Grant Support

This work was supported in part by a NCI FCCC-UPenn ovarian cancer SPORE (P50 CA083638) pilot project and SPORE career development award (to R. Zhang) and a DOD ovarian cancer academy award (OC093420 to R. Zhang). B.G. Bitler is supported by an NCI postdoctoral training grant (CA-009035-35). R. Zhang is an Ovarian Cancer Research Fund (OCRF) Liz Tilberis Scholar.

The costs of publication of this article were defrayed in part by the payment of page charges. This article must therefore be hereby marked *advertisement* in accordance with 18 U.S.C. Section 1734 solely to indicate this fact.

Received August 24, 2011; revised November 10, 2011; accepted November 14, 2011; published OnlineFirst December 5, 2011.

References

1. Farley J, Ozbun LL, Birrer MJ. Genomic analysis of epithelial ovarian cancer. Cell Res 2008;18:538–48.
2. Shih Ie M, Kurman RJ. Ovarian tumorigenesis: a proposed model based on morphological and molecular genetic analysis. Am J Pathol 2004;164:1511–8.
3. Cao R, Wang L, Wang H, Xia L, Erdjument-Bromage H, Tempst P, et al. Role of histone H3 lysine 27 methylation in Polycomb-group silencing. Science 2002;298:1039–43.
4. Li H, Cai Q, Godwin AK, Zhang R. Enhancer of zeste homolog 2 promotes the proliferation and invasion of epithelial ovarian cancer cells. Mol Cancer Res 2010;8:1610–8.
5. Lu C, Han HD, Mangala LS, Ali-Fehmi R, Newton CS, Ozbun L, et al. Regulation of tumor angiogenesis by EZH2. Cancer Cell 2010;18:185–97.
6. Rizzo S, Hersey JM, Mellor P, Dai W, Santos-Silva A, Liber D, et al. Ovarian cancer stem cell like side populations are enriched following chemotherapy and overexpress EZH2. Mol Cancer Ther 2011;10:325–35.
7. Kondo Y, Shen L, Cheng AS, Ahmed S, Boumber Y, Charo C, et al. Gene silencing in cancer by histone H3 lysine 27 trimethylation independent of promoter DNA methylation. Nat Genet 2008;40:741–50.
8. Tan J, Yang X, Zhuang L, Jiang X, Chen W, Lee PL, et al. Pharmacologic disruption of Polycomb-repressive complex 2-mediated gene repression selectively induces apoptosis in cancer cells. Genes Dev 2007;21:1050–63.
9. Kryczek I, Liu S, Roh M, Vatan L, Szeliga W, Wei S, et al. Expression of aldehyde dehydrogenase and CD133 defines ovarian cancer stem cells. Int J Cancer 2012;130:29–39.
10. Landen CN Jr, Goodman B, Katre AA, Steg AD, Nick AM, Stone RL, et al. Targeting aldehyde dehydrogenase cancer stem cells in ovarian cancer. Mol Cancer Ther 2010;9:3186–99.
11. Silva IA, Bai S, McLean K, Yang K, Griffith K, Thomas D, et al. Aldehyde dehydrogenase in combination with CD133 defines angiogenic ovarian cancer stem cells that portend poor patient survival. Cancer Res 2011;71:3991–4001.
12. Bitler BG, Nicodemus JP, Li H, Cai Q, Wu H, Hua X, et al. Wnt5a suppresses epithelial ovarian cancer by promoting cellular senescence. Cancer Res 2011;71:6184–94.
13. Zhang R, Chen W, Adams PD. Molecular dissection of formation of senescence-associated heterochromatin foci. Mol Cell Biol 2007;27:2343–58.
14. Tu Z, Aird KM, Bitler BG, Nicodemus JP, Beeharry N, Xia B, et al. Oncogenic RAS regulates BRIP1 expression to induce dissociation of BRCA1 from chromatin, inhibit DNA repair, and promote senescence. Dev Cell 2011;21:1077–91.
15. Cao Q, Yu J, Dhanasekaran SM, Kim JH, Mani RS, Tomlins SA, et al. Repression of E-cadherin by the polycomb group protein EZH2 in cancer. Oncogene 2008;27:7274–84.
16. Margueron R, Li G, Sarma K, Blais A, Zavadil J, Woodcock CL, et al. Ezh1 and Ezh2 maintain repressive chromatin through different mechanisms. Mol Cell 2008;32:503–18.
17. Shi B, Liang J, Yang X, Wang Y, Zhao Y, Wu H, et al. Integration of estrogen and Wnt signaling circuits by the polycomb group protein EZH2 in breast cancer cells. Mol Cell Biol 2007;27:5105–19.
18. Yu J, Rhodes DR, Tomlins SA, Cao X, Chen G, Mehra R, et al. A polycomb repression signature in metastatic prostate cancer predicts cancer outcome. Cancer Res 2007;67:10657–63.
19. Pasini D, Bracken AP, Hansen JB, Capillo M, Helin K. The polycomb group protein Suz12 is required for embryonic stem cell differentiation. Mol Cell Biol 2007;27:3769–79.
20. Lu Z, Luo RZ, Lu Y, Zhang X, Yu Q, Khare S, et al. The tumor suppressor gene ARHI regulates autophagy and tumor dormancy in human ovarian cancer cells. J Clin Invest 2008;118:3917–29.
21. Jiang X, Tan J, Li J, Kivimae S, Yang X, Zhuang L, et al. DACT3 is an epigenetic regulator of Wnt/beta-catenin signaling in colorectal cancer and is a therapeutic target of histone modifications. Cancer Cell 2008;13:529–41.
22. Hawkins RD, Hon GC, Lee LK, Ngo Q, Lister R, Pelizzola M, et al. Distinct epigenomic landscapes of pluripotent and lineage-committed human cells. Cell Stem Cell 2010;6:479–91.
23. van der Vlag J, Otte AP. Transcriptional repression mediated by the human polycomb-group protein EED involves histone deacetylation. Nat Genet 1999;23:474–8.
24. Bernstein BE, Mikkelsen TS, Xie X, Kamal M, Huebert DJ, Cuff J, et al. A bivalent chromatin structure marks key developmental genes in embryonic stem cells. Cell 2006;125:315–26.
25. Cancer Genome Atlas Research Network. Integrated genomic analyses of ovarian carcinoma. Nature 2011;474:609–15.
26. Pyronnet S, Bousquet C, Najib S, Azar R, Laklai H, Susini C. Antitumor effects of somatostatin. Mol Cell Endocrinol 2008;286:230–7.
27. Kurman RJ, Shih Ie M. The origin and pathogenesis of epithelial ovarian cancer: a proposed unifying theory. Am J Surg Pathol 2010;34:433–43.
28. Mok SC, Bonome T, Vathipadiekal V, Bell A, Johnson ME, Wong KK, et al. A gene signature predictive for outcome in advanced ovarian cancer identifies a survival factor: microfibril-associated glycoprotein 2. Cancer Cell 2009;16:521–32.
29. Sullivan JP, Spinola M, Dodge M, Raso MG, Behrens C, Gao B, et al. Aldehyde dehydrogenase activity selects for lung adenocarcinoma stem cells dependent on notch signaling. Cancer Res 2010;70:9937–48.
30. Deng S, Yang X, Lassus H, Liang S, Kaur S, Ye Q, et al. Distinct expression levels and patterns of stem cell marker, aldehyde dehydrogenase isoform 1 (ALDH1), in human epithelial cancers. PLoS One 2010;5:e10277.
31. Tanner B, Hengstler JG, Dietrich B, Henrich M, Steinberg P, Weikel W, et al. Glutathione, glutathione S-transferase alpha and pi, and aldehyde dehydrogenase content in relationship to drug resistance in ovarian cancer. Gynecol Oncol 1997;65:54–62.
32. Ginestier C, Hur MH, Charafe-Jauffret E, Monville F, Dutcher J, Brown M, et al. ALDH1 is a marker of normal and malignant human mammary

Published OnlineFirst December 5, 2011; DOI:10.1158/1940-6207.CAPR-11-0414

stem cells and a predictor of poor clinical outcome. Cell Stem Cell 2007;1:555–67.

33. Yang X, Lin X, Zhong X, Kaur S, Li N, Liang S, et al. Double-negative feedback loop between reprogramming factor LIN28 and microRNA let-7 regulates aldehyde dehydrogenase 1-positive cancer stem cells. Cancer Res 2010;70:9463–72.
34. Margueron R, Reinberg D. The Polycomb complex PRC2 and its mark in life. Nature 2011;469:343–9.
35. Villasante A, Piazzolla D, Li H, Gomez-Lopez G, Djabali M, Serrano M. Epigenetic regulation of Nanog expression by Ezh2 in pluripotent stem cells. Cell Cycle 2011;10:1488–98.
36. Yi JM, Tsai HC, Glockner SC, Lin S, Ohm JE, Easwaran H, et al. Abnormal DNA methylation of CD133 in colorectal and glioblastoma tumors. Cancer Res 2008;68:8094–103.
37. Ibragimova I, Ibanez de Caceres I, Hoffman AM, Potapova A, Dulaimi E, Al-Saleem T, et al. Global reactivation of epigenetically silenced genes in prostate cancer. Cancer Prev Res 2010;3:1084–92.

Cancer Research

Wnt5a Suppresses Epithelial Ovarian Cancer by Promoting Cellular Senescence

Benjamin G. Bitler, Jasmine P. Nicodemus, Hua Li, et al.

Cancer Res 2011;71:6184-6194. Published OnlineFirst August 4, 2011.

Published OnlineFirst August 4, 2011; DOI:10.1158/0008-5472.CAN-11-1341

Wnt5a Suppresses Epithelial Ovarian Cancer by Promoting Cellular Senescence

Benjamin G. Bitler[1], Jasmine P. Nicodemus[1], Hua Li[1], Qi Cai[2], Hong Wu[3], Xiang Hua[4], Tianyu Li[5], Michael J. Birrer[7], Andrew K. Godwin[8], Paul Cairns[6], and Rugang Zhang[1]

Abstract

Epithelial ovarian cancer (EOC) remains the most lethal gynecologic malignancy in the United States. Thus, there is an urgent need to develop novel therapeutics for this disease. Cellular senescence is an important tumor suppression mechanism that has recently been suggested as a novel mechanism to target for developing cancer therapeutics. Wnt5a is a noncanonical Wnt ligand that plays a context-dependent role in human cancers. Here, we investigate the role of Wnt5a in regulating senescence of EOC cells. We show that Wnt5a is expressed at significantly lower levels in human EOC cell lines and in primary human EOCs ($n = 130$) compared with either normal ovarian surface epithelium ($n = 31$; $P = 0.039$) or fallopian tube epithelium ($n = 28$; $P < 0.001$). Notably, a lower level of Wnt5a expression correlates with tumor stage ($P = 0.003$) and predicts shorter overall survival in EOC patients ($P = 0.003$). Significantly, restoration of Wnt5a expression inhibits the proliferation of human EOC cells both *in vitro* and *in vivo* in an orthotopic EOC mouse model. Mechanistically, Wnt5a antagonizes canonical Wnt/β-catenin signaling and induces cellular senescence by activating the histone repressor A/promyelocytic leukemia senescence pathway. In summary, we show that loss of Wnt5a predicts poor outcome in EOC patients and Wnt5a suppresses the growth of EOC cells by triggering cellular senescence. We suggest that strategies to drive senescence in EOC cells by reconstituting Wnt5a signaling may offer an effective new strategy for EOC therapy. *Cancer Res; 71(19); 6184–94. ©2011 AACR.*

Introduction

Cellular senescence is an important tumor suppression mechanism *in vivo* (1). In primary mammalian cells, cellular senescence can be triggered by various inducers including critically shortened telomeres and activated oncogenes (such as oncogenic *RAS*; ref. 1). Senescent cells are viable but nondividing (2). Senescent cells also exhibit several distinctive morphologic characteristics and molecular markers, including a large flat cellular morphology and expression of senescence-associated β-galactosidase (SA-β-gal) activity (3). In murine liver carcinoma and sarcoma models, reactivation of the tumor suppressor p53 induces senescence and is associated with tumor regression (4, 5). Hence, driving cancer cells to undergo cellular senescence represents a novel mechanism for developing cancer therapeutics (6, 7).

More than 85% of ovarian cancers are of epithelial origin (8). Epithelial ovarian cancers (EOC) are classified into distinct histologic types including serous, mucinous, endometrioid, and clear cell (9). The most common histology of EOC is serous (~60% of all cancers) and less common histologies include endometrioid, clear cell, and mucinous (9). Recently, an alternative classification has been proposed, in which EOC is broadly divided into 2 types (10). Type I EOC includes endometrioid, mucinous, low-grade serous, and clear-cell carcinomas, and type II EOC includes high-grade serous carcinomas (10). EOC remains the most lethal gynecologic malignancy in the United States (8). Thus, there is an urgent need to better understand the etiology of EOC to develop novel therapeutics for this devastating disease.

Wnt signaling is initiated by binding of the Wnt ligand to its cognate frizzled receptor (11). Canonical Wnt signaling results in stabilization of the key transcription factor β-catenin, which then translocates into the nucleus and drives expression of its target genes, such as *CCND1 (cyclin D1), FOSL1,* and *c-MYC* (12, 13). Canonical Wnt signaling is active in the putative somatic stem/progenitor cells of the coelomic epithelium of the mouse ovary (14). Underscoring the importance of Wnt signaling in EOC, in a murine ovarian cancer model, activation of canonical Wnt signaling cooperates with inactivation of the tumor suppressor PTEN in driving ovarian carcinogenesis (15). However, the role of Wnt signaling in EOC is not fully understood.

Authors' Affiliations: [1]Women's Cancer Program, [2]Biosample Repository Facility, [3]Department of Pathology, [4]Transgenic Facility, [5]Department of Bioinformatics and Biostatistics, and [6]Department of Surgical Oncology, Fox Chase Cancer Center, Philadelphia, Pennsylvania; [7]Massachusetts General Hospital Cancer Center, Boston, Massachusetts; and [8]University of Kansas Medical Center, Kansas City, Kansas

Note: Supplementary data for this article are available at Cancer Research Online (http://cancerres.aacrjournals.org/).

Corresponding Author: Rugang Zhang, W446, Fox Chase Cancer Center, 333 Cottman Avenue, Philadelphia, PA 19111. Phone: 215-728-7108; Fax: 215-728-3616; E-mail: rugang.zhang@fccc.edu

doi: 10.1158/0008-5472.CAN-11-1341

Published OnlineFirst August 4, 2011; DOI:10.1158/0008-5472.CAN-11-1341

Wnt5a is a noncanonical Wnt ligand that plays opposing roles in different types of cancer and has variable expression dependent on the cancer context (16). Specifically, in EOC the role of Wnt5a remains unclear. Thus, in this study, we investigated Wnt5a expression and its potential function in human EOC cells. We discovered that Wnt5a was expressed at significantly lower levels in primary human EOC compared with either primary human ovarian surface epithelium or fallopian tube epithelium. Notably, loss of Wnt5a expression was associated with tumor stage and predicted shorter overall survival in EOC patients. Significantly, Wnt5a reconstitution inhibited the growth of EOC cells both *in vitro* and *in vivo* in an orthotopic EOC mouse model by promoting cellular senescence. These studies show, for the first time, a functional role of the noncanonical Wnt ligand, Wnt5a, in promoting senescence. Importantly, they also suggest that promoting EOC cells to undergo senescence represents a potential novel strategy for developing urgently needed EOC therapeutics.

Materials and Methods

Cells and culture conditions

Primary human ovarian surface epithelial (HOSE) cells were isolated and cultured as previously described (17). Human EOC cell lines were obtained from American Type Culture Collection (ATCC) and were passaged for less than 6 months. EOC cell line identification was further confirmed by DNA Diagnostic Center (www.dnacenter.com). EOC cell lines were cultured according to ATCC in RPMI-1640 medium supplemented with 10% FBS. 5-Aza-cytidine (Aza-C; Sigma) was used at working concentration of 5 μmol/L (18).

Human ovarian specimens and immunohistochemistry

The protocol to evaluate deidentified human tissue specimens was approved by Fox Chase Cancer Center (FCCC) institutional review board. Ovarian tumor microarray and normal human ovary and fallopian tube specimens were obtained from the FCCC Biosample Repository Core Facility (BRCF). Histopathology of the selected specimens on the tumor microarrays was provided by BRCF. Immunohistochemistry (IHC) was conducted by using goat anti-Wnt5a polyclonal antibody (R&D Systems) and mouse anti–Ki-67 (Dako) with a DAKO EnVision System and the Peroxidase (DAB) kit (DAKO Corporation) following the manufacturer's instructions and as previously described (17). Wnt5a staining was scored in a double-blinded manner by Dr. Qi Cai at the BRCF, and a proportion of the cases were independently confirmed by Dr. Hong Wu, a board-certified pathologist, at the FCCC Department of Pathology.

Anchorage-independent soft agar colony formation assay

Soft agar assay were carried out as previously described (17). Briefly, 3,500 cells were resuspended in 0.35% low melt agarose dissolved in RPMI-1640 medium supplemented with 10% FBS and inoculated on top of 0.6% low melt agarose base in 6-well plates. After 2 weeks in culture, the plates were stained with 0.005% crystal violet, and the number of colonies was counted by using a dissecting microscope.

Retrovirus production, infection, and drug selection

The following retrovirus constructs were used: pBABE-puro was obtained from Addgene, hygro-pWZL-luciferase was a kind gift of Dr. Denise Connolly, and pBABE-Wnt5a was generated by using standard cloning protocol. Retrovirus packaging was done as previously described by using Phoenix packaging cells (19, 20). To increase infection efficacy, double virus infection was carried out. For drug selection, 3 μg/mL of puromycin was used for the OVCAR5 human EOC cell line.

Reverse transcriptase PCR, quantitative reverse transcriptase PCR, and immunoblotting

RNA from cultured primary HOSE cells or human EOC cell lines was isolated by using TRIzol (Invitrogen) according to manufacturer's instruction. For quantitative reverse transcriptase PCR (qRT-PCR), TRIzol-isolated RNA was further purified by using an RNeasy kit (QIAGEN) following manufacture's instruction. The *Wnt5a*, *CCND1, FOSL1,* and *c-MYC* primers used for qRT-PCR were purchased from SABiosciences. mRNA expression of the housekeeping gene β-2-microglobulin (B2M) was used to normalize mRNA expression. Soluble β-catenin was extracted, using a buffer that consisting of 10 mmol/L Tris-HCl (pH 7.5), 0.05% NP-40, 10 mmol/L NaCl, 3 mmol/L $MgCl_2$, 1 mmol/L EDTA, and protease inhibitors (Roche) as previously described (21, 22). The following antibodies were used for immunoblotting from the indicated suppliers, goat anti-Wnt5a (R&D Systems), mouse β-actin (Sigma), mouse anti-GAPDH (Millipore), mouse anti-β-catenin, mouse anti-Rb (BD Biosciences), and rabbit anti-pRBpS780 (Cell Signaling).

Immunofluorescence and SA-β-gal staining

Indirect immunofluorescence staining was carried out as previously described (19, 20, 22). The following antibodies were used for immunofluorescence: a cocktail of mouse anti-HIRA monoclonal antibodies (WC19, WC117, and WC119; 1:10; ref. 20) and a rabbit anti-PML antibody (Chemicon, 1:5,000). Images were captured by a DS-QilMc camera on a Nikon Eclipse 80i microscope and processed by NIS-Elements BR3.0 software (Nikon). SA-β-gal staining was carried out as described previously (3, 23). For SA-β-gal staining in sections from xenografted tumors, 8 separate fields were examined from 2 individual tumors for each of the groups.

In vivo orthotopic xenograft tumorigenesis study

The protocol was approved by the FCCC Institutional Animal Care and Use Committee. OVCAR5 cells were infected with a luciferase-encoding retrovirus (hygro-pWZL-luciferase) and infected cells were selected with 50 μg/mL hygromycin. Drug-selected cells were then infected with control or Wnt5a-encoding retrovirus and subsequently selected with 3 μg/mL puromycin and 50 μg/mL hygromycin. A total of 3×10^6 drug-selected cells were unilaterally injected into the ovarian bursa sac of immunocompromised mice (6 mice per group; ref. 24). From day 10 postinfection, tumors were visualized by injecting luciferin (intraperitoneal, 4 mg/mice) resuspended in PBS and

Published OnlineFirst August 4, 2011; DOI:10.1158/0008-5472.CAN-11-1341

imaged with an IVIS Spectrum imaging system every 5 days until day 30. Images were analyzed by Live Imaging 4.0 software. At day 30, tumors were surgically dissected and either fixed in 10% formalin or fresh-frozen in Optimal Cutting Temperature compound (Tissue-Tek). Sections of the dissected tumors were processed by the FCCC Histopathology Core Facility.

Statistical analysis

Quantitative data are expressed as mean ± SD, unless otherwise indicated. ANOVA with Student's t test was used to identify significant differences in multiple comparisons. The Pearson χ^2 test was used to analyze the relationship between categorical variables. Overall survival was defined as the time elapsed from the date of diagnosis and the date of death from any cause or the date of last follow-up. Kaplan–Meier survival plots were generated and comparisons were made by using the log-rank sum statistic. For all statistical analyses, the level of significance was set at 0.05.

Results

Wnt5a is expressed at significantly lower levels in human EOC cell lines and primary human EOCs compared with normal human ovarian surface epithelium or fallopian tube epithelium

To determine Wnt5a expression in human EOC cell lines and primary HOSE cells, we examined the relative Wnt5a mRNA levels by carrying out semiquantitative RT-PCR. We observed that Wnt5a mRNA levels were greatly diminished in human EOC cell lines compared with primary HOSE cells (Fig. 1A). This finding was further confirmed through qRT-PCR analysis of Wnt5a mRNA in multiple isolations of primary HOSE cells and human EOC cell lines, showing that the levels of Wnt5a mRNA were significantly lower in human EOC cell lines compared with primary HOSE cells (Fig. 1B; $P = 0.008$). Consistently, we observed that Wnt5a protein levels were also lower in human EOC cell lines compared with primary HOSE cells as determined by immunoblotting (Fig. 1C). On the basis of these results, we conclude that Wnt5a is expressed at lower levels in human EOC cell lines compared with primary HOSE cells.

We next determined whether the loss of Wnt5a expression found in human EOC cell lines was also observed in primary human EOCs. We examined Wnt5a expression in 130 cases of primary human EOC specimens and 31 cases of normal human ovary with surface epithelium by IHC, using an antibody against Wnt5a (Table 1). In addition, there is recent evidence to suggest that a proportion of high-grade serous EOC may arise from distant fallopian tube epithelium (25). Thus, we also included 28 cases of normal human fallopian tube specimens in our IHC analysis (Table 1). The specificity of the anti-Wnt5a antibody was confirmed in our study (Supplementary Fig. S1). A single band at predicted molecular weight (~42 kDa) was detected in OVCAR5 cells with ectopically expressed Wnt5a and was absent after expression of a short hairpin RNA to the human Wnt5a gene (shWnt5a), which effectively knocked down Wnt5a mRNA expression (Supplementary Fig. S1A and data not shown). In addition, Wnt5a staining was lost when primary anti-Wnt5a antibody was replaced with an isotype-matched IgG control (Supplementary Fig. S1B).

As shown in Figure 1D, in normal human ovarian surface epithelial cells and fallopian tube epithelial cells, both cytoplasm and cell membrane were positive for Wnt5a IHC staining (black arrows, Fig. 1D). In contrast, Wnt5a staining in EOC cells was dramatically decreased (Fig. 1D). We scored expression of Wnt5a as high (H-score ≥ 30) or low (H score < 30) on the basis of a histological score (H score; 26), which considers both intensity of staining and percentage of positively stained cells, as previously described (17). Wnt5a expression was scored as high in 58.1% (18/31) cases of normal human ovarian surface epithelium and 82.1% (23/28) cases of normal human fallopian tube epithelium (Table 1). In contrast, Wnt5a expression was scored as high in 37.7% (49/130) cases of primary human EOCs (Table 1). Statistical analysis revealed that Wnt5a was expressed at significantly lower levels in primary human EOCs compared with either normal human ovarian surface epithelium ($P = 0.039$) or normal human fallopian tube epithelium ($P < 0.001$; Table 1). On the basis of these studies, we conclude that Wnt5a is expressed at significantly lower levels in primary human EOCs compared with either normal human ovarian surface epithelium or fallopian tube epithelium.

Wnt5a expression negatively correlates with tumor stage and lower Wnt5a expression predicts shorter overall survival

We next examined the correlation between Wnt5a expression and clinical and pathologic features of human EOCs. Significantly, there was a negative correlation between Wnt5a expression and tumor stage ($P = 0.003$; Table 1). Notably, the majority of examined cases are high-grade serous subtypes that are usually of stage 3/4. In addition, we examined the correlation between expression of Wnt5a and a marker of cell proliferation, Ki-67 (ref. 27; Fig. 1E). There was a significant negative correlation between Wnt5a expression and Ki-67 ($P = 0.038$; Table 1). We next assessed whether Wnt5a expression based on H score might predict prognosis of EOC patients (High, H score ≥ 30; Low, H score < 30; $n = 123$), for which long-term follow-up data were available. Significantly, lower Wnt5a expression correlated with shorter overall survival in the examined EOC patients ($P = 0.003$; Fig. 1F). Together, we conclude that a lower level of Wnt5a expression correlates with tumor stage and predicts shorter overall survival in human EOC patients.

Wnt5a gene promoter hypermethylation contributes to its downregulation in human EOC cells

Wnt5a gene promoter hypermethylation has been implicated as a mechanism underlying its silencing in several types of human cancers (16). Consistently, we also observed *Wnt5a* gene promoter hypermethylation in a number of human EOC cell lines (Fig. 2A; Supplementary Table S1). Further supporting a role of promoter hypermethylation in suppression of Wnt5a expression, treatment with a DNA demethylation drug, Aza-C (28), in PEO1 EOC cells resulted in a significant increase in levels of both Wnt5a mRNA and protein (Fig. 2B and C). We

Published OnlineFirst August 4, 2011; DOI:10.1158/0008-5472.CAN-11-1341

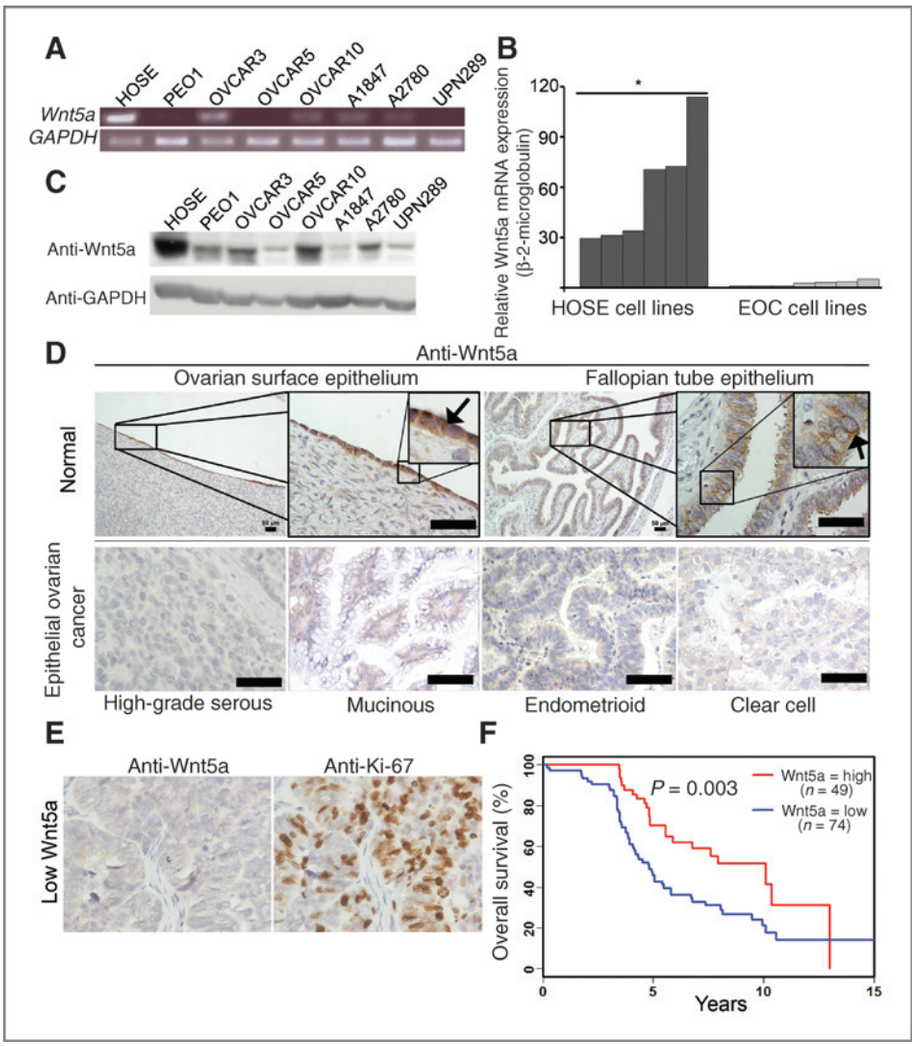

Figure 1. Wnt5a is expressed at significantly lower levels in human EOC cells compared with normal human ovarian surface or fallopian tube epithelial cells, and a lower level of Wnt5a expression predicts shorter overall survival in human EOC patients. A, expression of Wnt5a mRNA in primary HOSE cells and the indicated human EOC cell lines was determined by semiquantitative RT-PCR. Expression of glyceraldehyde 3-phosphate dehydrogenase (*GAPDH*) mRNA was used as a loading control. B, Wnt5a mRNA levels were quantified by qRT-PCR in 6 individual isolations of primary HOSE cells and 7 different EOC cell lines. Expression of β-2-microglobulin was used to normalize Wnt5a mRNA expression. *, $P = 0.008$ compared with human EOC cells. C, same as (A), but examined for Wnt5a and GAPDH protein expression by immunoblotting. D, examples of Wnt5a IHC staining in normal human ovarian surface epithelium, fallopian tube epithelium, and EOC of indicated histologic subtypes. Bar, 50 μm. Arrows point to examples of positively stained human ovarian surface epithelial cells and fallopian tube epithelial cells. E, representative images from tissue microarray depicting low Wnt5a expression correlated with high Ki-67, a cell proliferation marker. F, loss of Wnt5a expression is an independent poor prognosis marker in human EOC patients. A lower level of Wnt5a expression correlates with shorter overall survival in human EOC patients. The univariate overall survival curve (Kaplan–Meier method) for EOC patients ($n = 123$) with high- or low-Wnt5a expression as determined by immunohistochemical analysis.

conclude that *Wnt5a* gene promoter hypermethylation contributes to its downregulation in human EOC cells.

Wnt5a restoration inhibits the growth of human EOC cells by antagonizing the canonical Wnt/β-catenin signaling

We next sought to determine the effects of Wnt5a reconstitution in human EOC cells. Wnt5a expression was reconstituted in the OVCAR5 EOC cell line via retroviral transduction. Ectopically expressed Wnt5a was confirmed by both qRT-PCR and immunoblotting in OVCAR5 cells stably expressing Wnt5a or a vector control (Fig. 3A and B). Of note, the levels of ectopically expressed Wnt5a in OVCAR5 cells are comparable with the levels observed in primary HOSE cells (Fig. 3B). Interestingly, Wnt5a reconstitution in OVCAR5 human EOC cells significantly inhibited both anchorage-dependent and anchorage-independent growth in soft agar compared with vector controls (Fig. 3C and D). In addition, similar growth inhibition by Wnt5a reconstitution was also observed in the PEO1 human EOC cell line

Published OnlineFirst August 4, 2011; DOI:10.1158/0008-5472.CAN-11-1341

Table 1. Wnt5a expression in primary human EOCs and correlation of its expression with clinicopathologic variables

Patient characteristics	Wnt5a protein expression				
	Low (*n*)	High (*n*)	Total (*n*)	High (%)	*P*
Age (23–85 y; mean 59.2 y)					
≤55	24	16	40	40.0	
>55	52	33	85	38.8	0.900
Unknown	5	0	5		
Laterality					
Left	22	14	36	38.9	
Right	12	9	21	42.9	0.957
Bilaterality	35	24	59	40.7	
Undetermined	12	2	14		
Histotype					
EOC	81	49	130	37.7	
Type I	16	21	37	56.8	
Low-grade serous	1	1	2	50.0	
Endometrioid	4	9	13	69.2	
Mucinous	2	3	5	60.0	
Clear cell	5	4	9	44.4	
Others	4	4	8	50.0	
Type II					
High-grade serous	65	28	93	30.1	0.005[a]
Normal epithelium					
Ovarian surface	13	18	31	58.1	0.039[b]
Fallopian tube	5	23	28	82.1	<0.001[b]
Ki-67					
Low	22	23	44	52.3	
High	51	24	75	32.0	0.038
Undetermined	7	3	11		
Tumor grade					
1	3	7	10	70.0	
2	12	8	20	40.0	
3	64	31	95	32.6	
Undetermined	2	3	5		
Tumor stage					
Stage 1/2	12	18	30	60.0	
Stage 3/4	67	29	96	30.2	0.003[c]
Undetermined	2	2	4		

[a]Compared with type I EOC.
[b]Compared with EOC.
[c]Compared with stage 1/2.

(Supplementary Fig. S2A–C) suggesting that this effect is not cell line specific. On the basis of these results, we conclude that Wnt5a reconstitution inhibits the growth of human EOC cells *in vitro*.

Canonical Wnt signaling promotes cell proliferation and Wnt5a has been shown to antagonize the canonical Wnt/β-catenin signaling in certain cell contexts (16, 29–31). Because Wnt5a expression inversely correlated with expression of Ki-67 (Fig. 1E; Table 1), a cell proliferation marker, we hypothesized that Wnt5a would suppress the growth of human EOC cells by antagonizing canonical Wnt/β-catenin signaling. To test our hypothesis, we examined the effect of Wnt5a reconstitution on expression of markers of active Wnt/β-catenin signaling in human EOC cells, namely the levels of "active" soluble β-catenin (21, 22, 32) and expression of β-catenin target genes such as *CCND1, c-MYC,* and *FOSL1* (12, 13). Indeed, we observed a decrease in soluble β-catenin in Wnt5a-reconstituted OVCAR5 cells compared with vector controls (Fig. 3E). Consistently, we also observed a significant decrease in the levels of β-catenin target genes in these cells, namely *CCND1*

Published OnlineFirst August 4, 2011; DOI:10.1158/0008-5472.CAN-11-1341

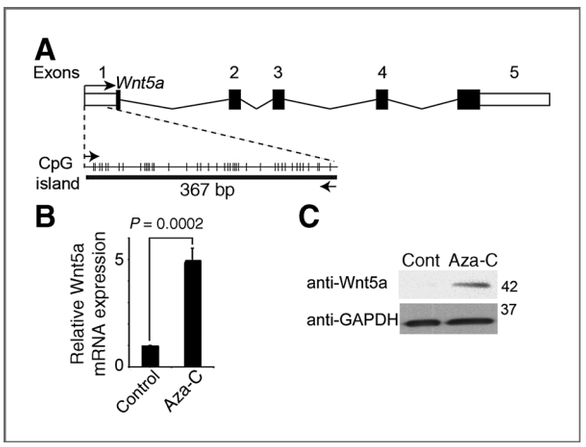

Figure 2. Promoter DNA CpG island hypermethylation contributes to Wnt5a downregulation in human EOC cells. A, schematic structure of the human *Wnt5a* gene transcript and its promoter CpG islands. Locations of exon 1 (open rectangle), CpG sites (vertical lines) and coding exons (filled rectangle), and the transcription start site (curved arrow) are indicated. Flat arrows indicate the positions of primers used for PCR amplification, and the size of PCR product is also indicated. B, PEO1 cells were treated with 5 μmol/L Aza-C for 4 days, and mRNA was isolated from control- and Aza-C–treated cells and examined for *Wnt5a* mRNA expression by qRT-PCR. Mean of 3 independent experiments with SD. C, same as (B) but examined for Wnt5a protein expression by immunoblotting.

($P = 0.0095$), *FOSL1* ($P = 0.0012$), and *c-MYC* ($P = 0.0286$; Fig. 3F). Similar effects of Wnt5a reconstitution on expression of markers of active Wnt/β-catenin signaling (such as decreased levels of soluble β-catenin) were also observed in PEO1 human EOC cells (Supplementary Fig. S2D), suggesting that this is not cell line specific. On the basis of these results, we conclude that Wnt5a suppresses the growth of human EOC cells by antagonizing canonical Wnt/β-catenin signaling in human EOC cells.

Wnt5a reconstitution drives cellular senescence in human EOC cells

Next, we sought to determine the cellular mechanism whereby Wnt5a inhibits the growth of human EOC cells. We have previously shown that suppression of canonical Wnt signaling promotes cellular senescence in primary human fibroblasts by activating the senescence-promoting histone repressor A (HIRA)/promyelocytic leukemia (PML) pathway (22). PML bodies are 20 to 30 dot-like structures in the nucleus of virtually all human cells. PML bodies are sites of poorly defined tumor suppressor activity and are disrupted in acute PML (33). PML has been implicated in regulating cellular senescence. For example, the foci number and size of PML bodies increase during senescence (33, 34) and inactivation of PML suppresses senescence (35). Activation of the HIRA/PML pathway is reflected by the recruitment of HIRA into PML bodies (36).

To determine whether Wnt5a reconstitution activates the HIRA/PML senescence pathway and induces senescence in EOC cells, we first sought to determine whether the HIRA/PML pathway is conserved in human ovarian epithelial cells. Ectopically expressing activated oncogenes (such as oncogenic *RAS*) is a standard approach for inducing senescence in a synchronized manner in primary human cells (1, 2, 19, 20). Indeed, ectopic expression of oncogenic *H-RAS*^{G12V} induced senescence of primary HOSE cells, as evident by an increase in SA-β-gal activity, a universal marker of cellular senescence (Supplementary Fig. S3A and B). Notably, the HIRA/PML pathway was activated during senescence of primary HOSE cells induced by oncogenic *RAS*, as evident by the relocalization of HIRA into PML bodies (Supplementary Fig. S3C and D). This result shows that the senescence-promoting HIRA/PML pathway is conserved in human ovarian epithelial cells. In addition, primary HOSE cells with HIRA foci displayed a marked decrease in BrdU incorporation, a marker of cell proliferation, compared with HIRA foci–negative cells (Supplementary Fig. S3E and F). This result is consistent with the idea that activation of the HIRA/PML pathway is directly correlated with senescence-associated cell growth arrest (37).

We next asked whether Wnt5a expression is regulated during natural senescence of primary HOSE cells. Indeed, we observed an increase in the levels of Wnt5a mRNA in senescent primary HOSE cells compared with young cells (Fig. 4A–C). In addition, we found that ectopic Wnt5a induces senescence of primary HOSE cells (Fig. 4D–F). Together, we conclude that Wnt5a plays a role in regulating senescence of primary HOSE cells.

As Wnt5a antagonizes canonical Wnt signaling in human EOC cells (Fig. 3E and F), we sought to determine whether Wnt5a restoration might activate the senescence-promoting HIRA/PML pathway and induce senescence in human EOC cells. Toward this goal, we examined the localization of HIRA in OVCAR5 EOC cells reconstituted with Wnt5a or vector control. Notably, there was a significant increase in the percentage of cells with HIRA localized to PML bodies in Wnt5a restored human EOC cells compared with controls (Fig. 5A and B; $P = 0.004$). In addition, we also observed an increase in the number and size of PML bodies in the Wnt5a restored OVCAR5 EOC cells (Fig. 5A), which are also established markers of cellular senescence (35, 38). Similarly, we observed activation of the HIRA/PML pathway by Wnt5a restoration in PEO1 human EOC cells (Supplementary Fig. S4A and B), suggesting that the observed effects are not cell line specific. Together, we conclude that Wnt5a reconstitution activates the HIRA/PML senescence pathway.

The p53 and pRB tumor suppressor pathways play a key role in regulating senescence (1). Thus, we sought to determine whether activation of the HIRA/PML pathway depends on the p53 and pRB pathways. Interestingly, p16^{INK4a}, the upstream repressor of pRB, is deleted in OVCAR5 human EOC cell line (39). In addition, the levels of total phosphorylated pRB were not decreased by Wnt5a, whereas the levels of cyclin D1/CKD4-mediated Serine 780 phosphorylation on pRB (pRBpS780) were decreased by Wnt5a (ref. 40; Fig. 5C and D). Furthermore, p53 is null in OVCAR5 cells (41). We conclude that activation of the HIRA/PML pathway is independent of the p53 and p16^{INK4a}.

We next sought to determine whether Wnt5a restoration induces SA-β-gal activity, a universal marker of cellular senescence (1). Indeed, SA-β-gal activity was notably induced by

Published OnlineFirst August 4, 2011; DOI:10.1158/0008-5472.CAN-11-1341

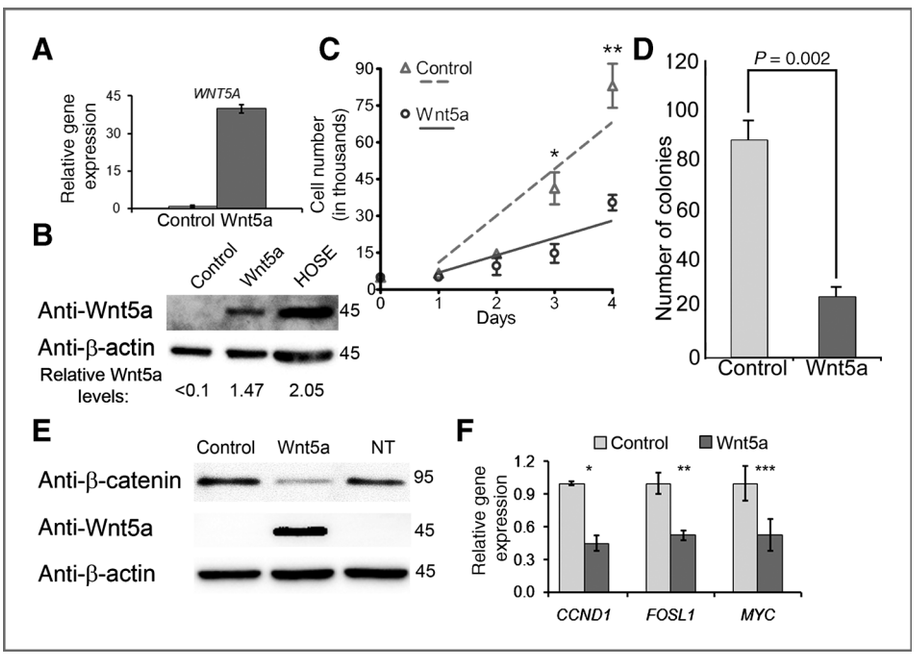

Figure 3. Wnt5a restoration inhibits the growth of human EOC cells by antagonizing canonical Wnt/β-catenin signaling. A, OVCAR5 cells were transduced with a control or Wnt5a-encoding puromycin-resistant retrovirus. The infected cells were drug-selected with 3 μg/mL puromycin. Expression of Wnt5a mRNA in drug-selected cells was determined by qRT-PCR. B, same as (A), but examined for expression of Wnt5a and β-actin in control or Wnt5a-infected OVCAR5 and primary HOSE cells by immunoblotting. Relative levels of Wnt5a expression was indicated on the basis of the densitometric analysis, using NIH ImageJ software. C, same as (A), but equal number (5,000) of drug-selected control (open triangles and dotted line) or Wnt5a-infected cells (open circles and solid line) were cultured on plastic plates for 4 days, and the number of cells was counted [control ± SD or Wnt5a ± SD ($n = 3$); Student's t test was used for calculating P value] at day 1 (6,666 ± 1,258 vs. 5,000 ± 1,000; $P = 0.1469$), day 2 (14,583 ± 954 vs. 9,583 ± 3,463; $P = 0.084$), day 3 (41,250 ± 6,538 vs. 14,750 ± 2,787; *, $P = 0.0038$), and day 4 (83,055 ± 8,978 vs. 35,416 ± 2,055; **, $P = 0.001$). Mean of 3 independent experiments with SD and linear regression. D, same as (C), but grown under anchorage-independent condition in soft agar. The number of colonies was counted 2 weeks after initial inoculation. Mean of 3 independent experiments with SD. E, same as (A), but examined for the levels of soluble β-catenin and β-actin expression by immunoblotting. NT, nontreated. F, same as (A), but examined for expression of indicated β-catenin target genes by qRT-PCR. Expression of β-2-microglobulin was used to normalize the expression of indicated genes. *, $P = 0.0095$; **, $P = 0.0012$; and ***, $P = 0.0286$ compared with controls.

Wnt5a reconstitution in both OVCAR5 and PEO1 human EOC cells compared with controls (Fig. 5E and F; Supplementary Fig. S4C and D, respectively). On the basis of these results, we concluded that Wnt5a restoration induced senescence of human EOC cells by activating the HIRA/PML senescence pathway.

Wnt5a inhibits the growth of human EOC cells *in vivo* by inducing cellular senescence

We next sought to determine whether Wnt5a would mediate growth inhibition and induce senescence *in vivo* in an orthotopic EOC model in immunocompromised mice. A luciferase gene was retrovirally transduced into control or Wnt5a-reconstituted OVCAR5 cells to monitor the cell growth *in vivo* via noninvasive imaging. These cells were injected unilaterally into the bursa sac covering the ovary in female immunocompromised mice ($n = 6$ for each of the groups; Supplementary Fig. S5). Tumor growth was monitored every 5 days starting at day 10 postinjection by measuring luciferase activity, and the growth of the tumor was followed for a total of 30 days (Fig. 6A). Wnt5a significantly suppressed the growth of xenografted OVCAR5 human EOC cells compared with controls (Fig. 6B; $P < 0.03$). Consistently, following general pathologic examination during surgical dissection at day 30, we observed that tumor sizes were notably smaller from mice injected with Wnt5a-reconstituted OVCAR5 cells compared with controls (data not shown). The expression of ectopic Wnt5a was confirmed by IHC staining in sections from dissected tumors (Fig. 6C).

We next sought to determine whether cell proliferation was suppressed by Wnt5a reconstitution in dissected tumors. Toward this goal, we examined the expression of Ki-67 by IHC. We observed, there was a significant decrease in the number of Ki-67–positive cells in tumors formed by Wnt5a-reconstituted OVCAR5 cells compared with controls (Fig. 6D and E). In addition, intensity of Ki-67 staining was also notably weaker in Ki-67–positive Wnt5A-reconstituted OVCAR5 cells than in control Ki-67–positive cells (Fig. 6D). On the basis of these results, we conclude that Wnt5a reconstitution inhibits the proliferation of human EOC cells *in vivo* in an orthotopic xenograft EOC model.

We next investigated whether the growth inhibition observed by Wnt5a reconstitution *in vivo* was due to induction of cellular senescence. Toward this goal, we examined the expression of SA-β-gal activity in fresh sections of dissected tumors formed by OVCAR5 cells reconstituted with Wnt5a or control cells. Indeed, we observed a significant increase in the number of cells positive for SA-β-gal activity in OVCAR5 cells reconstituted with Wnt5a compared with control tumors

Published OnlineFirst August 4, 2011; DOI:10.1158/0008-5472.CAN-11-1341

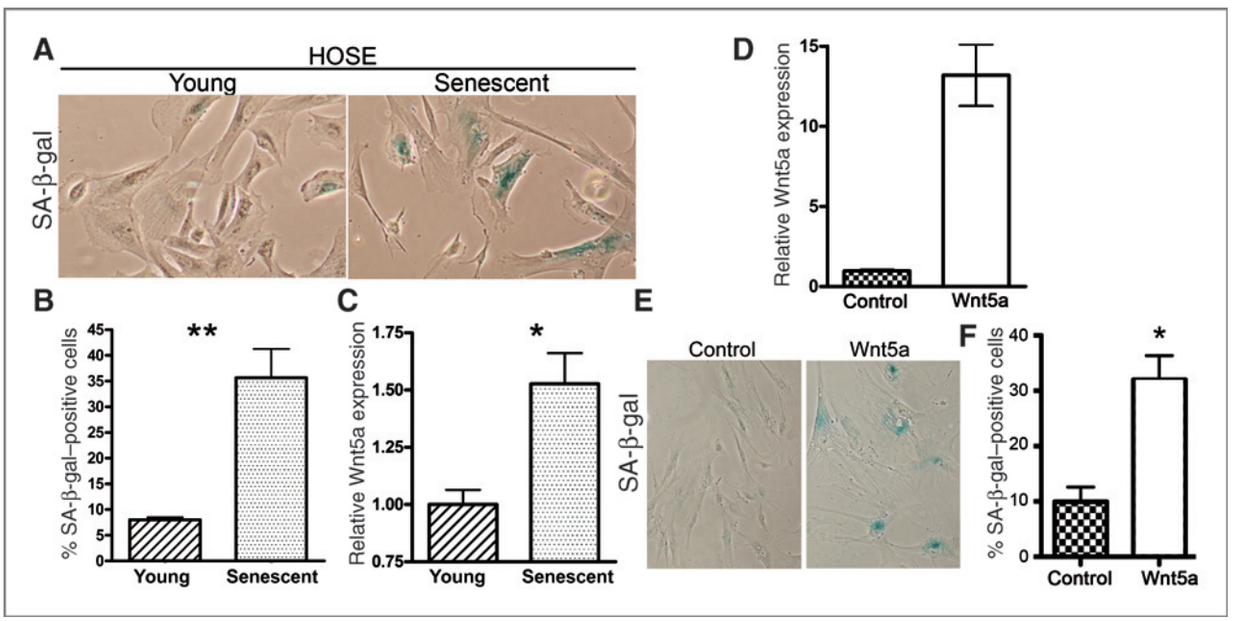

Figure 4. Wnt5a promotes senescence of primary HOSE cells. A, young proliferating primary HOSE cells were passaged to senescence (after 7 population doublings). Expression of SA-β-gal activity was measured in young and naturally senescent primary HOSE cells. B, same as (A). Quantitation of SA-β-gal–positive cells. **, $P < 0.001$. C, same as (A), but mRNA was isolated and examined for *Wnt5a* expression by qRT-PCR. Expression of B2M was used as a control. *, $P = 0.003$. D, young primary HOSE cells were transduced with retrovirus encoding human *Wnt5a* gene or a control. Expression of Wnt5a in indicated cells was determined by qRT-PCR. Expression of B2M was used as a control. E, same as (D), but stained for expression of SA-β-gal activity in drug-selected cells. F, quantitation of (E). Mean of 3 independent experiments with SD. *, $P < 0.05$.

(Fig. 6F and G; $P = 0.003$). Together, we conclude that Wnt5a reconstitution inhibits the growth of human EOC cells *in vivo* by inducing cellular senescence.

Discussion

Driving cancer cells to undergo cellular senescence has recently been proposed to be a novel mechanism to target for developing cancer therapeutics (1, 6). For example, pharmacologic inhibitor of *PTEN* drives senescence and, consequently, inhibits tumorigenesis *in vivo* in xenograft models of *PTEN* heterozygous prostate cancer cells (42, 43). Compared with apoptosis, therapeutics that drive cellular senescence are proposed to have less cytotoxic side effects (6), which makes prosenescence therapy attractive. Herein, we describe that restoration of Wnt5a signaling drives senescence of human EOC cells both *in vitro* and *in vivo* in an orthotopic mouse model of EOC (Figs. 5 and 6). Restoring gene expression by gene therapy has had limited success. Therefore, restoring Wnt5a signaling via exogenous ligand could prove to be an alternative approach. Interestingly, it has been previously reported that a Wnt5a-derived hexapeptide is sufficient to restore Wnt5a

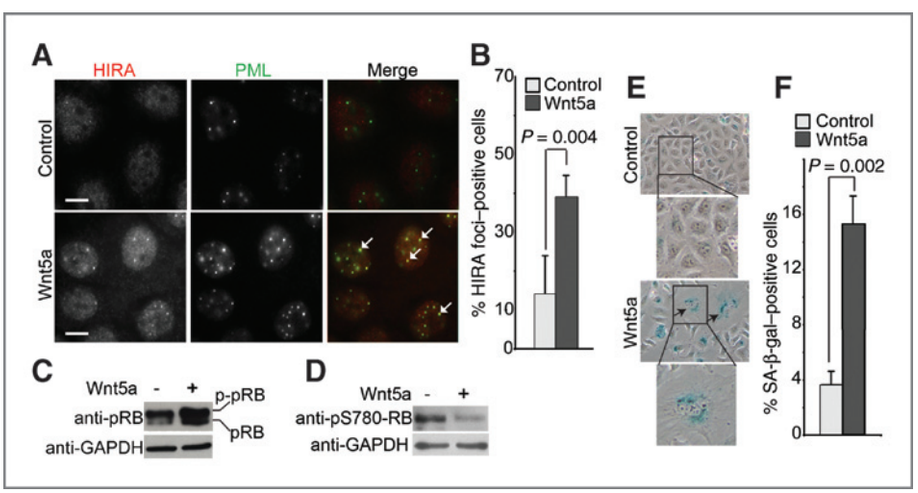

Figure 5. Wnt5a restoration triggers cellular senescence in human EOC cells. A, control and Wnt5a-expressing OVCAR5 EOC cells were stained with antibodies to HIRA and PML. Arrows point to examples of colocalized HIRA and PML bodies. Bar, 10 μm. B, quantitation of (A). A total of 200 cells from control and Wnt5a-expressing cells were examined for HIRA and PML colocalization. Mean of 3 independent experiments with SD. C, same as (A), but examined for pRB and GAPDH expression. D, same as (C), but examined for pRBpS780 and GAPDH expression. E, same as (A), but examined for SA-β-gal activity. F, quantitation of (E). Mean of 3 independent experiments with SD.

Published OnlineFirst August 4, 2011; DOI:10.1158/0008-5472.CAN-11-1341

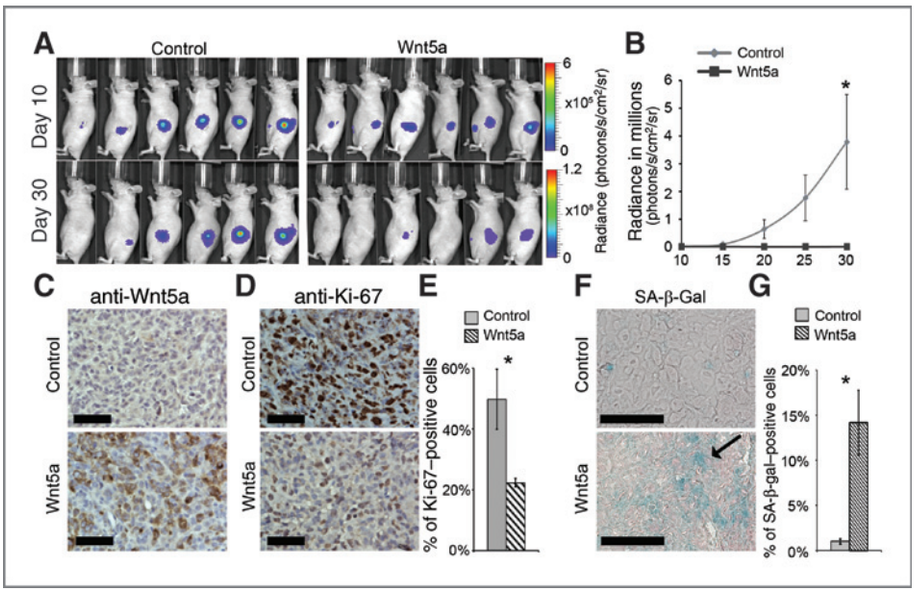

Figure 6. Wnt5a restoration inhibits tumor growth and promotes senescence of human EOC cells *in vivo*. A, OVCAR5 cells were transduced with luciferase-encoding hygromycin-resistant retrovirus together with a control or Wnt5a-encoding puromycin-resistant retrovirus. Drug-selected cells were unilaterally injected into the periovarian bursa sac of the female immunocompromised mice ($n = 6$ for each of the groups). The radiance of luciferase bioluminescence, an indicator of the rate for tumor growth, was measured every 5 days from day 10 until day 30 by using the IVIS imaging system. Shown are images taken at day 10 and day 30, respectively. B, quantitation of tumor growth from injected OVCAR5 cells expressing Wnt5a or control at indicated time points. *, $P = 0.038$ compared with controls. C, following tumor dissection, expression of Wnt5a in tumors formed by control or Wnt5a-expressing OVCAR5 EOC cells was determined by immunohistochemical staining against Wnt5a (magnification, 40×). Bar, 50 μm. D, same as (C), but examined for expression of Ki-67, a marker of cell proliferation (magnification, 40×). Bar, 50 μm. E, quantitation of (D). *, $P = 0.008$ compared with controls. F, expression of SA-β-gal activity was examined on sections of fresh-frozen tumors formed by OVCAR5 cells expressing control or Wnt5a (magnification, 40×). Bar, 100 μm. G, quantitation of (F). *, $P = 0.003$ compared with controls. Arrow points to an example of SA-β-gal positive cells.

signaling both *in vitro* and *in vivo* in xenograft models of breast cancer (44). It would be interesting to test whether the Wnt5a-derived hexapeptide will be sufficient to reconstitute Wnt5a signaling and drive senescence of EOC cells. Our data suggest that cellular senescence is a potential target for developing EOC therapeutics. In addition, these data imply that restoration of Wnt5a signaling represents a potential novel strategy to drive senescence of EOC cells.

This study is the first to show a role for Wnt5a in regulating senescence. We showed that Wnt5a activated the senescence-promoting HIRA/PML pathway in human EOC cells (Fig. 5A; Supplementary Fig. S4A). In primary human cells, activation of HIRA/PML pathway is sufficient to drive senescence by facilitating epigenetic silencing of proliferation-promoting genes (such as E2F target genes; ref. 19). Herein, we reported for the first time that the key HIRA/PML senescence pathway can be reactivated to drive senescence of human cancer cells. Further studies are warranted to elucidate the molecular basis by which Wnt5a restoration and activation of HIRA/PML pathway drive cellular senescence in human EOC cells.

Interestingly, senescence induced by Wnt5a restoration in human EOC cells was independent of both the p53 and $p16^{INK4a}$ tumor suppressors, which implies that EOC cells that lack p53 and $p16^{INK4a}$ retain the capacity to undergo senescence via HIRA/PML pathway through suppressing the canonical Wnt signaling. This is consistent with previous reports showing that cancer cells that lack p53 and pRB retain the capacity to undergo senescence when treated with anticancer agents or ionizing radiation (6). Notably, although the levels of total phosphorylated pRB were not decreased by Wnt5a, we observed a decrease in the levels of pRBpS780 that is mediated by cyclin D1/CDK4 (Fig. 5C and D). Future studies will determine whether the decrease in pRBpS780 levels plays a role in regulating senescence of human EOC cells.

Expression of Wnt5a is altered in many types of cancers (45). For example, in melanoma, Wnt5a overexpression correlates with cancer progression and a higher tumor stage (16). However, in colorectal and esophageal squamous cell carcinomas, Wnt5a has been described to be a tumor suppressor and was frequently silenced by promoter hypermethylation (16, 46). Consistently, we also observed *Wnt5a* promoter hypermethylation in a number of human EOC cell lines in which Wnt5a is downregulated (Fig. 2; Supplementary Table S1). This result is consistent with the idea that *Wnt5a* promoter hypermethylation contributes to Wnt5a downregulation in human EOC cells.

Wnt5a function is highly dependent on cellular context (45). For example, the cellular Wnt receptor/coreceptor context dictates the downstream signaling pathways upon the binding of Wnt5a, which include activating noncanonical Wnt signaling or antagonizing canonical Wnt/β-catenin signaling (47). These reports illustrate that Wnt5a expression and its resulting activity are cell type and context dependent. The Wnt receptor/coreceptor profile in EOC cells is currently unknown, and our future studies will elucidate the mechanism by which Wnt5a

Published OnlineFirst August 4, 2011; DOI:10.1158/0008-5472.CAN-11-1341

antagonizes Wnt/β-catenin signaling in human EOC cells. Regardless, our data show that Wnt5a downregulation is an independent predictor for overall survival in EOC patients. In contrast, 2 other studies showed that higher Wnt5a expression predicts poor survival in EOC patients (48, 49). The basis for this discrepancy remains to be elucidated. An explanation may be that our study included more cases than the other 2 studies (130 EOC cases in our study vs. 38 cases in the study by Badiglian and colleagues or 63 cases in the study by Peng and colleagues). It may also be due to the difference in the composition of type I and type II cases in this study compared with the other 2 studies. The vast majority of EOC cases in this study are of type II high-grade serous subtypes. Consistently, our data showed that there is a difference in Wnt5a expression between type I and type II EOC ($P = 0.005$; Table 1). Furthermore, it has been shown in microarray analysis that Wnt5a is expressed at lower levels in laser capture and microdissected high-grade serous EOC compared with normal primary HOSE cells (50).

In summary, the data reported here show that Wnt5a is often expressed at lower levels in human EOCs compared with either normal human ovarian surface epithelium or fallopian tube epithelium. A lower level of Wnt5a expression correlates with tumor stage and predicts shorter overall survival in EOC patients. Reconstitution of Wnt5a signaling inhibits the growth of human EOC cells both *in vitro* and *in vivo*. In addition, Wnt5a reconstitution suppresses the proliferation-promoting canonical Wnt/β-catenin signaling in human EOC cells. Significantly, Wnt5a reconstitution drives cellular senescence in human EOC cells and this correlates with activation of the senescence-promoting HIRA/PML pathway. Together, our data imply that reconstitution of Wnt5a signaling to drive senescence of human EOC cells is a potential novel strategy for developing EOC therapeutics.

Disclosure of Potential Conflicts of Interest

No potential conflicts of interest were disclosed.

Acknowledgments

The authors thank Dr. Denise Connolly for reagent, Dr. Harvey Hensley for technical assistance, and Drs. Katherine Aird and Maureen Murphy for critical reading of the manuscript.

Grant Support

R. Zhang is an Ovarian Cancer Research Fund (OCRF) Liz Tilberis Scholar. This work was supported in part by a NCI FCCC-UPenn ovarian cancer SPORE (P50 CA083638) pilot project and SPORE career development award (to R. Zhang), a DOD ovarian cancer academy award (OC093420 to R Zhang), an OCRF program project (to R. Zhang, M.J. Birrer, and A.K. Godwin), and a generous gift from Catherine and Peter Getchell. B.G. Bitler is supported by a NCI postdoctoral training grant (CA-009035-35).

The costs of publication of this article were defrayed in part by the payment of page charges. This article must therefore be hereby marked *advertisement* in accordance with 18 U.S.C. Section 1734 solely to indicate this fact.

Received April 18, 2011; revised July 28, 2011; accepted July 29, 2011; published OnlineFirst August 4, 2011.

References

1. Kuilman T, Michaloglou C, Mooi WJ, Peeper DS. The essence of senescence. Genes Dev 2010;24:2463–79.
2. Adams PD. Healing and hurting: molecular mechanisms, functions, and pathologies of cellular senescence. Mol Cell 2009;36:2–14.
3. Dimri GP, Lee X, Basile G, Acosta M, Scott G, Roskelley C, et al. A biomarker that identifies senescent human cells in culture and in aging skin *in vivo*. Proc Natl Acad Sci U S A 1995;92:9363–7.
4. Ventura A, Kirsch DG, McLaughlin ME, Tuveson DA, Grimm J, Lintault L, et al. Restoration of p53 function leads to tumour regression *in vivo*. Nature 2007;445:661–5.
5. Xue W, Zender L, Miething C, Dickins RA, Hernando E, Krizhanovsky V, et al. Senescence and tumour clearance is triggered by p53 restoration in murine liver carcinomas. Nature 2007;445:656–60.
6. Ewald JA, Desotelle JA, Wilding G, Jarrard DF. Therapy-induced senescence in cancer. J Natl Cancer Inst 2010;102:1536–46.
7. Peeper DS. PICS-ure this: prosenescence therapy? Cancer Cell 2010;17:219–20.
8. Ozols RF, Bookman MA, Connolly DC, Daly MB, Godwin AK, Schilder RJ, et al. Focus on epithelial ovarian cancer. Cancer Cell 2004;5:19–24.
9. Farley J, Ozbun LL, Birrer MJ. Genomic analysis of epithelial ovarian cancer. Cell Res 2008;18:538–48.
10. Shih Ie M, Kurman RJ. Ovarian tumorigenesis: a proposed model based on morphological and molecular genetic analysis. Am J Pathol 2004;164:1511–8.
11. Moon RT, Kohn AD, De Ferrari GV, Kaykas A. WNT and beta-catenin signalling: diseases and therapies. Nat Rev Genet 2004;5:691–701.
12. Katoh M. WNT signaling pathway and stem cell signaling network. Clin Cancer Res 2007;13:4042–5.
13. Mann B, Gelos M, Siedow A, Hanski ML, Gratchev A, Ilyas M, et al. Target genes of beta-catenin-T cell-factor/lymphoid-enhancer-factor signaling in human colorectal carcinomas. Proc Natl Acad Sci U S A 1999;96:1603–8.
14. Szotek PP, Chang HL, Brennand K, Fujino A, Pieretti-Vanmarcke R, Lo Celso C, et al. Normal ovarian surface epithelial label-retaining cells exhibit stem/progenitor cell characteristics. Proc Natl Acad Sci U S A 2008;105:12469–73.
15. Wu R, Hendrix-Lucas N, Kuick R, Zhai Y, Schwartz DR, Akyol A, et al. Mouse model of human ovarian endometrioid adenocarcinoma based on somatic defects in the Wnt/beta-catenin and PI3K/Pten signaling pathways. Cancer Cell 2007;11:321–33.
16. McDonald SL, Silver A. The opposing roles of Wnt-5a in cancer. Br J Cancer 2009;101:209–14.
17. Li H, Cai Q, Godwin AK, Zhang R. Enhancer of zeste homolog 2 promotes the proliferation and invasion of epithelial ovarian cancer cells. Mol Cancer Res 2010;8:1610–8.
18. Ibanez de Caceres I, Dulaimi E, Hoffman AM, Al-Saleem T, Uzzo RG, Cairns P. Identification of novel target genes by an epigenetic reactivation screen of renal cancer. Cancer Res 2006;66:5021–8.
19. Zhang R, Chen W, Adams PD. Molecular dissection of formation of senescence-associated heterochromatin foci. Mol Cell Biol 2007;27:2343–58.
20. Zhang R, Poustovoitov MV, Ye X, Santos HA, Chen W, Daganzo SM, et al. Formation of MacroH2A-containing senescence-associated heterochromatin foci and senescence driven by ASF1a and HIRA. Dev Cell 2005;8:19–30.
21. Cheyette BN, Waxman JS, Miller JR, Takemaru K, Sheldahl LC, Khlebtsova N, et al. Dapper, a Dishevelled-associated antagonist of beta-catenin and JNK signaling, is required for notochord formation. Dev Cell 2002;2:449–61.
22. Ye X, Zerlanko B, Kennedy A, Banumathy G, Zhang R, Adams PD. Downregulation of Wnt signaling is a trigger for formation of facultative heterochromatin and onset of cell senescence in primary human cells. Mol Cell 2007;27:183–96.

Published OnlineFirst August 4, 2011; DOI:10.1158/0008-5472.CAN-11-1341

23. Itahana K, Campisi J, Dimri GP. Methods to detect biomarkers of cellular senescence: the senescence-associated beta-galactosidase assay. Methods Mol Biol 2007;371:21–31.
24. Connolly DC, Hensley HH. Xenograft and transgenic mouse models of epithelial ovarian cancer and non invasive imaging modalities to monitor ovarian tumor growth *in situ* - applications in evaluating novel therapeutic agents. Curr Protoc Pharmacol 2009;45:14.12.1–26.
25. Kurman RJ, Shih Ie M. The origin and pathogenesis of epithelial ovarian cancer: a proposed unifying theory. Am J Surg Pathol 2010;34:433–43.
26. McCarty KS Jr, Szabo E, Flowers JL, Cox EB, Leight GS, Miller L, et al. Use of a monoclonal anti-estrogen receptor antibody in the immunohistochemical evaluation of human tumors. Cancer Res 1986;46: 4244s–8s.
27. Gerdes J, Lemke H, Baisch H, Wacker HH, Schwab U, Stein H. Cell cycle analysis of a cell proliferation-associated human nuclear antigen defined by the monoclonal antibody Ki-67. J Immunol 1984;133: 1710–5.
28. Baylin SB, Herman JG, Graff JR, Vertino PM, Issa JP. Alterations in DNA methylation: a fundamental aspect of neoplasia. Adv Cancer Res 1998;72:141–96.
29. Liang H, Chen Q, Coles AH, Anderson SJ, Pihan G, Bradley A, et al. Wnt5a inhibits B cell proliferation and functions as a tumor suppressor in hematopoietic tissue. Cancer Cell 2003;4:349–60.
30. Mikels AJ, Nusse R. Purified Wnt5a protein activates or inhibits beta-catenin-TCF signaling depending on receptor context. PLoS Biol 2006;4:e115.
31. Topol L, Jiang X, Choi H, Garrett-Beal L, Carolan PJ, Yang Y. Wnt-5a inhibits the canonical Wnt pathway by promoting GSK-3-independent beta-catenin degradation. J Cell Biol 2003;162:899–908.
32. Reya T, Clevers H. Wnt signalling in stem cells and cancer. Nature 2005;434:843–50.
33. Bernardi R, Pandolfi PP. Structure, dynamics and functions of promyelocytic leukaemia nuclear bodies. Nat Rev Mol Cell Biol 2007;8:1006–16.
34. Mallette FA, Goumard S, Gaumont-Leclerc MF, Moiseeva O, Ferbeyre G. Human fibroblasts require the Rb family of tumor suppressors, but not p53, for PML-induced senescence. Oncogene 2004;23:91–9.
35. Ferbeyre G, de Stanchina E, Querido E, Baptiste N, Prives C, Lowe SW. PML is induced by oncogenic *ras* and promotes premature senescence. Genes Dev 2000;14:2015–27.
36. Salomoni P, Pandolfi PP. The role of PML in tumor suppression. Cell 2002;108:165–70.
37. Ye X, Zerlanko B, Zhang R, Somaiah N, Lipinski M, Salomoni P, et al. Definition of pRB- and p53-dependent and -independent steps in HIRA/ASF1a-mediated formation of senescence-associated heterochromatin foci. Mol Cell Biol 2007;27:2452–65.
38. Pearson M, Carbone R, Sebastiani C, Cioce M, Fagioli M, Saito S, et al. PML regulates p53 acetylation and premature senescence induced by oncogenic *Ras*. Nature 2000;406:207–10.
39. Watson JE, Gabra H, Taylor KJ, Rabiasz GJ, Morrison H, Perry P, et al. Identification and characterization of a homozygous deletion found in ovarian ascites by representational difference analysis. Genome Res 1999;9:226–33.
40. Lundberg AS, Weinberg RA. Functional inactivation of the retinoblastoma protein requires sequential modification by at least two distinct cyclin-cdk complexes. Mol Cell Biol 1998;18:753–61.
41. Yaginuma Y, Westphal H. Abnormal structure and expression of the p53 gene in human ovarian carcinoma cell lines. Cancer Res 1992;52:4196–9.
42. Alimonti A, Nardella C, Chen Z, Clohessy JG, Carracedo A, Trotman LC, et al. A novel type of cellular senescence that can be enhanced in mouse models and human tumor xenografts to suppress prostate tumorigenesis. J Clin Invest 2010;120:681–93.
43. Collado M. Exploring a`pro-senescence' approach for prostate cancer therapy by targeting PTEN. Future Oncol 2010;6:687–9.
44. Safholm A, Tuomela J, Rosenkvist J, Dejmek J, Harkonen P, Andersson T. The Wnt-5a-derived hexapeptide Foxy-5 inhibits breast cancer metastasis *in vivo* by targeting cell motility. Clin Cancer Res 2008;14:6556–63.
45. Pukrop T, Binder C. The complex pathways of Wnt 5a in cancer progression. J Mol Med 2008;86:259–66.
46. Li J, Ying J, Fan Y, Wu L, Ying Y, Chan AT, et al. WNT5A antagonizes WNT/beta-catenin signaling and is frequently silenced by promoter CpG methylation in esophageal squamous cell carcinoma. Cancer Biol Ther 2007;10:617–24.
47. Nishita M, Enomoto M, Yamagata K, Minami Y. Cell/tissue-tropic functions of Wnt5a signaling in normal and cancer cells. Trends Cell Biol 2010;20:346–54.
48. Badiglian Filho L, Oshima CT, De Oliveira Lima F, De Oliveira Costa H, De Sousa Damiao R, Gomes TS, et al. Canonical and noncanonical Wnt pathway: a comparison among normal ovary, benign ovarian tumor and ovarian cancer. Oncol Rep 2009;21:313–20.
49. Peng C, Zhang X, Yu H, Wu D, Zheng J. Wnt5a as a predictor in poor clinical outcome of patients and a mediator in chemoresistance of ovarian cancer. Int J Gynecol Cancer 2011;21:280–8.
50. Mok SC, Bonome T, Vathipadiekal V, Bell A, Johnson ME, Wong KK, et al. A gene signature predictive for outcome in advanced ovarian cancer identifies a survival factor: microfibril-associated glycoprotein 2. Cancer Cell 2009;16:521–32.

Published OnlineFirst November 29, 2010; DOI:10.1158/1541-7786.MCR-10-0398

Molecular Cancer Research

Enhancer of Zeste Homolog 2 Promotes the Proliferation and Invasion of Epithelial Ovarian Cancer Cells

Hua Li, Qi Cai, Andrew K. Godwin, et al.

Mol Cancer Res 2010;8:1610-1618. Published OnlineFirst November 29, 2010.

Published OnlineFirst November 29, 2010; DOI:10.1158/1541-7786.MCR-10-0398

Cell Cycle, Cell Death, and Senescence

Molecular Cancer Research

Enhancer of Zeste Homolog 2 Promotes the Proliferation and Invasion of Epithelial Ovarian Cancer Cells

Hua Li[1], Qi Cai[2], Andrew K. Godwin[1], and Rugang Zhang[1,3]

Abstract

Enhancer of zeste homolog 2 (EZH2) is the catalytic subunit of the polycomb repressive complex 2 (PRC2) that includes noncatalytic subunits suppressor of zeste 12 (SUZ12) and embryonic ectoderm development (EED). When present in PRC2, EZH2 catalyzes trimethylation on lysine 27 residue of histone H3 (H3K27Me3), resulting in epigenetic silencing of gene expression. Here, we investigated the expression and function of EZH2 in epithelial ovarian cancer (EOC). When compared with primary human ovarian surface epithelial (pHOSE) cells, EZH2, SUZ12, and EED were expressed at higher levels in all 8 human EOC cell lines tested. Consistently, H3K27Me3 was also overexpressed in human EOC cell lines compared with pHOSE cells. EZH2 was significantly overexpressed in primary human EOCs ($n = 134$) when compared with normal ovarian surface epithelium ($n = 46$; $P < 0.001$). EZH2 expression positively correlated with expression of Ki67 ($P < 0.001$; a marker of cell proliferation) and tumor grade ($P = 0.034$) but not tumor stage ($P = 0.908$) in EOC. There was no correlation of EZH2 expression with overall ($P = 0.3$) or disease-free survival ($P = 0.2$) in high-grade serous histotype EOC patients ($n = 98$). Knockdown of EZH2 expression reduced the level of H3K27Me3 and suppressed the growth of human EOC cells both *in vitro* and *in vivo* in xenograft models. EZH2 knockdown induced apoptosis of human EOC cells. Finally, we showed that EZH2 knockdown suppressed the invasion of human EOC cells. Together, these data demonstrate that EZH2 is frequently overexpressed in human EOC cells and its overexpression promotes the proliferation and invasion of human EOC cells, suggesting that EZH2 is a potential target for developing EOC therapeutics. *Mol Cancer Res; 8(12); 1610–8. ©2010 AACR.*

Introduction

Enhancer of zeste homolog 2 (EZH2) is the catalytic subunit of polycomb repressive complex 2 (PRC2; refs. 1–4). In addition to EZH2, PRC2 also contains the noncatalytic subunits embryonic ectoderm development (EED) and suppressor of zeste 12 (SUZ12; ref. 5). PRC2 plays an important role in epigenetic gene silencing via methylation of lysine 27 residue of histone H3 (H3K27) and can add up to 3 methyl groups to the lysine side chain. EZH2 lacks enzyme activity on its own, and has to complex with EED and SUZ12 to attain robust histone methyltransferase activity (5, 6). The trimethylated form of H3K27 (H3K27Me3) is thought to be the main form that confers transcriptional silencing function (7–10).

EZH2 is overexpressed in several types of cancers (11–15) and is correlated with aggressiveness and poor prognosis in breast and prostate cancers (11–13). In breast epithelial cells, EZH2 overexpression causes anchorage-independent growth and increases cell invasiveness *in vitro* (11). In prostate cancer cells, inhibition of EZH2 blocked the growth of prostate cancer cells (13, 15). In addition, SUZ12 is also upregulated in certain types of cancer, including colon, breast, and liver (16–18).

More than 85% of ovarian cancers are of epithelial origin (19). Epithelial ovarian cancers (EOC) are classified into distinct histologic subtypes including serous, mucinous, endometrioid, and clear cell (19). The most common histology of EOC is serous (50%–60% of all EOCs), approximately, 75% of which is high-grade and 25% is low-grade (20–22). Less common histologies include endometrioid (25%), clear cell (4%), and mucinous (4%; ref. 20, 21). Recently, an alternative classification has gained traction, in which EOC is broadly divided into 2 types (22). Type I EOC includes endometrioid, mucinous, low-grade serous, and clear cell carcinomas, and type II EOC includes high-grade serous carcinomas (22). EOC remains the most

Authors' Affiliations: [1]Women's Cancer Program, [2]Biosample Repository Facility, and [3]Epigenetics and Progenitor Cells Keystone Program, Fox Chase Cancer Center, Philadelphia, Pennsylvania

Note: Supplementary data for this article are available at Molecular Cancer Research Online (http://mcr.aacrjournals.org/).

Authors' Contributions: H. Li performed all the experiments and drafted the manuscript. Q. Cai and A.K. Godwin reviewed and provided primary human ovarian carcinoma and normal ovary specimens. R. Zhang conceived the study, designed the experiments and wrote the manuscript.

Corresponding Author: Rugang Zhang, Women's Cancer Program, Fox Chase Cancer Center, W446, 333 Cottman Avenue, Philadelphia, PA 19111. Phone: 215-728-7108; Fax: 215-728-3616. E-mail: rugang.zhang@fccc.edu

doi: 10.1158/1541-7786.MCR-10-0398

Published OnlineFirst November 29, 2010; DOI:10.1158/1541-7786.MCR-10-0398

lethal gynecologic malignancy in the Western world (19). Thus, there is an urgent need to identify new targets for developing novel therapeutics for EOC. Although EZH2 is overexpressed in tumor-associated endothelial cells in invasive EOC (23) and regulates tumor angiogenesis in EOC (24), its role in pathogenesis of EOC remains poorly understood. Here, we examined the expression of the subunits of PRC2 and H3K27Me3 in human EOC cell lines. In addition, we determined EZH2 expression in primary human EOCs of different histologic subtypes by immunohistochemistry (IHC). Further, we investigated the effects of EZH2 knockdown by short hairpin RNA (shRNA) on H3K27Me3 expression, cell growth, and invasion of human EOC cells.

Material and Methods

Cell culture

Primary human ovarian surface epithelial (pHOSE) cells were isolated and cultured as previously described (25). The protocol was approved by Fox Chase Cancer Center (FCCC) institutional review board. Human EOC cell lines A1847, A2780, OVCAR3, OVCAR5, OVCAR10, PEO1, SKOV3, and UPN289 were kindly provided by Drs. Thomas Hamilton and Steve Williams at FCCC and were maintained in 1640 medium, supplemented with 10% FBS, 2 mmol/L of L-glutamine, penicillin (100 units/mL), and streptomycin (100 μg/mL).

shRNA, lentivirus packaging, and infection

The sense sequences of 2 individual shRNA EZH2 are: 5′-CCAACACAAGTCATCCCATTA-3′ and 5′-CGGAAATCTTAAACCAAGAAT-3′, respectively. Lentivirus packaging was performed using virapower system (Invitrogen) according to manufacturer's instruction. PEO1 and SKOV3 at 40% to 50% confluence were infected with lentivirus expressing shRNA to the human *EZH2* gene or vector control. The infected cells were drug-selected with 1 μg/mL (for PEO1) or 3 μg/mL (for SKOV3) of puromycin, respectively.

Human ovarian tissue microarrays

Tissue microarrays, including core samples from 134 primary human EOCs and 46 cases of normal ovary tissues were obtained from FCCC Biosample Repository Core Facility. Use of these human specimens was approved by the Institutional Review Board.

Immunohistochemical staining and scoring

The expression of EZH2 and Ki67 proteins was detected using avidin–biotin–peroxidase methods. Briefly, tissue sections were subjected to antigen retrieval by steaming in 0.01 mol/L of sodium citrate buffer (pH 6.0) for 30 minutes. After quenching endogenous peroxidase activity with 3% hydrogen peroxide and blocking nonspecific protein binding with 1% bovine serum albumin, sections were incubated overnight with primary monoclonal antibody (anti-EZH2: Millipore, 1:100; anti-Ki67: DAKO, 1:100) at 4°C, followed by biotinylated goat anti-mouse IgG (DAKO, 1:400) for 1 hour, detecting the antibody complexes with the labeled streptavidin-biotin system (DAKO), and visualizing them with the chromogen 3,3′-diaminobenzidine. Sections were lightly counterstained with hematoxylin. Tissues in which nuclei were stained for EZH2 or Ki67 protein were considered positive. Two 1-mm cores were examined in each specimen on the tissue microarray and cells were counted in at least 5 high-power fields, with approximately 200 cells analyzed per high-power field.

FACS, immunoflurescence staining, and Western blot analysis

FACS and indirect immunoflurescence (IF) staining were performed as described previously (26–28). The following antibodies were used for IF: rabbit anti-H3K27Me3 (Cell Signaling, 1:1,000), and rabbit anti-H3K9Me3 (Abcam, 1:500). The antibodies used for Western blotting were from indicated suppliers: mouse anti-EZH2 (Millipore; 1:2,500), rabbit anti-H3K27Me3 (Cell signaling, 1:1,000), rabbit anti-H3K9Me3 (Abcam, 1:2,000), mouse anti-histone H3 (Millipore, 1:10,000), mouse anti-GAPDH (Millipore, 1:10,000), rabbit anti-PARP p85 fragment (Promega, 1:1,000), rabbit anti-cleaved caspase 3 (Cell Signaling, 1:1,000), and rabbit anti-cleaved Lamin A (Cell signaling, 1:1,000).

Soft agar colony formation assay

A total of 1×10^4 cells per well were inoculated in a 6-well plate in 1.5 mL of RPMI 1640 medium supplemented with 10% FBS and 0.35% agar on a base layer of 1.5 mL of the same medium containing 0.6% agar. Three weeks after plating, the cells were stained with 1% crystal violet (Sigma) in PBS to visualize the colonies. Number of colonies that were larger than 50 μm (approximately 100 cells) in diameter in each well was counted.

Matrigel invasion assay

BD BioCoat Matrigel Invasion Chamber was used to measure cell invasion according to manufacturer's instruction. Cells (1×10^5 cells per well) suspended in 0.5 ml RPMI 1640 medium were added to the upper compartment of 24-well matrigel-coated or noncoated 8 μm membrane, and RPMI 1640 medium supplemented with 10% FBS was applied to the lower compartment. After incubating 22 hours at 37°C, 5% CO_2, the cells were fixed with 4% formaldehyde and stained with 1% crystal violet in PBS. The number of cells that migrated across control membrane or invaded through Matrigel-coated membrane was determined in 9 fields across the center and the periphery of the membrane.

Annexin V staining for detecting apoptotic cells

Phosphatidylserine externalization was detected using an Annexin V staining kit (Millipore) following manufacture's instruction. Annexin V positive cells were detected by

Published OnlineFirst November 29, 2010; DOI:10.1158/1541-7786.MCR-10-0398

Guava system and analyzed with Guava Nexin software Module (Millipore).

In vivo tumorigenicity assay

A total of 5×10^6 cells in PBS (pH 7.3) per mouse were injected subcutaneously into the flank of 6-week-old female nude athymic mice. The mice were sacrificed 4 weeks post-inoculation. Width and length of tumor size were measured and the tumor volume (mm^3) was calculated using the following formula: tumor volume (in mm^3) = length $\times$ width^2 $\times$ 0.52.

Statistical analysis

Quantitative data were expressed as mean $\pm$ SD, unless otherwise stated. analysis of variance (ANOVA) with Student's *t* test was used to identify significant differences in multiple comparisons. The χ^2 test was used to analyze the relationship between categorical variables. Overall survival was defined as the time elapsed from the date of diagnosis and the date of death from any cause or the date of last follow-up. Disease-free survival was defined as the time elapsed from the date of surgery and the date of the first recurrence. Kaplan–Meier survival plots were generated and comparisons made using the log-rank statistic. For all statistical analyses, the level of significance was set at 0.05.

Results

The catalytic and noncatalytic subunits of PRC2 complex and H3K27Me3 are expressed at higher levels in human EOC cell lines compared with pHOSE cells

Expression of EZH2, EED, and SUZ12 was examined by Western blotting in cultures of pHOSE cells isolated from 5 different individuals and 8 human EOC cell lines. When compared with pHOSE cells, EZH2, EED, and SUZ12 were expressed at higher levels in all human EOC cell lines tested (Fig. 1A). Consistently, the levels of H3K27Me3, the product of EZH2 histone H3 lysine 27 methyltransferase activity, was also increased in human EOC cell lines compared with pHOSE cells (Fig. 1A). On the basis of these results, we conclude that the catalytic and noncatalytic subunits of PRC2 and H3K27Me3 are expressed at higher levels in human EOC cell lines compared with pHOSE cells.

EZH2 is overexpressed in primary human EOCs and its expression positively correlates with expression of Ki67, a cell proliferation marker

We next sought to examine the expression of EZH2, the catalytic subunit of PRC complex, in 134 primary human EOCs and 46 normal ovary tissue specimens by IHC staining (Table 1; Fig. 1B; Supplementary Fig. S1). The specificity of the EZH2 antibody used for IHC staining was confirmed by the following (Supplementary Fig. S1A and B). First, a single band at right molecule weight (~95KD) was obtained in Western blotting of human EOC cell line SKOV3 using the EZH2 antibody, and this band was absent after expression of shRNA to the human *EZH2* gene (shEZH2) that effectively knocked down EZH2

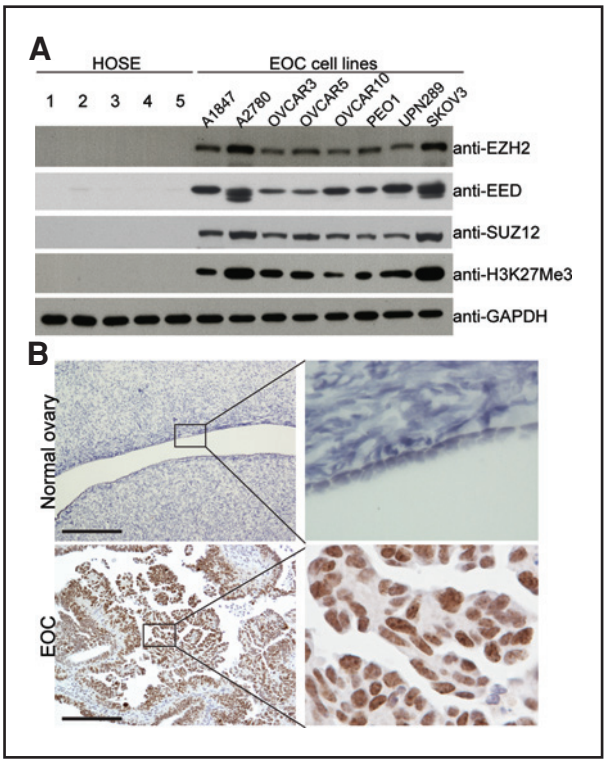

Figure 1. EZH2 is expressed at higher levels in human EOC cell lines and primary human EOCs compared with normal ovarian surface epithelium. A, expression of EZH2, EED, SUZ12, H3K27Me3, and GAPDH in 5 individual batches of pHOSE cell cultures and indicated human EOC cell lines was determined by Western blotting. B, examples of EZH2 immunohistochemical staining in normal ovary and primary human EOC (shown is an example of high-grade serous histotype EOC). Bar = 50 μm.

mRNA expression (Supplementary Fig. S1A and data not shown). In addition, EZH2 staining signal was lost when primary anti-EZH2 was replaced with an isotype-matched IgG control (Supplementary Fig. S1B). Importantly, the nuclei of human EOC cells were strongly stained by the anti-EZH2 antibody (Fig. 1B; Supplementary Fig. S1C). By contrast, ovarian surface epithelial cells were negative for EZH2 staining (Fig. 1B).

We scored expression of EZH2 as low (H-score $\leq$ 100) or high (H-score > 100) based on the histochemical score (29, 30), which considers both the intensity of staining and the percentage of positively stained cells. EZH2 expression in the surface epithelium of all 46 normal ovaries was scored as low (in fact, negative EZH2 staining). EZH2 was scored as low in 34% (46 of 134) and high in 66% (88 of 134) of primary EOCs tested, respectively. When compared with normal ovarian surface epithelium, EZH2 was expressed at significantly higher levels in primary human EOCs ($P < 0.001$). Because EZH2 has been implicated in promoting cell proliferation (12), we stained the same set of primary human EOC specimens with Ki67, a cell proliferation marker, and compared the expression of EZH2 and Ki67 expression in consecutive sections. There

Published OnlineFirst November 29, 2010; DOI:10.1158/1541-7786.MCR-10-0398

Table 1. Correlation between EZH2 expression and tumor cell proliferation (Ki67) or clinicopathologic variables

	EXH2 protein expression				
Patient characteristics	**Low (*n*)**	**High (*n*)**	**Total (*n*)**	**High (%)**	***P***
Age (23–85 y, mean 59.6 y)					
≤55	17	31	48	64.58	
>55	29	57	86	66.28	0.843
Laterality					
Left	12	25	37	67.57	
Right	7	18	25	72.00	
Bilaterality	22	39	61	63.93	0.764
Undetermined	5	6	11	54.55	
Histotype					
Epithelial ovarian cancer	46	88	134	65.67	
Type I	11	25	36	69.44	
Low-grade serous	2	0	2		
Endometrioid	5	8	13		
Mucinous	1	4	5		
Clear cell	2	6	8		
Others	1	7	8		
Type II	35	63	98	64.29	0.577[a]
High-grade serous	35	63	98	64.29	
Normal ovarian epithelium	46	0	46	0.00	<0.001[b]
Ki67					
0%–10%	27	2	29	6.90	
10%–40%	10	17	27	62.96	
40%–100%	9	69	78	88.46	<0.001
Tumor grade					
Well differentiation	6	3	9	33.33	
Moderate differentiation	10	12	22	54.55	
Poor differentiation	29	70	99	70.71	0.034
Undetermined	1	3	4	75.00	
Tumor stage					
Stage 1/2	12	21	33	63.64	
Stage 3/4	33	55	88	62.50	0.908
Undetermined	1	12	13	92.31	

[a]Compared with type I, $P = 0.577$.
[b]Compared with epithelial ovarian cancer, $P < 0.001$.

was a significant correlation between EZH2 expression and Ki67 expression ($P < 0.001$; Table 1). Together, we conclude that EZH2 is significantly overexpressed in primary human EOCs compared with normal ovarian surface epithelium and its expression correlates with a high proliferation index revealed by Ki67 staining.

EZH2 expression is positively correlated with tumor grade but not tumor stage, or overall or disease-free survival

We next sought to determine the correlation between EZH2 expression and clinical and pathologic features of human EOCs. There was a significantly positive correlation between EZH2 expression and tumor grade ($P = 0.034$; Table 1). However, EZH2 expression was not associated with tumor stage ($P = 0.908$; Table 1). Next, we sought to determine whether EZH2 expression correlates with prognosis of type II high-grade serous histotype EOC patients for which long-term follow-up data were available ($n = 98$). The difference in overall ($P = 0.3$) or disease-free ($P = 0.2$) survival between low EZH2 expression group ($n = 35$) and high EZH2 expression group ($n = 63$) was not significant (Fig. 2).

EZH2 knockdown inhibits the growth of human EOC cells *in vitro* and *in vivo*

Because EZH2 expression positively correlates with Ki67 expression (Table 1), we sought to determine the effects of EZH2 knockdown on proliferation of human EOC cells. To

Published OnlineFirst November 29, 2010; DOI:10.1158/1541-7786.MCR-10-0398

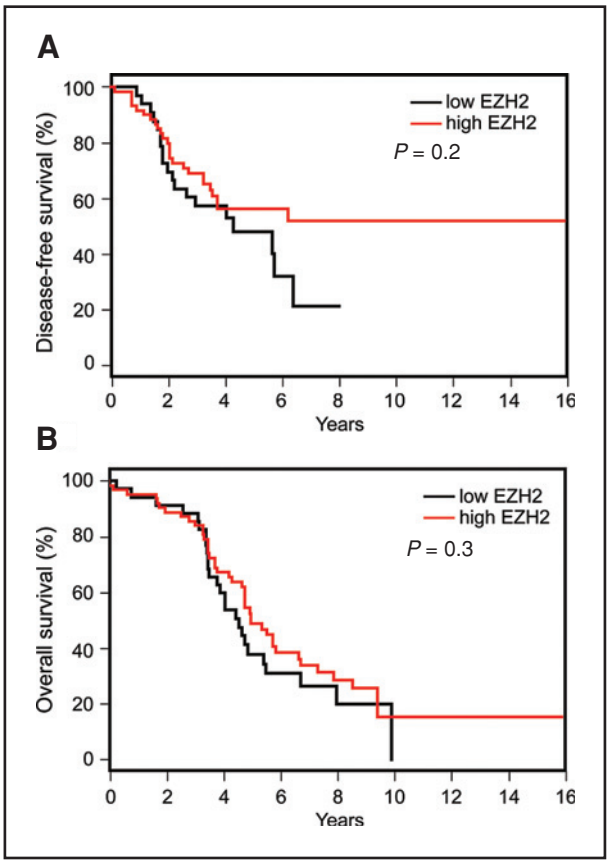

Figure 2. EZH2 expression does not correlate with disease-free or overall survival in high-grade serous histotype EOC patients. The univariate disease-free (A) and overall survival (B) curves (Kaplan–Meier method) for high-grade serous histotype EOC patients with low or high EZH2 protein levels as assessed by immunohistochemistry analysis.

knockdown EZH2 expression in SKOV3 cells, we developed 2 individual lentivirus encoded shEZH2. The knockdown efficacy of shEZH2 in SKOV3 cells was confirmed by Western blotting (Fig. 3A). Consistently, the level of H3K27Me3 level was significantly reduced by shEZH2 expression in SKOV3 cells as determined by both Western blotting and IF staining (Fig. 3B and C). As a negative control, shEZH2 expression has no effects on the level of trimethylated lysine 9 histone H3 (H3K9Me3) that is generated by histone methyltransferase Suv39H (ref. 31; Fig. 3B and C). Compared with controls, EZH2 knockdown significantly reduced both anchorage-dependent and -independent growth in soft agar in SKOV3 cells ($P < 0.001$; Fig. 3D and E). The degree of growth inhibition by shEZH2 correlated with the level of EZH2 knockdown in SKOV3 cells by 2 individual shEZH2 (Fig. 3), suggesting that the observed growth inhibition by shEZH2 was not because of off-target effects. In addition, EZH2 knockdown in PEO1 cells has same effects on the expression of H3K27Me3 and also suppressed both anchorage-dependent and -independent cell growth (Supplementary Fig. S2), suggesting that the observed growth inhibition is not cell line specific.

We next sought to determine the effects of EZH2 knockdown on the growth of SKOV3 cells *in vivo* in immunocompromised nude mice. Control and shEZH2 expressing SKOV3 cells were injected subcutaneously into nude mice with 5×10^6 cells per mice and 5 mice in each group. Four weeks after injection, the sizes of xenografted tumors were compared between control and shEZH2 expressing cells (Fig. 4A and B). EZH2 knockdown by shEZH2 in the xenograft tumors was confirmed by IHC staining (Fig. 4C). shEZH2 expression significantly inhibited the growth of xenografted SKOV3 cells (Fig. 4A and B).

EZH2 knockdown inhibits the invasion of human EOC cells

EZH2 has been implicated in regulating cell invasion in several types of cancer cells (11, 15, 32, 33). Thus, we sought to determine the effects of EZH2 knockdown on invasion of human EOC cells. Toward this goal, control and shEZH2 expressing SKOV3 cells were tested for their ability to migrate through uncoated control membrane or invade through matrigel-coated membrane. Compared with controls, EZH2 knockdown significantly inhibited the invasion of SKOV3 cells as revealed by a decreased invasion index that is calculated as the ratio between the number of cells invaded through matrigel-coated membrane and the number of cells migrated through control membrane (Fig. 5). Inhibition of invasion was observed by 2 individual shEZH2 in SKOV3 cells (Fig. 5). In addition, the degree of invasion inhibition correlated with the degree of EZH2 knockdown (Figs. 3 and 5), suggesting that this is not because of off-targets effects. On the basis of these results, we conclude that EZH2 knockdown inhibits the invasion of human EOC cells.

EZH2 knockdown triggers apoptosis in human EOC cells

We next sought to determine the mechanisms by which EZH2 knockdown inhibits the growth of human EOC cells. DNA content analysis determined by FACS showed that there was no statistical difference in cell-cycle distribution between control and shEZH2 expressing cells (Supplementary Fig. S3). We next examined the markers of apoptosis in control and shEZH2 expressing SKOV3 cells. When compared with controls, markers of apoptosis were significantly induced by shEZH2 expression (Fig. 6). Those apoptotic markers include increased percentage of cells at sub-G1 phase as measured by FACS analysis (Fig. 6A), increased percentage of Annexin V positively stained cells as measured by Guava Nexin assay (Fig. 6B), upregulation of cleaved Lamin A, PARP p85, and caspase 3 (Fig. 6C; ref. 34). Together, we conclude that EZH2 knockdown induces apoptosis of human EOC cells.

Discussion

Consistent with our findings, EZH2 mRNA expression was upregulated 2-fold or more in more than 80% of high-grade serous human EOC specimens in the newly released

Published OnlineFirst November 29, 2010; DOI:10.1158/1541-7786.MCR-10-0398

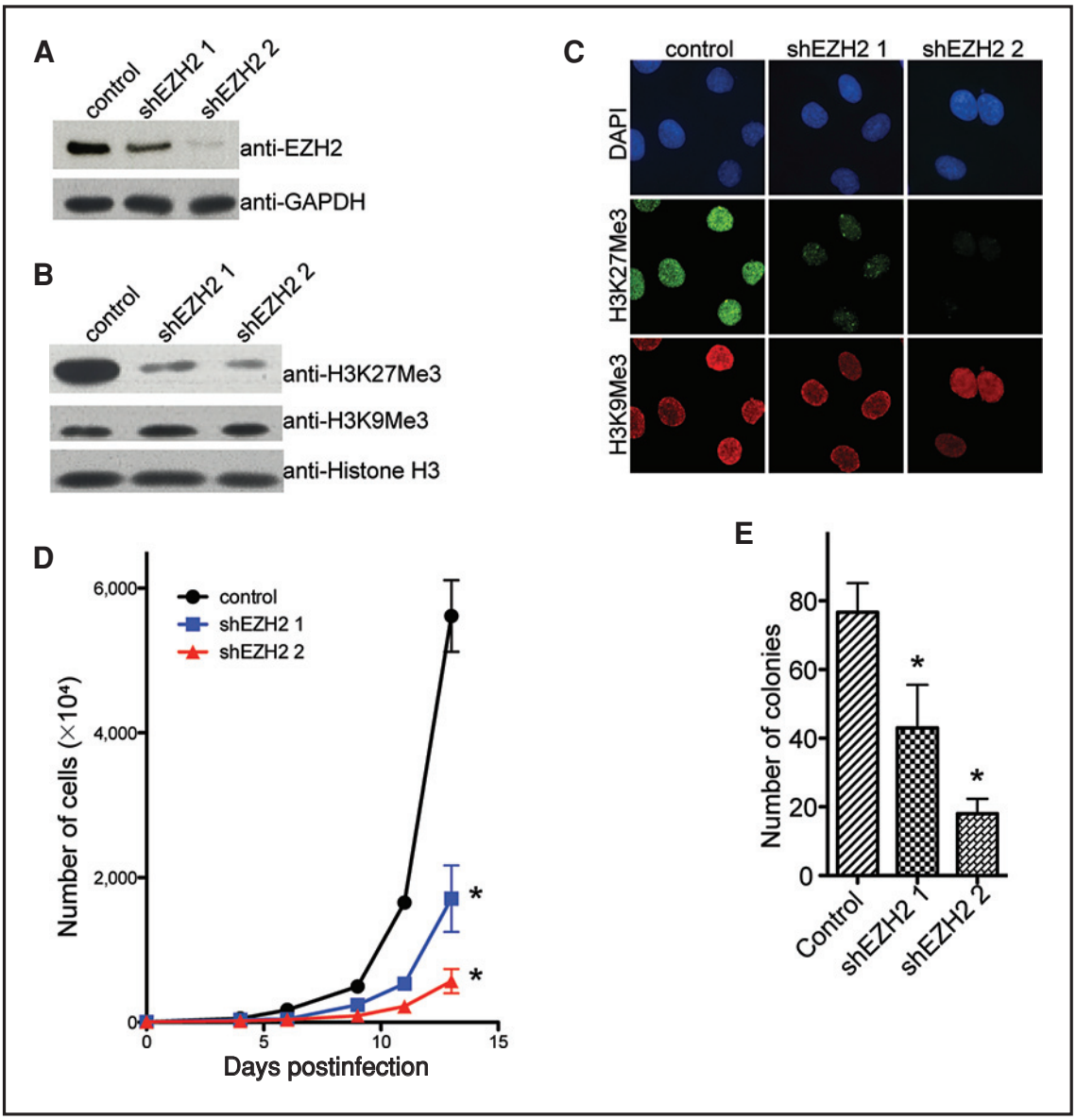

Figure 3. EZH2 knockdown inhibits the growth of SKOV3 cells *in vitro*. A, SKOV3 cells were infected with 2 individual lentivirus encoded shEZH2 or control. Drug-selected cells were examined for expression of EZH2 and GAPDH by Western blotting. B, same as A, but examined for expression of H3K27Me3 and H3K9Me3 by Western blotting. C, same as A, but examined for expression of H3K27Me3 and H3K9Me3 by immunofluorescence staining. DAPI counterstaining was used to visualize the cell nuclei. D, same as A, but equal number of drug-selected cells were seeded and counted at indicated time points. Mean of 3 independent experiments with SD. *, $P < 0.001$. E, same as A, 1×10^4 cells were seeded in soft agar and the number of colonies were counted after 3 weeks of culture. Mean of 3 independent experiments with SD. *, $P < 0.001$.

the Cancer Genomics Atlas (TCGA) serous ovarian cystoadenocarcinoma gene expression database (http//cancergenome.nih.gov/). *EZH2* gene is located at chromosome 7q36.1. Gene amplification contributes to EZH2 overexpression in several types of cancer (14, 35). However, TCGA gene copy-number analysis indicates that *EZH2* gene amplification occurs only in a very small percentage of EOCs (<10% specimens show >4 copy of EZH2 gene; http//cancergenome.nih.gov/), suggesting that gene amplification is not a major mechanism that leads to EZH2 upregulation in human EOCs. EZH2 is an E2F target gene (35). A very recent study showed that VEGF stimulates EZH2 expression in human EOC cells via E2F family members, E2F1 and E2F3 (24). However, VEGF only stimulates the expression of EZH2 mRNA up to 3-fold (24), which is far below the level of increase in EZH2 mRNA or protein in human EOC cells compared with cultured pHOSE cells (Fig. 1 and data not shown), suggesting additional mechanisms contribute to EZH2 upregulation in human EOC cells. In the future, we will elucidate

Published OnlineFirst November 29, 2010; DOI:10.1158/1541-7786.MCR-10-0398

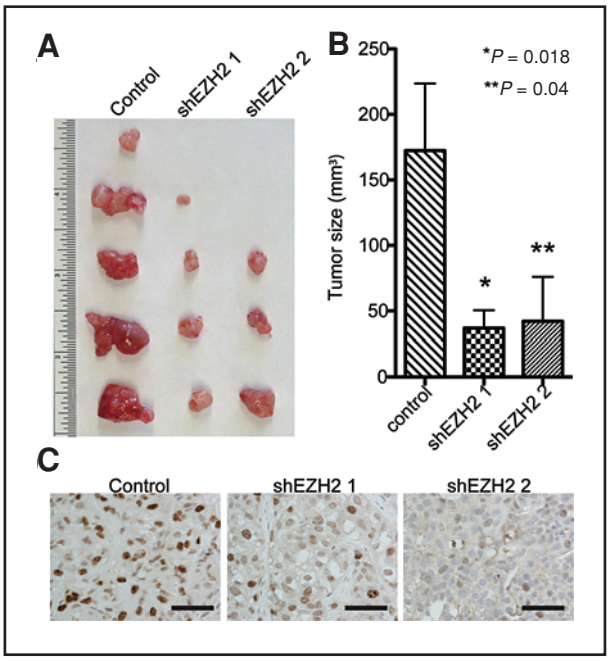

Figure 4. EZH2 knockdown suppresses the growth of SKOV3 cells *in vivo* in immunocompromised mice. A, 5×10^6 control or shEZH2 expressing SKOV3 cells were injected subcutaneously into immunocompromised nude mice ($n = 5$). Four weeks postinjection, tumors were removed from mice. B, quantitation of A, the size of tumors was measured. Mean of tumor sizes with SEM. C, xenografted tumors formed by control or shEZH2 expressing SKOV3 cells were sectioned and stained for EZH2 expression. Bar = 50 μm.

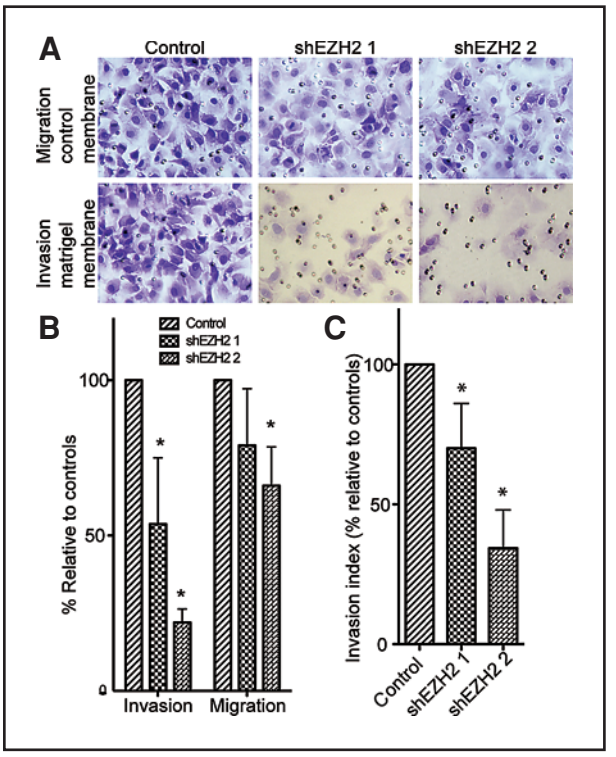

Figure 5. EZH2 knockdown suppresses the invasion of SKOV3 cells. A, equal number of control and shEZH2 expressing SKOV3 cells were assayed for migration through uncoated control membrane or invasion through matrigel-coated membrane. The cells migrated through control membrane or invaded through matrigel-coated membrane were stained with 1% crystal violet in PBS. B, quantitation of A. Relative percentage of shEZH2 expressing cells migrated through control membrane or invaded through matrigel-coated membrane compared with controls was indicated. Mean of 3 independent experiments with SD. *, $P < 0.05$. C, invasion index of shEZH2 expressing SKOV3 cells compared with controls. Invasion index is the ratio between cells invaded through matrigel-coated membrane and cells migrated through control membrane. Mean of 3 independent experiments with SD. *, $P < 0.05$.

additional mechanisms that contribute to EZH2 upregulation in human EOCs.

EZH2 has been demonstrated as a prognostic marker for breast and prostate cancers and positively correlates with disease-free survival and overall survival in those patient populations (11–13). In addition, EZH2 overexpression correlates with more advanced disease stages of breast and prostate cancers (11, 13). However, EZH2 expression was not a prognostic marker in other types of cancers including renal clear cell carcinoma and hepatocellular carcinomas (33, 36). We showed that there was no significant correlation between EZH2 expression and disease-free or overall survival in high-grade serous EOC patients (Fig. 2). Consistent with our findings, low expression of H3K27Me3 has been demonstrated to be a poor prognostic marker in EOC (37). In contrast, a very recent study showed that EZH2 expression in either EOC cells or ovarian tumor vasculature is predictive of poor clinical outcome (24). The basis for the discrepancy between our study and that of Lu et al.'s is unclear. A possible reason may be that we correlated EZH2 expression with overall or disease-free survival only in high-grade serous histotype EOCs (Fig. 2), whereas the study by Lu et al. includes additional histotypes of EOCs (24).

We showed that EZH2 expression positively correlated with Ki67 expression in EOCs (Table 1). There are conflicting results regarding the prognostic value of Ki67 in ovarian carcinoma (38–42). A recent study by Kobel et al. (43) suggests that differences in Ki67 index among different subtypes of EOCs confound the Ki67 survival analysis because nearly all high-grade serous EOCs have a high Ki67 index. In analysis of each individual subtypes, Ki67 is no longer a prognostic marker. Consistent with this, although EZH2 correlates with Ki67 expression (Table 1), EZH2 expression was not a prognostic indicator for either overall or disease-free survival in the tested high-grade serous histotype EOC patients (Fig. 2).

Interestingly, when compared with normal ovarian surface epithelium, EZH2 expression is significantly upregulated (up to 23-fold) in ovarian epithelial inclusion cysts (44), which are thought to be the precursor lesion of a subset of EOC (45). This suggests that EZH2 overexpression is an early event during EOC development. Although ovarian surface epithelium is thought to be the cell origin of EOC (46), there are still several histopathology-based theories that differ in their explanations about the origins of EOC (46–48). Notably, recent evidence suggests that a proportion of high-grade serous EOC may arise from distal fallopian tube

Published OnlineFirst November 29, 2010; DOI:10.1158/1541-7786.MCR-10-0398

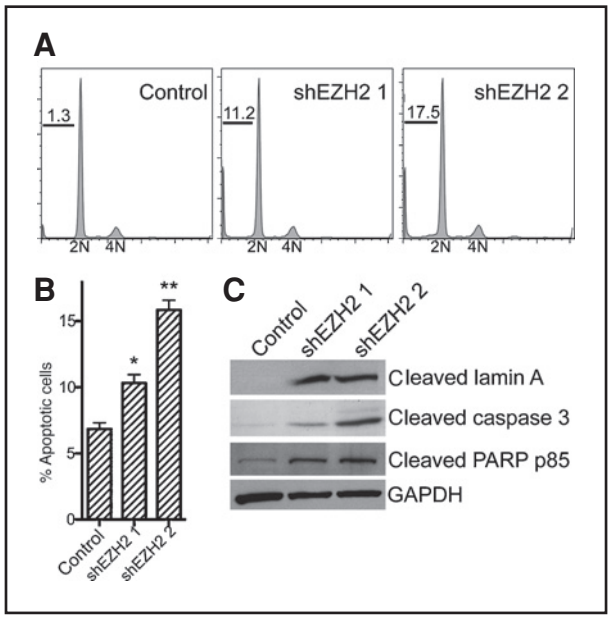

Figure 6. EZH2 knockdown induces apoptosis of SKOV3 cells. A, control and shEZH2 expressing SKOV3 cells were examined for cell-cycle distribution by FACS. The percentage of sub-G1 cells was indicated. B, control and shEZH2 expressing cells were stained for Annexin V, a cell surface marker of apoptosis. Annexin V–positive cells were measured by Guava Nexin assay. Mean of 3 independent experiments with SD. *, P, 0.019 and **, $P < 0.001$ compared with controls. C, same as B, but examined for expression of cleaved Lamin A, PARP p85, and caspase 3, all markers of apoptosis in control and shEZH2 expressing cells.

(48). Therefore, it will be interesting to examine EZH2 expression in normal fallopian tube epithelium.

Multiple genes have been implicated in EZH2 inhibition–induced apoptosis. For example, FBXO32 contributes to EZH2 inhibition induced–apoptosis in breast cancer cells (45), and Bim expression has been demonstrated to mediate EZH2 inhibition–induced apoptosis in prostate cancer cells (49). Likewise, E-cadherin, DAB2IP, and SLIT2 have all been implicated in mediating increased invasiveness conferred by high levels of EZH2 expression (32, 50–52). Further studies are warranted to delineate the molecular mechanisms by which EZH2 overexpression promotes proliferation and invasion of human EOC cells.

In summary, the data reported here show that EZH2 is overexpressed in approximately 66% of primary human EOCs and its overexpression correlates with a high proliferation index and tumor grade in EOCs. Knockdown of EZH2 inhibits the growth of human EOC cells *in vitro* and *in vivo*. EZH2 knockdown induces apoptosis of human EOC cells. In addition, EZH2 knockdown suppresses the invasion of human EOC cells. Further, inhibition of the growth and invasion of human EOC cells induced by EZH2 knockdown correlates with a decrease in the levels of H3K27Me3, suggesting that EZH2 histone methyltransferase activity is critical for its function in human EOC cells. Together, our data imply that EZH2 is a potential target for developing epigenetic modifying therapeutics for EOC.

Disclosure of Potential Conflicts of Interest

No potential conflicts of interest were declared.

Acknowledgments

We thank Drs. Thomas Hamilton and Steve Williams at Fox Chase Cancer Center for human epithelial ovarian cancer cell lines, Tianyu Li at Fox Chase Cancer Center Biostatistics and Bioinformatics facility for statistical analysis, and JoEllen Weaver at Fox Chase Cancer Center Biosample Repository facility for technical support, and Dr. Denise Connolly for critical reading of the manuscript.

Grant Support

R. Zhang is an Ovarian Cancer Research Fund (OCRF) Liz Tilberis Scholar. This work was supported, in part, by a NCI FCCC-UPenn ovarian cancer SPORE (P50 CA083638) pilot project and career development award (R. Zhang), a Department of Defense Ovarian Cancer Academy award OC093420 (R. Zhang) and an OCRF program project (A. K. Godwin and R. Zhang).

The costs of publication of this article were defrayed in part by the payment of page charges. This article must therefore be hereby marked *advertisement* in accordance with 18 U.S.C. Section 1734 solely to indicate this fact.

Received 08/30/2010; revised 09/30/2010; accepted 10/08/2010; published OnlineFirst 11/29/2010.

References

1. Cao R, Wang L, Wang H, Xia L, Erdjument-Bromage H, Tempst P, et al. Role of histone H3 lysine 27 methylation in Polycomb-group silencing. Science 2002;298:1039–43.
2. Czermin B, Melfi R, McCabe D, Seitz V, Imhof A, Pirrotta V. Drosophila enhancer of Zeste/ESC complexes have a histone H3 methyltransferase activity that marks chromosomal Polycomb sites. Cell 2002;111:185–96.
3. Kuzmichev A, Nishioka K, Erdjument-Bromage H, Tempst P, Reinberg D. Histone methyltransferase activity associated with a human multiprotein complex containing the Enhancer of Zeste protein. Genes Dev 2002;16:2893–905.
4. Muller J, Hart CM, Francis NJ, Vargas ML, Sengupta A, Wild B, et al. Histone methyltransferase activity of a Drosophila Polycomb group repressor complex. Cell 2002;111:197–208.
5. Cao R, Zhang Y. SUZ12 is required for both the histone methyltransferase activity and the silencing function of the EED-EZH2 complex. Mol Cell 2004;15:57–67.
6. Ketel CS, Andersen EF, Vargas ML, Suh J, Strome S, Simon JA. Subunit contributions to histone methyltransferase activities of fly and worm polycomb group complexes. Mol Cell Biol 2005;25:6857–68.
7. Schwartz YB, Kahn TG, Nix DA, Li XY, Bourgon R, Biggin M, et al. Genome-wide analysis of Polycomb targets in Drosophila melanogaster. Nat Genet 2006;38:700–5.
8. Schuettengruber B, Ganapathi M, Leblanc B, Portoso M, Jaschek R, Tolhuis B, et al. Functional anatomy of polycomb and trithorax chromatin landscapes in Drosophila embryos. PLoS Biol 2009;7:e13.
9. Boyer LA, Plath K, Zeitlinger J, Brambrink T, Medeiros LA, Lee TI, et al. Polycomb complexes repress developmental regulators in murine embryonic stem cells. Nature 2006;441:349–53.
10. Lee TI, Jenner RG, Boyer LA, Guenther MG, Levine SS, Kumar RM, et al. Control of developmental regulators by Polycomb in human embryonic stem cells. Cell 2006;125:301–13.
11. Kleer CG, Cao Q, Varambally S, Shen R, Ota I, Tomlins SA, et al. EZH2 is a marker of aggressive breast cancer and promotes neoplastic

Published OnlineFirst November 29, 2010; DOI:10.1158/1541-7786.MCR-10-0398

transformation of breast epithelial cells.Proc Natl Acad Sci USA 2003;100:11606–11.
12. Bachmann IM, Halvorsen OJ, Collett K, Stefansson IM, Straume O, Haukaas SA, et al. EZH2 expression is associated with high proliferation rate and aggressive tumor subgroups in cutaneous melanoma and cancers of the endometrium, prostate, and breast. J Clin Oncol. 2006;24:268–73.
13. Varambally S, Dhanasekaran SM, Zhou M, Barrette TR, Kumar-Sinha C, Sanda MG, et al. The polycomb group protein EZH2 is involved in progression of prostate cancer. Nature 2002;419:624–9.
14. Saramaki OR, Tammela TL, Martikainen PM, Vessella RL, Visakorpi T. The gene for polycomb group protein enhancer of zeste homolog 2 (EZH2) is amplified in late-stage prostate cancer. Genes Chromosomes Cancer 2006;45:639–45.
15. Bryant RJ, Cross NA, Eaton CL, Hamdy FC, Cunliffe VT. EZH2 promotes proliferation and invasiveness of prostate cancer cells. Prostate 2007;67:547–56.
16. Kuzmichev A, Margueron R, Vaquero A, Preissner TS, Scher M, Kirmizis A, et al. Composition and histone substrates of polycomb repressive group complexes change during cellular differentiation. Proc Natl Acad Sci USA 2005;102:1859–64.
17. Kirmizis A, Bartley SM, Kuzmichev A, Margueron R, Reinberg D, Green R, et al. Silencing of human polycomb target genes is associated with methylation of histone H3 Lys 27. Genes Dev 2004;18:1592–605.
18. Kirmizis A, Bartley SM, Farnham PJ. Identification of the polycomb group protein SU(Z)12 as a potential molecular target for human cancer therapy. Mol Cancer Ther 2003;2:113–21.
19. Ozols RF, Bookman MA, Connolly DC, Daly MB, Godwin AK, Schilder RJ, et al. Focus on epithelial ovarian cancer. Cancer Cells 2004;5:19–24.
20. Farley J, Ozbun LL, Birrer MJ. Genomic analysis of epithelial ovarian cancer. Cell Res 2008;18:538–48.
21. Stany MP, Bonome T, Wamunyokoli F, Zorn K, Ozbun L, Park DC, et al. Classification of ovarian cancer: a genomic analysis. Adv Exp Med Biol 2008;622:23–33.
22. Shih Ie M, Kurman RJ. Ovarian tumorigenesis: a proposed model based on morphological and molecular genetic analysis. Am J Pathol 2004;164:1511–8.
23. Lu C, Bonome T, Li Y, Kamat AA, Han LY, Schmandt R, et al. Gene alterations identified by expression profiling in tumor-associated endothelial cells from invasive ovarian carcinoma. Cancer Res 2007;67:1757–68.
24. Lu C, Han HD, Mangala LS, Ali-Fehmi R, Newton CS, Ozbun L, et al. Regulation of tumor angiogenesis by EZH2.Cancer Cell 2010;18:185–97.
25. Bellacosa A, Godwin AK, Peri S, Devarajan K, Caretti E, Vanderveer L, et al. Altered gene expression in morphologically normal epithelial cells from heterozygous carriers of BRCA1 or BRCA2 mutations. Cancer Prev Res (Phila). 2010;3:48–61.
26. Zhang R, Chen W, Adams PD. Molecular dissection of formation of senescence-associated heterochromatin foci. Mol Cell Biol 2007;27:2343–58.
27. Zhang R, Liu ST, Chen W, Bonner M, Pehrson J, Yen TJ, et al. HP1 proteins are essential for a dynamic nuclear response that rescues the function of perturbed heterochromatin in primary human cells. Mol Cell Biol 2007;27:949–62.
28. Zhang R, Poustovoitov MV, Ye X, Santos HA, Chen W, Daganzo SM, et al. Formation of MacroH2A-containing senescence-associated heterochromatin foci and senescence driven by ASF1a and HIRA. Dev Cell 2005;8:19–30.
29. McCarty KS, Jr/surname>., Miller LS, Cox EB, Konrath J, McCarty KS, Sr. Estrogen receptor analyses. Correlation of biochemical and immunohistochemical methods using monoclonal antireceptor antibodies. Arch Pathol Lab Med 1985;109:716–21.
30. McCarty KS Jr., Szabo E, Flowers JL, Cox EB, Leight GS, Miller L, et al. Use of a monoclonal anti-estrogen receptor antibody in the immunohistochemical evaluation of human tumors. Cancer Res. 1986;46:4244s-8s.
31. Jenuwein T. The epigenetic magic of histone lysine methylation. FEBS J. 2006;273:3121–35.
32. Cao Q, Yu J, Dhanasekaran SM, Kim JH, Mani RS, Tomlins SA, et al. Repression of E-cadherin by the polycomb group protein EZH2 in cancer. Oncogene. 2008;27:7274–84.
33. Sudo T, Utsunomiya T, Mimori K, Nagahara H, Ogawa K, Inoue H, et al. Clinicopathological significance of EZH2 mRNA expression in patients with hepatocellular carcinoma. Br J Cancer. 2005;92:1754–8.
34. Nicholson DW, Thornberry NA. Caspases: killer proteases. Trends Biochem Sci. 1997;22:299–306.
35. Bracken AP, Pasini D, Capra M, Prosperini E, Colli E, Helin K. EZH2 is downstream of the pRB-E2F pathway, essential for proliferation and amplified in cancer. EMBO J. 2003;22:5323–35.
36. Hinz S, Weikert S, Magheli A, Hoffmann M, Engers R, Miller K, et al. Expression profile of the polycomb group protein enhancer of Zeste homologue 2 and its prognostic relevance in renal cell carcinoma. J Urol 2009;182:2920–5.
37. Wei Y, Xia W, Zhang Z, Liu J, Wang H, Adsay NV, et al. Loss of trimethylation at lysine 27 of histone H3 is a predictor of poor outcome in breast, ovarian, and pancreatic cancers. Mol Carcinog 2008;47:701–6.
38. Munstedt K, von Georgi R, Franke FE. Correlation between MIB1-determined tumor growth fraction and incidence of tumor recurrence in early ovarian carcinomas. Cancer Invest 2004;22:185–94.
39. Khouja MH, Baekelandt M, Nesland JM, Holm R. The clinical importance of Ki-67, p16, p14, and p57 expression in patients with advanced ovarian carcinoma. Int J Gynecol Pathol 2007;26:418–25.
40. Korkolopoulou P, Vassilopoulos I, Konstantinidou AE, Zorzos H, Patsouris E, Agapitos E, et al. The combined evaluation of p27Kip1 and Ki-67 expression provides independent information on overall survival of ovarian carcinoma patients. Gynecol Oncol 2002;85:404–14.
41. Green JA, Berns EM, Coens C, van Luijk I, Thompson-Hehir J, van Diest P, et al. Alterations in the p53 pathway and prognosis in advanced ovarian cancer: a multi-factorial analysis of the EORTC Gynaecological Cancer group (study 55865).Eur J Cancer 2006;42:2539–48.
42. Anttila M, Kosma VM, Ji H, Wei-Ling X, Puolakka J, Juhola M, et al. Clinical significance of alpha-catenin, collagen IV, and Ki-67 expression in epithelial ovarian cancer. J Clin Oncol 1998;16:2591–600.
43. Kobel M, Kalloger SE, Boyd N, McKinney S, Mehl E, Palmer C, et al. Ovarian carcinoma subtypes are different diseases: implications for biomarker studies. PLoS Med. 2008;5:e232.
44. Pothuri B, Leitao MM, Levine DA, Viale A, Olshen AB, Arroyo C, et al. Genetic analysis of the early natural history of epithelial ovarian carcinoma. PLoS One 2010;5:e10358.
45. Salazar H, Godwin AK, Daly MB, Laub PB, Hogan WM, Rosenblum N, et al. Microscopic benign and invasive malignant neoplasms and a cancer-prone phenotype in prophylactic oophorectomies.J Natl Cancer Inst 1996;88:1810–20.
46. Kurman RJ, Shih Ie M. The origin and pathogenesis of epithelial ovarian cancer: a proposed unifying theory.Am J Surg Pathol 34:433–43.
47. Dubeau L. The cell of origin of ovarian epithelial tumours. Lancet Oncol 2008;9:1191–7.
48. Levanon K, Crum C, Drapkin R. New insights into the pathogenesis of serous ovarian cancer and its clinical impact. J Clin Oncol 2008;26:5284–93.
49. Wu ZL, Zheng SS, Li ZM, Qiao YY, Aau MY, Yu Q. Polycomb protein EZH2 regulates E2F1-dependent apoptosis through epigenetically modulating Bim expression.Cell Death Differ 2010;17:801–10.
50. Herranz N, Pasini D, Diaz VM, Franci C, Gutierrez A, Dave N, et al. Polycomb complex 2 is required for E-cadherin repression by the Snail1 transcription factor. Mol Cell Biol 2008;28:4772–81.
51. Min J, Zaslavsky A, Fedele G, McLaughlin SK, Reczek EE, De Raedt T, et al. An oncogene-tumor suppressor cascade drives metastatic prostate cancer by coordinately activating Ras and nuclear factor-kappaB. Nat Med 2010;16:286–94.
52. Chen H, Tu SW, Hsieh JT. Down-regulation of human DAB2IP gene expression mediated by polycomb Ezh2 complex and histone deacetylase in prostate cancer. J Biol Chem 2005;280:22437–44.

AACR Annual Meeting Abstract

Wnt5a-dependent induction of senescence suppresses epithelial ovarian cancer.

Benjamin G. Bitler [1], Jasmine P. Nicodemus [1], Hua Li [1], Qi Cai [2], Keri Soring [3], Michael J. Birrer [6], Denise C. Connolly [1], Andrew K. Godwin [2], Paul Cairns [3], Hong Wu [4], Rugang Zhang [1, 5]

[1] Women's Cancer Program, [2] Biosample Repository Facility, [3] Department of Surgical Oncology, [4] Department of Pathology, [5] Epigenetic and Progenitor Cell Keystone Program, Fox Chase Cancer Center; [6] Massachusetts General Hospital Cancer Center, Harvard Medical School.

Epithelial Ovarian Cancer (EOC) remains the most lethal gynecological malignancy in US and is the fifth leading cause of cancer deaths among American women. Thus, there is an urgent need to understand the etiology of EOC to develop novel therapies for this disease. Here, we demonstrated that a non-canonical Wnt ligand, Wnt5a, is expressed at significantly lower levels in human EOC cell lines and in primary human EOC compared with either normal ovarian surface epithelial cells or fallopian tube epithelial cells. Importantly, expression of Wnt5a in primary human EOC inversely correlates with tumor stage but not tumor grade. Interestingly, Wnt5a expression is significantly lower in Type II high-grade serous EOC compared to Type I EOC that includes low-grade serous, mucinous, clear cell and endometrioid subtypes of EOC. In addition, we discovered that hypermethylation of promoter CpG island contributes to Wnt5a downregulation in human EOC cells. Significantly, restoration of Wnt5a expression in human EOC cells promoted senescence of EOC cells and resulted in a dramatic decrease in cell proliferation both *in vitro* and *in vivo* in an orthotopic model of EOC in the ovary of SCID mice. Mechanistically, Wnt5a inhibited canonical Wnt/β-catenin signaling and resulted in the activation of senescence-promoting histone repressor A/PML pathway. In summary, we show that Wnt5a is often expressed at lower levels in primary human EOC and Wnt5a expression suppresses the growth of EOC cells by triggering senescence through antagonizing canonical Wnt signaling. These results also suggest that loss of Wnt5a expression is a putative marker of EOC and that non-canonical Wnt signaling is a potent target for developing novel EOC therapeutics.

An abstract presented at the 3rd International Symposium on Ovarian Cancer

Wnt Signaling, Cellular Senescence and Ovarian Cancer Therapy

Rugang Zhang, Ph.D.

Program in Gene Expression and Regulation, The Wistar Institute, Philadelphia, PA 19104.

Epithelial ovarian cancer (EOC) remains the most lethal gynecological malignancy in the US. Thus, there is an urgent need to develop novel therapeutics for this disease. Cellular senescence is a tumor suppression mechanism that has been suggested as a novel mechanism for developing cancer therapeutics. Wnt5a is a non-canonical Wnt ligand that plays a context-dependent role in human cancers. Recently, we discovered a lower level of Wnt5a expression predicted shorter overall survival in EOC patients. Significantly, Wnt5a restoration inhibited proliferation of EOC cells both *in vitro* and *in vivo* in an orthotopic mouse model. Mechanistically, Wnt5a antagonizes Wnt/β-catenin signaling and induces cellular senescence by activating the epigenetic histone repressor A (HIRA)/promyelocytic leukemia (PML) senescence pathway. These data suggest that promoting cells to undergo senescence by reconstituting Wnt5a signaling represents a novel strategy for developing urgently needed EOC therapeutics. Here we performed preliminary experiments with a Wnt5a-mimetic hexapeptide, Foxy5. In EOC cell lines, Foxy5 significantly inhibits the proliferation of EOC cells by downregulating β-catenin and its transcriptional target, *CCND1* (cyclin D1). In addition, Foxy5 inhibits EOC cell migration in a classical wound-healing assay. In summary, we show that loss of Wnt5a predicts poor outcome in EOC patients and Wnt5a suppresses the growth of EOC cells by triggering cellular senescence. We suggest that strategies to drive senescence in EOC cells by reconstituting Wnt5a signaling via using Foxy5 may offer an effective new strategy for EOC therapy.